Fluvial erosion of St-Lawrence and Ottawa River valleys clays: erosion mechanics, critical shear stress and geotechnical properties

Liliane Gonthier – 260 588 161

Thesis

Department of Civil Engineering and Applied Mechanics

McGill University, Montreal

December 15th, 2021

A thesis submitted to McGill University in partial fulfillment of the requirements of the degree of Master of Civil Engineering

Abstract

The landscape of the St-Lawrence and Ottawa River valleys was formed by the events of the last three glaciations and interglaciations, which laid thick deposits of glaciolacustrine, glaciomarine, lacustrine and fluvial sediments. In the past 50 years, land use changes in the St-Lawrence Lowlands as well as an increased frequency of larger flood and drought events have led to the exacerbation of the erosion (increased erosion rates) of these cohesive sediment deposits. Fluvial erosion of cohesive sediments is complex due to the influence of depositional history, internal structure and moisture content. There is limited knowledge of the erosion processes of river clay deposits, particularly for cemented sediments commonly found in post-glacial environments. The objective of this research was to increase knowledge on the erosion behavior of clay deposits and to identify their controlling characteristics. A new coring method was designed to sample large undisturbed samples and used at six sites located in the St-Lawrence Lowlands. Its performance was compared directly to the Sherbrooke sampler at one site. The samples had wide range of geotechnical characteristics; with a clay content varying from 24 to 63%, a liquidity index varying from 33 to 92%, a consistency varying from non-plastic to highly plastic and with distinct structures linked to diverse depositional environments such as varved clays, rhythmites and remolded glaciomarine sediments. Floc erosion, slaking, surface erosion as well as mass erosion were observed during uni-directional flume erosion tests, in a flume equipped with a lifting mechanism to align the eroded sample surface flush with the channel bed and a catchment basin to collect eroded blocks. The critical shear stress of the samples varied from 0.2Pa up to >11.5Pa and the mass erosion rate varied from 0.04 to 7.16mm/h; samples with planes of weaknesses such as thin stratification, presence of cohesionless sediments pockets and fissures were more erodible than other samples taken at the same site. The results also show that the degree of cementation present in the clays significantly affected their erosion behavior. Air-drying for 48 hours only had a significant impact on the erosional behavior of the loam as its moisture content decreased and a significant loss of cohesion occurred during the wet-dry cycle indicated by the decrease in critical shear stress from >11.5Pa to 0.9Pa.

Résumé

Le paysage des vallées du St-Laurent et la rivière des Outaouais a été façonné par les évènements des trois dernières périodes de glaciation desquels découlent la présence d'épais dépôts glaciolacustrins, glaciomarins, lacustrins et fluviaux. Depuis les années 1950, des changements dans l'occupation du territoire ainsi que l'intensification d'inondations et de sécheresses ont exacerbés l'érosion de ces dépôts cohésifs. L'érosion fluviale de sédiments cohésifs est un mécanisme complexe lié à l'influence de l'historique de déposition, leur structure interne et leur teneur en eau. Il existe très peu de connaissances sur les processus d'érosion de dépôts cohésifs riverains et encore moins pour les dépôts cimentés présents dans des environnements post-glaciaires. Le but de cette recherche était de dresser un meilleur portrait de la résistance au cisaillement liée à l'érosion de dépôts cohésifs locaux ainsi qu'identifier des facteurs déterminants. Une nouvelle méthode de carottage fût développée pour échantillonner de larges spécimens non-remaniés à six sites situés dans les basses-terres du Saint-Laurent et sa performance fût comparée à celle de l'échantillonneur de Sherbrooke à un emplacement. Les échantillons avaient des caractéristiques géotechniques variées; avec une teneur en argile variant entre 24 et 63%, une limite de liquidité variant entre 33 et 92%, une consistance allant de non-plastique à très plastique ainsi qu'avec des structures internes distinctes incluant des argiles varvées, des rythmites et des sédiments glaciomarins remaniés. De l'érosion par floculation, de surface et de masse ainsi que de la battance furent observées lors de tests d'érosion dans un canal droit unidirectionnel avec un mécanisme de levée pour des échantillons confinés et un basin de capture pour récupérer les masses érodées. Le seuil critique de cisaillement des échantillons variait entre 0.2 and >11.5Pa et le taux d'érosion de masse variaient entre 0.04 et 7.16mm/h. Ceux contenant des faiblesses comme des strates fines, des poches de sédiments non-cohésifs et des fissures étaient plus érodables que les autres échantillons des mêmes sites. Les résultats montrent aussi que le degré de cimentation présent dans les argiles influence hautement leur résistance au cisaillement. Le séchage pendant 48 heures n'a eu un impact significatif que sur la résistance à l'érosion d'une glaise alors que celle-ci a perdu considérablement d'eau à sa surface et qu'elle encourut une perte de cohésion durant le cycle sec/humide menant à une diminution de la résistance au cisaillement de >11.5Pa à 0.9Pa.

Acknowledgments

This project is the fruit of three years of dedicated work and benefited from a great deal of support and assistance.

I would first like to thank WSP, Mitacs and NSERC for their financial support and for making this project a reality. I am grateful for the support of Julian Gacek who supported me and helped me ground the project to the reality of practitioners in the field of river engineering.

I would also like to thank my supervisor, Professor Susan Gaskin, for her guidance and extraordinary counsel throughout this project. She taught me immensely about river engineering and encouraged me to think critically by directing and monitoring the project thoroughly. I'm forever grateful for her patience and her passion for this project.

I also wish to thank Professor Mourad Karray for his invaluable expertise on the behavior of clays and enthusiasm towards this project. I am thankful for the collaboration that took place at Université de Sherbrooke under his direction and the assistance of Alexandre Sévigny, Ahmed Mhenni et Valérie Dumoulin during all the geotechnical tests.

I am indebted to my partner Dorothy Yeats for all the work she has done by my side during the last three years. Her sense of organization, her wits and her sense of humor have me helped me immensely throughout this journey. We accomplished much more as a team than I could have done by myself, and I am grateful for her help designing the sampling methods and the flume setup as well as the sampling that occurred during the first year of this project.

I am beholden to the McGill Civil Engineering lab technicians: John Barczak, William Dumais and Damon Kiperchuk for making this project possible. They helped me design and build all the setups as well as allowing me to try and develop innovative sampling and measurement techniques.

I would also like to thank Peter Yeats, Pierre-William Breau and Junho Park for assisting me during the sample collection in Chelsea, Prévost and Quebec City. Their help was inestimable as sampling was arduous and under straining conditions.

Table of contents

List of Figures

List of Tables

Notation

- A channel area
- a_c activity of the clay minerals
- A_s surface area
- C_u or S_u undrained shear strength of a soil
- c_{ur} remoulded shear strength
- D diameter of the particles
- D diameter of the vane blades
- D_{50} diameter at which 50% of a sample's mass is comprised of smaller particles
- E specific energy
- F spring constant
- F correction factor based on the use of a hydrometer 151H
- Fr Froude number
- g gravitational constant
- H height of the vane blades
- H total head
- $\hat{I}_b$ near-bed turbulence intensity
- k constant associated with the geometry of the cone
- K calibration coefficient for drag and gravitational acceleration
- LI liquidity index of a cohesive soil
- LL liquid limit of a cohesive soil
- m moisture content of a soil
- M_{loss} Mass of eroded material
- m_s dry mass of the clay particles
- m_w mass of the calibration pycnometer
- m_{s+w} mass of the pycnometer filled
- p or h penetration depth of a fall cone
- PF percentage of fine particles
- PI plasticity index of cohesive soil
- PL plastic limit of a cohesive soil
- $\bar{P}$ average depth of submersion of the hydrometer
- Q weight of the cone
- R hydraulic radius
- R_{init} is the initial angle of the vane rotation
- R_{final} is the final angle of the vane rotation
- R_v distance between water surface and Z_0
- Re Reynolds' number
- Re_* boundary Reynolds number or roughness Reynolds number
- S_o bed slope of channel
- S_f energy slope of channel
- S_G or G_s specific gravity of a soil or the solid fraction of a soil
- S_{tv} sensitivity of a clay
- T temperature
- T torque of the vane
- u streamwise velocity
- U* shear velocity
- W_{loss} Eroded material weight
- $\dot{Z}$ scour, or erosion, rate
- Z_0 height above the datum at which the velocity equals zero
- γ_b soil bulk unit weight
- γw specific weight of water
- Δdz roughness change
- ΔS salinity difference between eroding fluid and clay pore water
- η dynamic viscosity of water
- κ von Karman's constant
- with sediments and water
- ρ_w density of water
- τ shear stress
- τ* non-dimensional shear stress
- τc critical shear stress
- ν kinematic viscosity of a fluid

1 Introduction

Glacial marine and lacustrine deposits originating from the last three stadials (glaciation) and interstadials during the Wisconsin, dating from 191 kya to the most recent ending only 11 kya, underlie the St. Lawrence and Ottawa River valleys. During this time, lakes and marine inlets (from example the Champlain Sea) resulted in layers of clay deposits. Clays, defined by particle sizes less than 0.002mm, are cohesive due to the van der Waals forces between them, which results in their being more resistant to fluvial erosion than larger alluvial materials (Thorne & Tovey, 1981). As both the St. Lawrence and Ottawa Rivers and their tributaries are incised into these clays, it is of interest to determine their resistance to fluvial erosion and the fluvial erosion mechanisms occurring. In Eastern Canada, marine clay deposits can be sensitive (defined as the ratio of the undistributed to the remoulded shear strength), which describes their loss of strength when disturbed, for example by bank failure due to fluvial erosion, which can induce large retrogressive landslides (Evans and Brooks, 1993; Lévy et al., 2012). The fluvial erosion of estuarine clays and their scouring near hydraulic structures has been well studied. However, few erosion studies have been made on well cemented clays, such as the ones found in the river systems of Quebec and Eastern Ontario (Mitchell and Klugman, 1979), although the impact of regional and compositional variations on the undrained shear strength has been obtained through geotechnical testing (e.g., Ewane et al., 2020; Leroueil et al., 1991; Liu et al., 2021). No relationships are currently defined to predict the erosion resistance behaviour of cohesive sediments (Briaud et al., 2017; Van Rijn, 2020); field practitioners either need to perform site specific erosion testing to obtain values for the critical shear strength of clays or design erosion mitigation measures with a high factor of safety.

The objective of this research was to study the fluvial erosion behaviour of undisturbed cohesive sediments (clays) found in the fluvial system of the St-Lawrence and the Ottawa River valleys. The goal was to compare the geotechnical properties of clays from a wide range of depositional environments as well as to study and define key parameters controlling their fluvial erosional behavior.

A sampling methodology was developed to collect samples, obtained from six different deposits lying within the St. Lawrence and Ottawa River valleys, using a method that minimally disturbs the sample in order to test both the geotechnical properties and the fluvial erosion behaviour of the material in as close to *in-situ* condition as possible. The material properties of the clays will be determined using standard geotechnical tests. The fluvial erosion will be assessed under unidirectional flow in a straight open channel laboratory flume under incremental increases of bed shear stress, during which the critical shear strength, mass erosion behavior, surface roughness (using an optical sensor) and erosion rate are observed. The bed shear stress will be estimated using the bed shear stress equation and a method of direct measurement in real-time is developed and tested.

2 Literature Review

2.1 Geological history

During periods of glaciation ice sheets extended far south in North America. Extended stadials (glaciations) followed by interstadials have shaped the surface of the Northern Hemisphere for 3Mya depositing sediments in valleys and exposing the bedrock at higher elevations. In the St-Lawrence Lowlands, exposed surface sediments were deposited during three glaciations during the Wisconsin dating from 191kya to the most recent episode that ended 11kya (Lamothe, 1989). In the St-Lawrence Lowlands, the deposition history followed similar sequences during stadials (glaciations) and interstadials (interglaciations); glaciolacustrine sediments were deposited during the advance and the retreat of the Laurentide Ice Sheet, when the outlet of the St-Lawrence River was blocked by an ice lobe downstream of Quebec City, glaciomarine and marine sediments were deposited during the retreat of the Laurentide Ice Sheet as the sea transgressed into the Lowlands as the crust had settled under the weight of the ice and, finally, lacustrine sediments were deposited as the crust rebounded and the sea retreated. At the end of the last glaciation, glaciolacustrine sediments deposited at the bottom glacial of Lake Candona (also designated as glacial Lake St-Lawrence by Rodrigues, 1992; 1994) from 12.1 – 11.1kya (Dubois Verret, 2015; Parent and Ochietti, 2002; Tremblay, 2008), while marine sediments deposited as the Champlain Sea flooded the St-Lawrence Lowlands from 12.0 – 9.4kya (Lamarche, 2006; Tremblay, 2008) and then lacustrine sediments deposited at the bottom of Lake Lampsilis from 9.8 – 9.0kya (Lamontagne et al., 2000; Ochietti, 2004; Parent & Occhietti, 1988; Tremblay, 2008). The layers of finer sediments glaciolacustrine, glaciomarine, marine and lacustrine sediments are separated by glacial sediments such as tills, deposited during the stadials, as well as fluvial and organic sediments, deposited during the warmer interstadials. Regional variations in the deposition history and characteristics of the fine sediments studied in this research are discussed with the site descriptions in section 3.1.

2.2 Incipient motion of cohesive soils

Geomorphologists as well as engineers in the field of sediment transport are well aware of the mechanisms of erosion of non-cohesive alluvial sediments as there exists an extensive literature on the subject as well as prediction methods most often based on a couple of factors to describe erosive force and resistance to erosion. This is not the case for the mechanisms of erosion of cohesive sediments and more particularly for consolidated cohesive deposits found in river environments where a complex set of factors comes into play.

However, certain underlying principles have proven to be generally true for both types of sediments. Assumptions made by Shields (1936), who presented groundwork for incipient motion of non-cohesive sediments by observing the shear stress acting at the bottom of the boundary layer τ_b on sand particles of various size, about a critical erosion threshold, the critical shear stress τ_{cr}, under which no erosion occurs and above which general continuous erosion occurs still holds true for cohesive sediments (Briaud et al., 2017; Partheniades, 1965; Van Rijn, 2020). In the same decade, other work on incipient motion by geomorphologists, such as the thesis presented by Hjulström (1935), based the study of incipient motion on flow velocity, which is easier to understand and easily applicable, but is limited as it is not a unique and standard characteristic like the boundary shear stress. Both concepts, of boundary shear stress and flow velocity, are still commonly used in the study of incipient motion of all types of sediments including cohesive sediments.

Shields (1936) also made important contributions by defining two non-dimensional parameters based on the physical properties of cohesionless sediments: dimensionless shear stress τ^* and the boundary Reynolds' number Re_*. The non-dimensional shear stress is based on a balance of forces acting on cohesionless particles that erode when the moment due to drag and lift is larger than the moment due to gravity at the point of contact between particles. The non-dimensional shear stress is defined as:

$$\tau^{*} = \frac{\tau}{g(S_G - 1)\rho d_{50}} \tag{2.1}$$

Where τ is the shear stress (Pa) acting on the grains and $g(S_G - 1)\rho d_{50}$ is the submerged weight of the particles times the median height of the particles d_{50} (m). In a fluvial environment, the shear stress in uniform and non-uniform flow is defined based on the principles of energy and momentum conservations and defined as:

$$\tau = \gamma R S_f \tag{2.2}$$

where γ is the unit weight of water, R is the hydraulic radius above the sample and S_f is the energy slope:

$$S_f = \frac{H_1 - H_2}{dx} = \frac{E_1 - E_2}{dx} + S_0 \tag{2.3}$$

where *H* is the total head (m), *E* is the specific energy (m), *dx* is the distance between the two readings along the flume (m) and S_0 is the bed slope.

Shields (1936) found a dependency between the dimensionless shear stress τ^{*} and the boundary Reynolds' number, or roughness Reynolds number, defined as:

$$Re_{*} = \frac{U_{*} d_{50}}{\nu} \tag{2.4}$$

where U_{*} is the shear, or friction, velocity (m/s), ν is the kinematic velocity of the fluid (m^2/s) and d_{50} is the mean diameter of the grains.

An important assumption in Shields' definition of the boundary Reynolds number is that grain size is the dominating source of roughness present at the solid-fluid interface (Shields, 1936). Shields noted that bedforms have an impact on incipient motion, but it was only proven and quantified in later work (e.g., Buffington and Montgomery, 1997; Miller et al., 1977). Later contributions have also defined two type of initiation of motion in cohesionless sediments: a critical initiation of motion and a critical initiation of suspension (Van Rijn, 2020). Work on the incipient motion of cohesionless sediments have been compiled over the years and Shields' diagram has been revised to account for initiation of bed forms, which creates an envelope for critical shear stress instead of a definite threshold condition (Lavelle and Mofjeld, 1987; Miller et al., 1977 on coarser sediments; Van Rijn, 2020 on laminar Re*). Additionally, this allowed accounting for the stochastic nature of incipient motion due to the occurrence of instantaneous changes on the resultant forces acting on bed particles and as the probability of a local shear stresses overcoming the resisting forces in a local area of the bed increases with a general increase in flow forces (Grass, 1970; Vanoni, 1964).

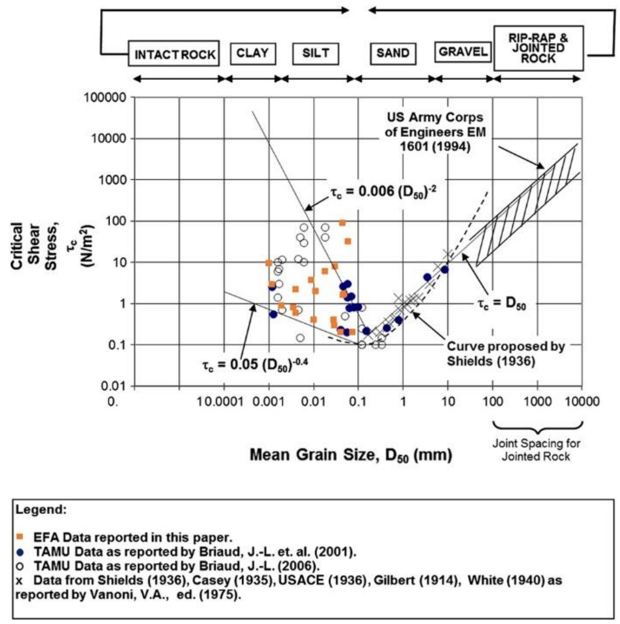

Figure 2-1. Revised Shields' diagram (1936) based on Erosion Flume Apparatus (EFA) tests results for fine grained soils (Briaud et al., 2017; Briaud et al., 2006; Briaud et al., 2001) and other studies on coarse grained soils (reported by Vanoni, 1975). From Briaud et al. (2017).

Cohesive sediments have a greater resistance to erosion than non-cohesive sediments for a given particle size (Bernhardt, 2009; Partheniades, 1965; Van Rijn, 2020). Silts are the smallest cohesionless particles and at the center of the silt size range of 0.01mm, they erode at a critical shear stress of 0.04Pa (Briaud et al., 2017; Shields 1936). Beyond a size of 2mm, the dimensionless critical shear stress is a constant, $\tau_{cr}^{*} = 0.006 = \tau_{cr} / (\gamma_s - \gamma) d_{50}$, which means that critical shear stress of larger alluvial material is only a function of particle size and density of the sediment (with a usual range of $S_g = [2.4, 2.65]$). Cohesive fine grain sediments, that is those smaller than 2μm have been found to erode at bed shear stresses between 0.15-20Pa (e.g., Briaud et al., 2017; Gaskin et al., 2003; Kamphuis et al., 1990; Shafii et al., 2016), shear stresses that would erode alluvial particles of 1.5mm to 212mm. An overview of the critical shear stress of different material, alluvial and cohesive, is presented below in Figure 2-1. Revised Shields' diagram (1936) based on Erosion Flume Apparatus (EFA) tests results for fine grained soils (Briaud et al., 2017; Briaud et al., 2006; Briaud et al., 2001) and other studies on coarse grained soils (reported by Vanoni, 1975).. Understanding the key characteristics controlling the erosion mechanisms of cohesive sediments is important as erosion of clay banks is not uncommon and not well understood. A review of the current literature indicates observed trends in erosion resistance as a function of a combination of soil properties, fluid properties and the ratio of shear stress to critical shear stress.

2.2.1 Erosion mechanisms

In comparison to cohesionless sediments, the nature of the cohesion and bonding of particles in cohesive sediments results in different erosion modes. The failure mode occurring during erosion depends on the applied shear stress acting on the surface of the sediments, on the general shear strength of the cohesive sediments as well as on the presence of local weaker planes close to or at the fluid-soil interface. In the study of both soft and firm clays, four different erosion modes are identified: particle erosion, floc erosion, surface erosion and mass erosion. The erosion mechanism occurring depends on the properties of the cohesive material, and, therefore, a critical shear stress can be identified independent of the erosion mechanism. Previous research identified critical shear stress occurring for all erosion mechanisms, although surface erosion and mass erosion are the dominant mechanisms.

At lower applied shear stresses to shear strength ratio, particle erosion, as defined by Mostafa et al. (2008), is the result of plucking and lifting of individual grains from the surface of cohesive sediments. Particle erosion occurs at a slow rate as the plucking happens in a random manner and is dependent on pressure fluxes, due to turbulent fluctuations, occurring at localized regions on the surface of the samples (Raudkivi, 1990).As particles disperse (cloudy water) into the eroding fluid, it can be observed through the use of a collecting siphon placed downstream from the eroding sample (Mostafa et al., 2008). In a similar manner, in the study of estuarine clays or muds, characterized by low density, low consolidation and high moisture contents, floc erosion is observed at low shear stresses (Winterwerp et al., 2012), in which involves loosely connected particles as well as flocs are removed from the sediment surface by turbulent vortices.

When the ratio of applied shear stresses to shear strength increases, surface erosion starts to occur. Several layers start to break off/detach from the sediment’s main skeleton as a whole (Winterwerp et al., 2012). At this point, the shear stresses and pressure fluxes acting at the surface of the sediments are large enough to detach larger particles-flocs from the sediments core; almost as if they are being peeled off the surface. Additionally, surface erosion is described as the onset of pit and streak marks as a generalized phenomenon across the surface as evidence of material being eroded (Kamphuis, 1983; Smeardon and Beasley, 1959).

Lastly, at higher shear stresses, general failure starts to occur below the surface of the sediment in a process called mass erosion (Mostafa et al., 2008; Winterwerp et al., 2012). It occurs when the applied shear stress at the surface of the soil is greater than the undrained shear strength of an embedded plane resulting in the removal of all material above it. In other words, this shear failure mode occurs at a larger scale and along deeper planes of weaknesses resulting in the erosion of solid blocks. Mostafa et al. (2008) defined mass erosion as the general erosion of blocks of 2-5mm diameter, but larger eroded blocks have also been observed (Gaskin et al. 2003).

In unsaturated soils, during sudden immersion, certain cohesive soils are more likely to undergo slaking, the fragmentation of unconfined aggregates, which can influence the type and threshold of the different erosion modes (Moriwaki and Mitchell, 1977). Slaking is often accompanied by dispersion, a separation of the aggregates into individual particles (Lim, 2006). Shaikh et al. (1988) attributed slaking as the primary cause of an increase in erosion rate for unsaturated non-dispersive soils. Le Bisonnais (1996) identified several mechanisms that might contribute to slaking that include, from the most to the least severe, (1) expansion of entrapped air during re-wetting, (2) differential swelling and shrinkage, (3) physio-chemical dispersion and (4) raindrop impact. These mechanisms are likely to occur in cohesive soils located at the surface of river banks, and during dry periods in the river bed, as they are exposed to sun, rain and wind, and as they desiccate when subject to wet-dry cycles (Gaskin, 2003; Lefebvre, 1985).

2.2.2 Erosion testing methods

Several testing methods have been developed since the 1930's to obtain the critical shear stress and the erosion rates of cohesive sediments. A non-exhaustive list of different laboratory and field erosion mechanisms is provided below.

Table 2-1. Existing erosion testing methods

Device	Simulated environment	Author(s)
SED Flume	Open channel flow	McNeil et al. (1996)
ASSET Flume	Open channel flow	Roberts et al. (2003)

Flume	Open channel flow	Gaskin et al. (2003)
ASETS Flume	Open channel flow	Lee et al. (2004)
ESTD Flume	Open channel flow	Shan et al. (2015)
SEAWOLF Flume	Oscillatory and linear flow	Jepsen et al. (2002)
EFA	Conduit flow erosion	Briaud et al. (2001)
SERF	Conduit flow erosion	Trammell (2004)
SETEG	Conduit flow erosion	Beckers et al. (2020)
HET	Seepage process	Wan and Fell (2004)
JET	Erosion under a jet	Hanson and Cook (2004)
CSM	Erosion under a jet	Tohurst et al. (2006)
RCT	Rotating flow	Moore and Masch (1962), Chapuis and Gatien (1986)
CCFED	Shallow circular Couette flow	Moore and Masch (1961)

To test the erosion of cohesive sediments, a cohesive sample is cored and placed in a flume subjected to incrementally increasing near-bed shear stress by changing the flow conditions. The surface of the sample is positioned flush with the floor of the flume, to represent the *in-situ* condition in a river bed, lifting mechanisms were designed to either lift the surface of the samples to the elevation of the flume floor as they erode (e.g., Lee et al., 2004) or lift them after a layer has eroded (e.g. Briaud et al., 2001). A complication present in all the flume devices is the transition from a smooth surface to the sediment's (rougher) surface, which might affect the erosion areas; there is a disagreement on the significance of its impact (Roberts et al., 2003; Tolhurst et al., 2006). Sophistication of flume devices for the measurement of erosion have improved over time. Examples of improvements made are described below.

A few methods have been developed to mimic the scour process occurring in river flows. Earlier work include the shallow circular Couette flow (CCFED), a simple apparatus designed to measure the erosion rate of a cylindrical specimen (Moore and Masch, 1961). The clay specimen is placed on a stationary mount attached to a torsion wire in drum filled with an eroding fluid. As the outer drum rotates, shear stress is measured by the angular displacement of the torsion wire and the erosion rate is determined by measuring the loss of mass over the testing time interval (Shan et al., 2015). Moore and Masch (1962) also developed an erosion apparatus called the rotating cylinder test (RCT) machine in which the sample rotates in a stationary tank. Chapuis and Gatien (1986) later reworked the RCT design and allowed for testing of both undisturbed and remoulded samples.

Since the 1990's, many flume apparatus have been designed using piston-type like devices (Crowley, 2014), or lifting apparatus (Gaskin et al. 2003) to lift the samples as they erode. Most of these flume apparatuses are rectangular and allow for the flow to fully develop over a short length (Trammel, 2004). First, the sediment erosion at depth flume (SEDFlume) was developed to measure the transport of sediments and contaminants during large flood events and allows for the correlation of critical shear stress and erosion rate to the sediment bulk properties as a function of depth (McNeil et al., 1996). A sample placed in coring test container, measuring 10x15cm and 1m in depth, is lifted to be flush with the false floor of a straight-channel flume continuously by the operator as it erodes (McNeil et al., 1996). Larger sample sizes (0.3m x 0.45 m) have been used to assess the effect of internal clay structure on erosion (Gaskin et al. 2003).

Likewise, the erosion function apparatus (EFA) was designed to provide a standard and efficient way to measure scour rate around bridge piers and consists of a rectangular close conduit flume that can produce flow velocities ranging from 0.1 to 6.0m/s (Briaud et al., 2001). Samples taken in Shelby tubes are inserted into the flume to be flush with the false floor and are then projected (1mm at a time) into the flow for an hour or until the 1mm has eroded (Trammell, 2004). The ex-situ erosion-testing device (ESTD) is very similar to the EFA but has a moving upper wall which allows for deeper flow (Wibowo and Robbins, 2018). The shear stress measurement of the EFA and the SED flumes is based on average flow velocity measurements. Beckers et al. (2020) designed another closed conduit flume allowing for higher applied bed shear stresses, the erosion flume to determine the depth-dependent erosion stability of aquatic sediments (SETEG), that has a Laser Doppler Velocitymeter (LDV) and photogrammetric measurements to measure the relationship between near-bed shear stress and surface roughness (Beckers et al., 2020).

The adjustable shear stress erosion and transport flume (ASSET) is an improved SEDFlume as several modifications were implemented by Roberts et al. (2003) to quantify the erosion modes occurring at different depths of erosion. Roberts et al. (2003) enlarged the flume to minimize wall disturbances and installed three traps in the bed of the flume downstream from the eroding specimen to qualify and quantify the bedload. The automated sediment erosion testing system (ASETS) was developed around the same time as the ASSET and uses real-time black-lighted imaging to maintain the eroding specimen flush with flume bottom and to calculate the erosion rate in relation to the depth of scour (Lee et al., 2004).

The sediment erosion rate flume (SERF) is also a piston-type erosion device and was developed to measure directly and continuously the erosion rate and applied shear stress over eroding specimen (Crowley et al., 2014). The device is more complex and uses several sensors and pressure transducers to calibrate the flume shear stress measurements. The most important distinguishing designs of the SERF are a mounted disc-spring setup connected to a Servo magnet and a Hall sensor to measure shear stress for a given roughness, an ultrasonic depth and laser system connected to a stepper motor to keep the samples flush with the floor of the flume and a temperature control system to protect the sensors and to observe constant eroding fluid properties during the erosion tests (Crowley et al., 2014).

Furthermore, the ex-situ erosion testing device (ESTD) was designed to mimic more accurately open channel flow conditions by including a rotating belt in a closed conduit flume in order to produce a log law velocity profile over the eroding specimen (Shan et al., 2015). The samples are mounted on direct force gage setup which includes two horizontally mounted magnets, a Servo solenoid and a Hall sensor to measure shear force and counteract the force.

Other researchers have looked into the erosion modes of cohesive sediments in marine environments, scour caused by free overfalls and internal piping caused by seepage. In 2002, Jepsen et al. modified the SEDFlume to cause sediment erosion by wave oscillations and linear flow (SEAWOLF) to mimic a wave-dominated environment and allowed for the superimposition of oscillatory flow upon a unidirectional current. Oscillatory flow is generated by pistons at the end of the flume (Jepsen et al., 2002).

Additionally, the submerged jet erosion test (JET) mimics the scouring process that occurs at a headcut or a free overfall (Wahl, 2010). A nozzle is installed on top of a submerged specimen and attacks the soil surface while the scouring rate is measured using a point gage passing through the nozzle (Hanson and Cook, 2004). The latest addition to jet erosion testing is the cohesive strength meter (CSM) which allows for the measurement of spatial and temporal changes in the erosion threshold of intertidal muds (Tohurst et al., 2016).

Lastly, the hole erosion test (HET) mimics a seepage process, or internal erosion occurring due to surface erosion, as water flow enlarges a pinhole initially bored in the middle of a clay specimen (Wan and Fell, 2004). The specimen is placed in a confining tube and connected to two water tanks with differential water levels which are used to measure the shear stress. The flow velocity is increased steadily until entrainment is observed, the eroded soil is collected and measured and the hole diameter measured to determine erosion rates.

Each method mimics specific flow conditions and few direct comparison studies exist to compare different erosion apparatus. In recent research, a direct comparison of the Jet Erosion Tests (JET) and an Erosion Flume Apparatus (EFA) yielded consistent results for the soil types tested (a range of fine and coarse grained soils) (Wibowo and Robbins, 2018; Al-Madhhachi et al., 2013). However, direct comparison of the Hole Erosion Test (HET) and the Jet Erosion Test (JET) yielded very different quantitative results (Regazzoni et al., 2008).

2.2.3 Strength of cohesive sediments

The shear strength of cohesive sediments is governed by cohesion forces at the microscopic level, interparticle forces created by chemical and electrochemical bonds, as well as by their structure at the macroscopic scale which can be affected by many factors such as biological activity, consolidation and environmental weathering.

Cohesive sediments are defined as containing a fraction of at least 10% clay particles (Hosny, 1995), which are particles of <0.002mm diameter (USCS, 2012; USDA, 2012). According to the USDA soil classification system (2012), clays are defined as containing at least 40% clay particles while containing less than 40% silts and 45% sands.

During the formation of clay deposits, the type of minerals found in the clay as well as the salinity of the depositional environment affect the alignment of the skeleton of the clay, the type of interparticle bonds (e.g., Van der Wall forces, cationic bonds, cation exchange) and the presence of chemical cementation (Mostafa et al., 2008). In settling of clays from suspensions, flocculation is the main source of strength. According to the electrical double-layer theory (Mitchell, 1993), in a colloidal system (a system with many particle sizes), there exists a region under the surface of the particles, called the double layer, where ions are of the same charge, positive or negative, and are repulsed. The double layer is created when water particles are absorbed and adsorbed by clay particles. As it is mostly negatively charge, the smaller it is the greater the attraction of particles in a solution and the greater the cohesion. Osipov (1975) describes three types of contact in a clay: (1) a coagulated contact: found in quick clays or clays with a high moisture content, with very weak valent and molecular bonds; (2) an atomic contact: in drier consolidated clays, with stronger ion-electrostatic bonds; (3) a phase contact: due to the plastic deformation of clays, found in highly consolidated clays. By adding water to a clay with atomic bonds, the contact between clay particles changes to a coagulated contact, or an increase in the size of the double layer, which induces a loss of shear strength (Osipov, 1975).

The ability of clay minerals to adsorb water makes clay malleable. The plasticity of a clay is governed by its water content, but also by its clay content and the nature of its clay minerals. The clay fraction in a cohesive sediment affects its plasticity in a linear manner (Seed et al., 1964; Skempton, 1953), while different clay minerals carry a wide array of adsorption abilities, which influences its plasticity in relation to its water content. Smectites have the greatest adsorption ability of all clay-like minerals, and are found in more plastic clays, whereas illite and chlorite minerals, which are the most common, retain less water on their surface and decrease the plasticity of clays (Wagner, 2013).

The interactions of clay mineral surfaces and pore water, as well as its deposition history can cause a clay to be sensitive. Sensitivity is the ratio of interparticle cohesion in the undisturbed state to that in its remoulded state. The strength of undisturbed samples is substantially higher than their strength in the remoulded state (Prince and Strauß, 2006). The undisturbed strength of Champlain Sea clays, found in the St-Lawrence and the Ottawa River valleys, is governed by natural cementation, unlike other quick clays, for which leaching of salt after deposition is the primary cause of sensitivity (Mitchell and Klugman, 1979). Cementation occurs when the least resistant primary minerals in a clay are weathered and are rendered soluble creating a bonding agent between the clay particles (Torrance, 1975). By reviewing numerous retrogressive landslide events, Mitchell and Klugman (1979) concluded that the cementation in the Champlain Sea clays varies regionally, which leads to regional behavioural and compositional characteristics. The timing of the cementation process during the consolidation of the clays also influences its subsequent undisturbed strength; when cementation happens soon after deposition the soil structure resists the subsequent overburden pressure and does not consolidate as much as if cementation occurs at a later stage (Torrance, 1975).

Previous studies have mostly focused on the influence of individual macroscopic properties on the fluvial erosion behavior of clays. However, the accurate prediction of fluvial erosion of cohesive sediment depends on a large number of governing properties (Lim, 2006) and such extended analyses are costly (Trammell, 2004). At the macroscopic scale, many environmental factors might affect the shear strength of cohesive sediments. The critical shear strength of clays for entrainment (critical shear stress) diverges from the shear strength defined in geotechnical settings as it represents the resistance to shear stress at the surface of a soil in comparison to the resistance to shearing under compression or tension in a bulk manner (e.g. loading of a soil). The critical shear stress of clays can vary depending on their degree of consolidation, on stratification, grain size distribution outside the cohesive range, void ratio and moisture content. In a river environment, influencing factors also include biological activity found in a river ecosystem, mixing of sediments during deposition as well as environmental weathering.

A summary of the properties influencing the cohesion and the critical shear stress of cohesive sediments is presented below in Table 2-2. The list of properties is based on a review of the current literature and based on the works of Shan et al. (2015), Wagner (2013), Mostafa et al. (2008), Raudkivi (1990), Lefebvre et al. (1985).

Table 2-2. Soil properties controlling the critical shear stress of cohesive sediments

Chemical and electrochemical	▪ Dominant ions of the clay, NaCl adsorption ratio, cation exchange capacity ▪ Type of clay minerals ▪ Clay size ▪ Chemical cementation
Physical	▪ Temperature ▪ Swelling ▪ Plasticity, plastic limit and liquid limit ▪ Clay content, fine grains content, grain size distribution ▪ Void ratio water content, saturation, consolidation, stratification
Biological	▪ Organic matter content and nature, reactivity with clay-water system, ▪ Presence of vegetation (e.g., roots) ▪ Burrowing of animals

In recent developments, the extensive review done by Briaud et al. (2017) has made possible multivariable linear regressions. The regression curves developed by Shafii et al. (2016) and Briaud et al. (2017) for fine grained sediments are defined in the table below. The experiments and their significance are discussed in Section 2.2.4.

Additionally, Mostafa et al. (2008) performed a dimensional analysis relating the dimensionless shear stress to the following independent parameters:

$$\tau^* = f\left(LI, S_G, \Delta S, \hat{I}_b\right) \qquad 2.5$$

where ΔS is defined as the salinity difference between the eroding water and the clay pore water to represent the type of anions present in the soil and $\hat{I}_b$ represents the near-bed turbulence intensity due to the flow of the eroding fluid. Mostafa et al. (2008) found a dependency between the non-dimensional shear stress and a non-dimensional parameter χ that relates to the liquidity index and the excess moist bulk density of the soil, $S_G - 1$, which is defined as:

$$\chi = \frac{LI}{S_G - 1} \qquad 2.6$$

Table 2-3. Model expression used to define erosion threshold of fine-grained sediments

Model expression		Number of tests	R^2
Briaud et al. (2017)			
$\tau_c = 3.347 \times 10^{-10} \times PI^{-1.855} \times {d_{50}}^{-1.05} \times m^{6.707}$	2.7	17	0.72
$\tau_c = 2.28 \times 10^{-15} \times PI^{-1.732} \times m^{-3.106} \times PF^{6.412}$	2.8	55	0.6
$\tau_c = 1.354 \times 10^{-7} \times PL^{0.666} \times {d_{50}}^{-0.189} \times m^{4.046}$	2.9	17	0.5
Shafii et al. (2016)			
$\tau_c = 0.005 \times PI^{0.44} \times {S_u}^{0.83} \times m^{1.03} \times {d_{50}}^{0.29}$	2.10	Unknown fraction of 182 tests*	0.517
Mostafa et al. (2008)			
$\tau_* = -107.56\chi + 79.59$	2.11	4	0.8704

PI: plasticity index (%), PL: plastic limit (%), d_{50}: median grain size (mm), PF: percent fine or particles passing through sieve no 200 (%), S_u: undisturbed shear strength obtained in the vane shear test (kPa), m: moisture content (%), * Exact number of tests performed on fine grained soils is not mentioned in Shafii et al. (2016)'s paper.

2.2.4 Erodibility of cohesive soils

To understand the erosion behaviour of cohesive sediments once the bed shear stress is greater than the critical shear stress threshold, also defined as the excess shear stress, the concept of erodibility was used by researchers to quantify scour, mostly occurring around bridge piers. Erodibility is defined as the relationship between the erosion rate $\dot{Z}$ and the shear stress τ applied at the water-soil interface:

$$\dot{Z} = f(\tau) \tag{2.12}$$

Briaud et al. (2001) also reported scour rates (mm/h), or erosion rates, as:

$$\dot{Z} = \frac{dz}{dt} = \frac{dW_{loss}}{dt \cdot A_s} \times \frac{1}{\gamma_b} \tag{2.13}$$

where z is defined as the scour depth (mm) over time t (h), W_{loss} is defined as the weight loss (kN) occurring on a bed, A_s is the surface area (m^2) and γ_b is the bulk unit weight (kN/m^3) of the soil.

Different methods have been used to define and correlate the erosion rate to the excess shear stress in order to define erodibility categories and create design charts. Methods used to produce regression curves to define erosion rates such as the ones performed by Wan and Fell (2004a, b) and Briaud et al. (2001) assumed that the erosion rate and the excess shear stress are linearly dependent. Briaud et al. (2001) added a tangent slope to define critical shear stress which diverged from the assumptions made by previous methods that assume a linear relationship below critical shear stress (Lim, 2006). Briaud et al. (2017) defined arbitrarily the critical shear stress as that occurring when the soil erodes at a rate of 0.1mm/hr.

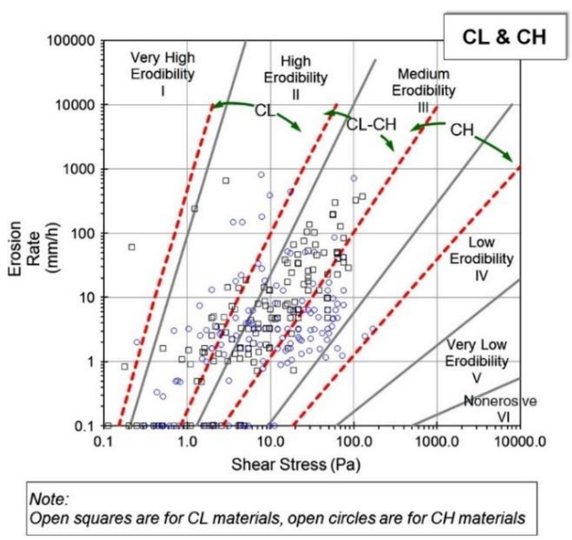

Figure 2-2. Erosion charts for clays (From Briaud et al., 2017)

Recent work from Briaud et al. (2017) and Shafii et al. (2016), based on a compilation of the results of 84 and 182 erosion tests performed at in an EFA flume apparatus at Texas A&M University and Texas Department of Transportation over the course of 25 years, have led to the development of erodibility charts and regression curves used to classify geomaterials. They provide a qualitative assessment of erosion properties during preliminary river studies. CL are defined as lean clays and CH are defined as heavy clays (USCS, 2012).

Table 2-4. Erosion categories and erosion thresholds (adapted from Briaud et al., 2017 et Anerson et al., 2012)

Erosion category	Degree of erodibility	Type of geomaterials	Critical shear stress (Pa)	Critical velocity (m/s)
I	Very high	Fine sand, non-plastic silt	0.1	0.1
II	High	Medium sand, low plasticity silt	0.2	0.2
III	Medium	Jointed rock (spacing < 30mm), fine gravel, coarse sand, high plasticity silt, low plasticity clay, all fissured clays	1.3	0.5
IV	Low	Jointed rock (30-150mm spacing), cobbles, coarse gravel, high plasticity clay	9.3	1.35
V	Very low	Jointed rock (150-1500mm spacing), riprap	62.0	3.5
VI	Non-erosive	Intact rock, jointed rock (spacing > 1500mm)	500	10

2.2.5 Erosion testing on undisturbed consolidated clays

Few studies have been done on undisturbed consolidated clays and those performed have mostly been on a limited number of samples except for the review of Briaud et al. (2017). As shown in Table 2-5 below, the geomaterials studied were from different locations and exhibited a wide range of properties. The type of test method also highly influenced the resistance to erosion of the different cohesive sediments tested as the observed critical shear stress of the samples tested in flume-like apparatus ranged between 0.1 and 20Pa, the ones tested in an RCT ranged between 2 - >10 while the ones tested a drill hole manner exhibited a resistance to erosion of an order of magnitude higher ranging from 100 to >450Pa.

Table 2-5. Results of erosion tests on undisturbed stiff clays (updated version of table presented in Gaskin et al., 2003)

Study	Geomaterial	Test method	Critical shear stress (Pa)
Laflen and Beasley (1960)	Five silty clays from the State of Missouri	Flume	0.5 -2.6
Rohan et al. (1980)	Two unweathered sensitive marine clays from Eastern Canada	Flume	7.5
Lefebvre et al. (1985, 1986)	Four unweathered brittle glaciomarine clays: 3 Champlain Sea clays and one Tyrell Sea clay	Drill hole	>350 - >450, 100 – 200

Chapuis (1986)	Two northern Quebec clays	RCT	4 - 9
Kamphuis et al. (1990)	One glaciolacustrine silty clay, three silty clays	Flume	0 – 2
Gaskin et al. (2003)	Six weathered Champlain Sea clays	Flume	6 – 20
Lim (2006)	Nine natural clays from Australia and the USA	RCT, HET and slaking test (SLT)	2 - >10
Mostafa et al. (2008)	Seven natural clays from the USA	Flume	1.6 – 2.7
Le Hir (2008)	Natural clay muds from Mont St-Michel, France	ASSET	0.25 – 2.0
Mobley et al. (2009)	One stiff clay and one hard clay from Alabama	EFA	0.8
Briaud et al. (2017)	79 natural cohesive fine sediments from the USA	EFA	0.1 - 20

The main conclusions from these tests, and previous studies on remoulded samples, can be summarized as:

The critical shear stress is unique to each fluid-soil system (e.g., Briaud et al., 2017; based on a review made Lim, 2006). For example, the flow conditions in a tidal environment and in a fluvial environment will exert different shear stresses and pressure gradients on a solid interface.

The critical shear strength of soft to firm cohesive muds increases with the following changes in the following parameters:

Table 2-6. Geotechnical parameters increasing the critical shear stress of soft to firm cohesive sediments

	Authors (e.g.)
Soil properties	
Increase in dry density	Krone (1999), Wan and Fell (2004b)
Increase in water content	Christensen and Das (1973), Hanson and Robinson (1993), Wan and Fell (2004b)
Increase in clay content, percentage of fine grains	Utley and Wynn (2008), Wan and Fell (2004b)
Decrease in the activity of clay minerals	Arulanandan (1975)
Decrease in slaking	Lim (2006), Shaik et al. (1988)
Increase in plasticity index	Briaud et al. (2017), Partheniades (2009)
Increase in undrained shear strength	Shaik et al. (1988a), Wan and Fell (2004b)
Fluid properties	
Decrease in temperature	Ariathurai and Arulanandan (1978), Christensen and Das (1973)
Decrease in salinity	Reddi et al. (2000)

The critical shear stress of well consolidated cohesive sediments increases with an increase in the following parameters:

Table 2-7. Geotechnical parameters increasing the critical shear stress of undisturbed consolidated cohesive sediments

	Authors (e.g.)
Soil properties	
Increase in bulk density	Mobley (2009), Mostafa et al. (2008), Laflen and Beasley (1960)
Increase in clay content, percentage of fine grains	Briaud et al. (2017), Kamphuis and Hall (1990), Le Hir (2008), Mostafa et al. (2008)
Increase in field condition moisture content	Briaud et al. (2017), Mostafa et al. (2008)
Increase in liquid limit and plastic limit	Briaud et al. (2017)
Increase in plasticity index	Shafii et al. (2016)

The soils with a smaller critical shear stress have a greater erosion rate (see Figure 2-2).

Undisturbed cohesive sediments erode far less than artificially made, remoulded and recompacted, cohesive sediments (Chapuis, 1983; Lefebvre, 1986).

The erosion initiates at the zones of weaknesses. These include fissures, silty or sand pockets and other planes of weaknesses (Gaskin et al., 2003; Kamphuis et al., 1990).

The present recommendations for the design of erosion mitigation measures still include site specific erosion testing (Briaud et al., 2017) as the erosion behavior of cohesive sediments is dependent on unique combinations of soil properties and flow conditions (Briaud et al., 2001; Lim, 2006).

2.3 Sampling of cohesive soils

In the geotechnical field, several methods have been developed to sample clay specimens and offer a wide range of sample sizes, efficiency and sample quality. These methods involve either coring the sample, using a tube, or carving the sample, obtaining blocks. Coring is a simpler method than carving as the sampling can be done without digging a trench but it is more likely to decrease the samples' quality as it disturbs the structure of the clay as well as it induces an uneven propagation of pore water pressure where the protrusion and the undercutting occurred (La Rochelle et al., 1981). To obtain samples with minimal disturbance, two methods were developed by geotechnical researchers in the province of Quebec: the Sherbrooke sampler (Lefebvre and Poulin, 1979), a block sampler, and the Laval sampler (La Rochelle et al., 1981), a tube sampler. Both sampling methods allow for the sampling of large specimens at great depths. The Sherbrooke sampler consists of a rotating diaphragm that uses blades and a water jet to carve out large clay blocks (30cm Ø or larger), while the Laval sampler uses a large rotating coring tube (20cm Ø) that includes an inner tube with no inside clearance and sharpened edges to minimize disturbances and an outer tube that is used to remove the surrounding soil. Both methods include removal of overlaying soil and are usually used in the vicinity of a road since they require a frame and a power output to penetrate the ground.

The samplers are used by field practitioners and researchers when high quality clay specimens are required (e.g., Amundsen et al., 2016, Karlsrud & Hernandez-Martinez, 2013; Nash et al., 1992). The Sherbrooke and Laval sampler are also used as a standard of quality in comparison to other sampling methods (e.g., Lunne et al., 2019; Pineda et al., 2016; Tanaka et al., 2001). Several studies conducted on clays found in Canada and in Norway have concluded that block sampling results in less disturbance to the clays than piston sampling (e.g., Holtz et al., 1986; Lunne et al., 2019; Tanaka et al., 2001;)

2.4 Roughness of clay beds

Surface roughness has a considerable effect on flow resistance and hence on bed shear stress. In the field of sediment transport, many definitions exist to describe surface roughness (Pokrajac et al., 2006; Smart et al., 2002) and several authors have studied and compared its effect on shear resistance in uniform flow (Smart et al., 2002) and in non-uniform flow conditions (Afzalimehr & Rennie, 2009; Afzalimehr & Anctil, 2000; Kironoto & Graf, 1994; Song & Graf, 1994).

The arrival of LIDAR and other depth sensing devices in the 1990's, that have led to the development of Digital Elevation Models (DEMs), allowed researchers to establish a relationship between geometric roughness and resistance to flow (Smart et al., 2002). Recent developments by Beckers et al. (2020) have shown that erosion on a silt core is a self reinforcing process as it propagates and progresses in already affected areas. Hence, to understand the dynamic relationship between erosion of cohesive soils and near-bed shear stress there is a need to acquire high spatial-temporal resolution (Beckers et al., 2020; Tolhurst et al., 2006).

The different definitions of surface roughness result from a wide range of theoretical approaches for defining incipient motion. The conversion of surface roughness data into roughness or friction factor coefficients also varies with experimental approaches and results. Roughness and friction factors include the Nikuradse sand grain size or equivalent k_s (or d_{50}), the Darcy-Weisbach friction factor f_D, Manning's friction coefficient *n* and Chezy's friction coefficient *C*.

The effect of shear stress on a flow can be determined by observing the local variations in flow characteristics (i.e., velocity and pressure). In order to compare the findings of different studies, the shear velocity is used to create dimensional consistency as it scales the turbulence level in a flow to the fluid shear stress. The shear velocity can be estimated at a macroscopic scale – averaged over an area –or deduced by careful measurements of the flow's velocity profile at specific points, commonly done with Acoustic Doppler Velocitymeters (ADVs) or a Laser Doppler Velocitymeters (LDVs).

For steady flow, the shear velocity for prismatic rectangular channels can be defined as follows:

$$U^* = \sqrt{ghS} \qquad 2.14$$

where h is the mean depth of flow over the area and S is based on the bed slope S_0 in uniform flows and the friction slope S_f in non-uniform flows (Chow, 1959).

In uniform flow, the effect of the bed shear stress on flow results in a velocity profile that follows a logarithmic curve as hypothesized by Monin and Yaglon (1971) and confirmed by an many of experimental studies (Smart et al., 2002). The well-known log law is:

$$\frac{u}{U^*} = \frac{1}{\kappa} ln\left(\frac{z}{Z_0}\right) \qquad 2.15$$

where u is the streamwise velocity at an elevation z, κ is von Karman's constant and Z_0 is the height above the datum at which the velocity equals zero.

The depth average velocity U as presented by Kuelegan (1938) is found by integrating equation 2.15 over the depth of flow. Z_0 is located at the mean level of the bed which is at a distance R_v below the surface of water (Smart, 1999).

$$\frac{U}{U^*} = \frac{1}{\kappa}\left[\left(\frac{R_v}{R_v - Z_0}\right) ln\left(\frac{R_v}{Z_0}\right) - 1\right] \quad 2.16$$

In non-uniform flow, the effect of roughness on the pressure gradient at the boundary changes in accelerating and decelerating flow, and thus, form a velocity profile that deviates from the log law. In accelerating flows, roughness elements create a favourable pressure region at the boundary interface, while in decelerating flows they generate a greater adverse pressure region (Afzalimehr & Anctil, 2000). The boundary layer is divided into two regions: an inner region near the solid-fluid interface where the viscous sublayer lies and an outer region that merges into the outer flow. If the pressure gradients caused by non-uniformity in the inner region are negligible, the velocity profile resembles a log profile in the inner region and a parabolic profile in the outer region (Afzalimehr & Rennie, 2009). Therefore, the shear velocity tends to be smaller in non-uniform flows and is even smaller in accelerating flows (Song and Graf, 1994; Kironoto & Graf, 1995; Afzalimehr & Anctil, 2000). Several methods and definitions exist to plot and scale the velocity profile of non-uniform flows based on extended velocity profile measurements. Deriving the depth average velocity for non-uniform flows has not been attempted when the boundary between the inner and the outer regions varies based on discharge, slope and geometry (Afzalimehr & Rennie, 2009).

Additionally, the roughness layer in rough turbulent flows, in which roughness elements are protruding significantly from the viscous sublayer and affect the flow characteristics in the outer region, may cover the region usually covered by the log layer and the outer region (Pokrajac et al., 2006).

Greater knowledge on non-uniform and uncommon surfaces, such as the surface of clays, could help better our understanding of the turbulent and shear stress mechanisms at the boundary layer in sediment transport.

3 Methods

Due to the limited knowledge of the complex erosion processes of rivers in clay deposits and of their critical shear stresses, particularly for sensitive clays, a selection of deposits will be sampled and the fluvial erosion behaviour studied and assessed for any correlation with their geotechnical properties. The first step was to find sampling locations in the St. Lawrence and Ottawa River valleys providing samples from clay deposits having different properties to indicate the possible range of behaviours in the study area. A sampling method was developed to collect, transport and store the samples such that sample disturbance was minimized, so that the fluvial erosion tests would represent as closely as possible the *in-situ* conditions. To differentiate and compare the clays with previously studied clays, standard geotechnical testing was performed at Université de Sherbrooke. Lastly, samples from all sites were prepared for erosion testing and subjected to fluvial erosion in a straight channel flume. The samples were tested at *in-situ* moisture content and also after 48 hours of air drying.

3.1 Site selection for sampling of clays

After careful consideration and investigation of numerous sites across the regions of Montérégie, Bas-St-Laurent, Laurentides, Outaouais, Quebec City and the South Nation River basin, the following sites were selected for sampling. The sites had different geomorphologic history, resulting in the clay deposits at the banks and the bed of the tributaries presenting a wide range of geotechnical characteristics. Clay deposits were sampled at six sites, whose locations are shown on the map of Figure 3-1 and whose map coordinate are given in Table 3-1. The clay type and general characteristic is also summarized in Table 3-1.

Table 3-1. Selected study sites

Site	Tributary of	Coordinates	Type of deposit	Clay characteristics	Presence of fissures in-situ
1	Rivière de la Tortue	45°18'50"N, 73°33'30"W	Remoulded Champlain Sea clay	Firm heterogeneous clay	
2	Castor River	45°16'50"N, 75°16'01"W	Champlain Sea sediments	Stiff rhythmite silty clay	X
3	Rivière du Nord	45°49'41"N, 74°03'17"W	Champlain Sea sediments	Stiff rhythmite silty clay	X
4	Chelsea Creek, lower tributary	45°29'46"N, 75°47'07"W	Lacustrine or glaciolacustrine sediments	Stiff varves of clay and sand	
5	Chelsea Creek, upper tributary	45°30'02"N, 75°47'03"W	Champlain Sea clay	Firm rhythmite clay	X (at one sampling location)
6	Rivière St-Charles	46°50'03"N, 71°19'47"W	Champlain Sea sediments	Very stiff loam	

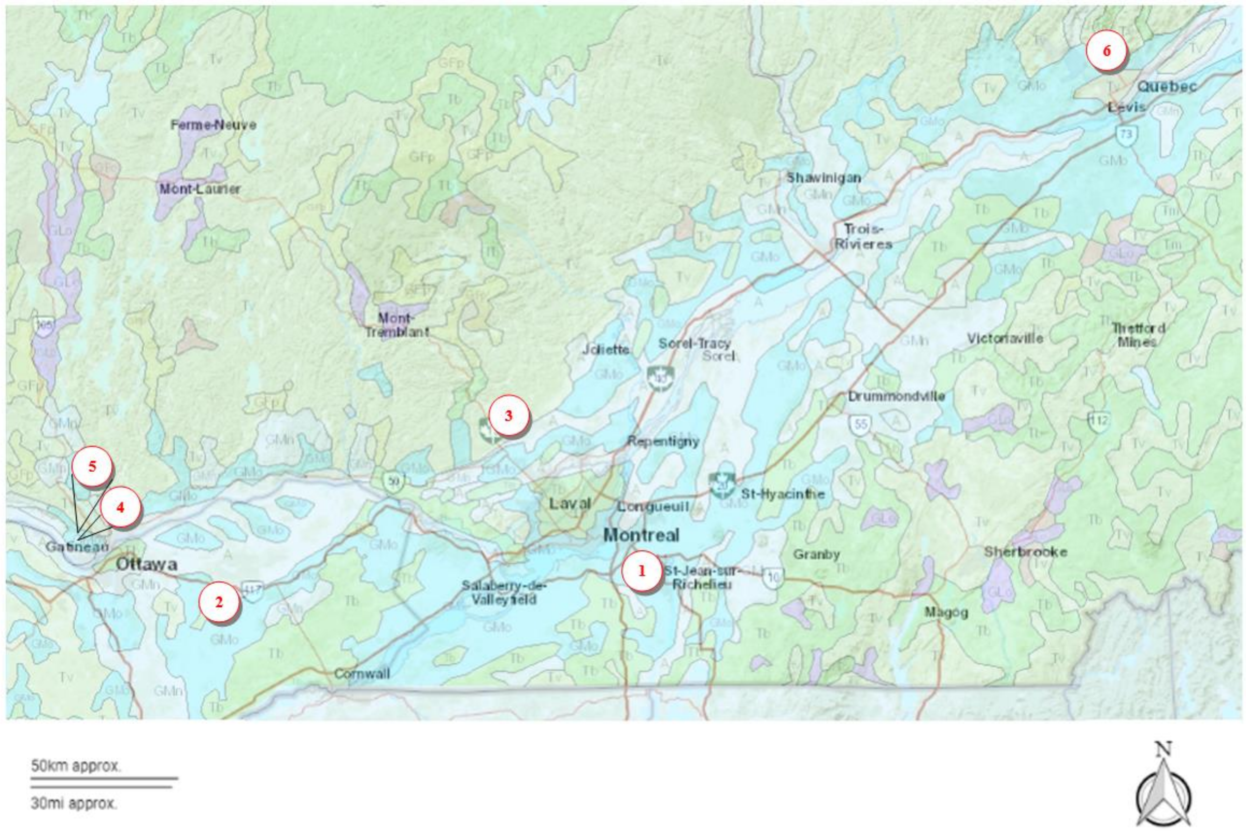

Figure 3-1. Location of study sites overlying the Surficial Geology Map of the St-Lawrence Lowlands with clay deposits in blue and alluvial deposits in beige (Geological Survey of Canada, 2014).

The process of site selection involved a literature review of the Quaternary geology of the St-Lawrence Lowlands, the use of surficial geology maps (Geological Survey of Canada, 2014) and invaluable help from the South Nation Conservation Authority, the city of Quebec, WSP and other individuals.

Tributaries were surveyed to identify clay deposits and the site selection that followed involved following considerations: the sites needed to be accessible by public roads or through private properties where permission of access was given, relatively low water levels to allow for safe sampling and access to the bed at with low depth of overlying water as samples were collected from below the water line of the river to ensure *in-situ* moisture content, safe access to the river reach, low river pollution as well as the absence of trees in the vicinity of potential sampling locations to avoid the presence of roots in the samples collected.

A detailed description of each of the six selected sites follows.

3.1.1 Site 1 – Rivière de la Tortue tributary

The Rivière de la Tortue is located on the South shore of Montreal, its source is upstream of St-Mathieu and it discharges into the St-Lawrence River at the municipal border between Delson and Candiac. The tributary studied has its headwaters North of St-Rémi and it flows into Rivière de la Tortue south of Delson. The tributary, formed of straight reaches with very few bends, runs through the flat base of a valley covered by farmland. Alluvial material, ranging in size from sand to gravel, forms a heterogenous cover on the bed and banks of the tributary. The alluvial material is thicker at the center of the bed and only a thin layer close to the banks. The location of the sampling site is in St-Mathieu south-west of the intersection of Chemin de la Petite Côte and Montée de la Petite Côte, as shown in Figure 3-2. The tributary is slightly incised into the surrounding strata with 2-3m high banks and it is 2-2.5m wide. The clay deposit is rarely exposed as it is overlain by a thick layer (1-2m) of organic matter. The presence of exposed clay banks and debris downstream suggests minor bank failures occurred upstream and downstream of the sampling locations, see Figure 3-4. Samples were taken at two different locations: a square mould sample was taken just upstream of lot 554 Chemin de la Petite Côte (Figure 3-3) and a circular mould sample, as well as a sample taken with the Sherbrooke sampler, were taken downstream of the same lot (Figure 3-5). The first location was sampled in August 2019 when water levels were ankle deep and the second location was sampled in early October 2019 when water levels were knee deep. The surrounding farmland is at an elevation of 41m while the bed of the river is at an elevation in between 38 and 39m (Google Earth Pro).

The region is known for its gleysolic soil and poorly drained clay deposits (Jobin et al., 2010). There are three main sources of finer sediments in the upper surficial geology found in western Montérégie: the Lake Candona brown or red silts deposited from 12.1 to 12kya (Tremblay, 2008; Parent and Ochietti, 2002), the grey Champlain Sea clay deposited from 12 to 10kya and the Lake Lampsilis brown loams or silty clays deposited from 9.5 – 9.0kya (Tremblay, 2008; Lamontagne et al., 2000). The transition between marine and lacustrine sediments occurs at an elevation of 52m in the region, while the transition between the latter and fluvial sediments occurs at 30-40m elevation (Tremblay, 2008). The retreat of Lake Lampsilis lead to the remoulding of Champlain Sea clay and other sediments in the region (Delage, 1997; Bariteau, 1988) as well as the formation of the current river system of western Montérégie (Tremblay, 2008). The clay sampled is most likely to be remoulded Champlain Sea clay due to its consistency and the presence of pockets of red silts and sands as well as rare cobbles.

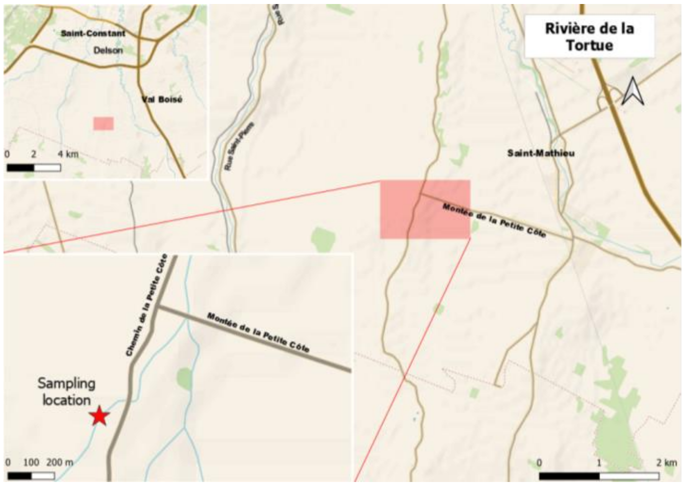

Figure 3-2 Geographic location of the Rivière de la Tortue tributary studied and the sampling location. Map data: Google, Stamen Design and Carto

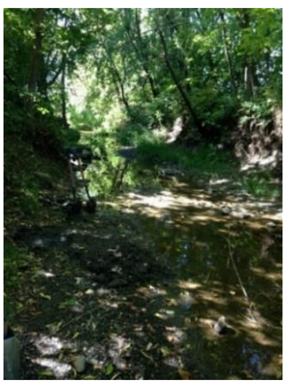

Figure 3-3. First sampling location upstream of the lot of 554 Chemin de la Petite Côte

Figure 3-4. Minor bank failure along the sampling reach of the tributary

Figure 3-5. Exposed clay north of the lot where a small overturn occurred

3.1.2 Site 2 – Castor River tributary

The Castor River is located in south-eastern Ontario; the headwaters of the main Castor River is in Embrun, where numerous branches converge, and it flows into the South Nation River in Casselman (South Nation Conservation, 2014). The surrounding area is mainly farmland with small areas of forest overlying till. The tributary studied has its source south of Vars and flows into the Castor River east of Embrun. The location of the sampling site is in the municipal lot connecting Renoir Dr and Cologne Street in Embrun, see Figure 3-6. The samples were taken at the outer edge of a sharp meander where clay is exposed along the river banks (Figure 3-7, Figure 3-8, Figure 3-9). There is an absence of alluvial material along the study reach. At the location of the sampling site, the tributary is 3-4m wide with steep 4-5m high banks. The elevation of the bed is approximately 61-62m (Google Earth Pro).

The landscape in the area was shaped, after the retreat of the Champlain Sea, as the Ottawa River system started to take its current form. The surface geology of the region is dominated by the Russell and Prescott sand plains overlying a deep deposit of Champlain Sea clay (Chapman and Putnam, 1984). The latter is exposed where the post-glacial Ottawa River system dissected the land around 10kya (Richard, 1982; Gadd 1976). The dominance of Champlain Sea clay in the bed and banks of the Castor River and South Nation River systems explains the absence of floodplains in the region (Evans and Brooks, 1993). The area is also prone to retrogressive landslides with four major landslides occurring close to Lemieux in 1895, 1910, 1971 and 1993 (Evans and Brooks, 1993; Mitchell, 1978) and numerous other minor landslides occurring in the area (Evans and Brooks, 1993).

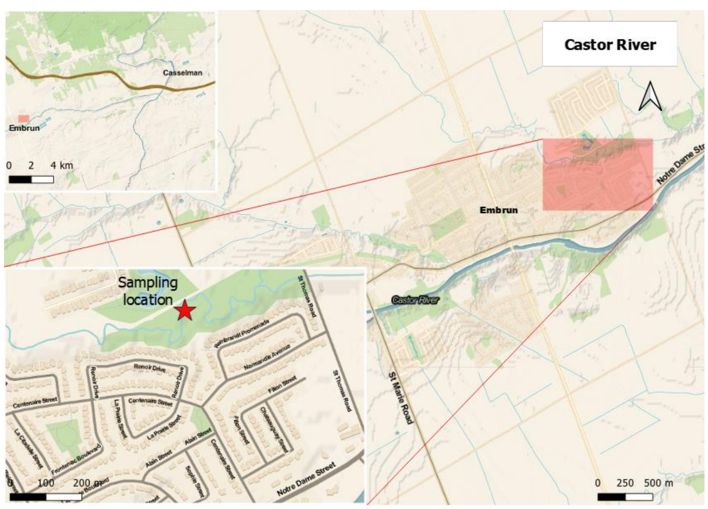

Figure 3-6. Geographic location of the Castor River tributary studied and the sampling location. Map data: Google, Stamen Design and Carto.

Figure 3-7. The sampling site is located in the bed of the meander of this Castor River tributary

Figure 3-8. Exposed bank downstream from the sampling location along the Castor River tributary

Figure 3-9. Fissured clay at the sampling location in November 2019

3.1.3 Site 3 – Rivière du Nord tributary

Rivière du Nord is located in the Laurentides region of Quebec, with its headwaters at the outlet of Lac Brûlé east of Ste-Agathe-des-Monts and it flows into the Ottawa River. The tributary studied is located in Prévost, to the west of highway 117, which flows directly into the Rivière du Nord, see Figure 3-10. Its runoff comes from a development east of highway 117. Both banks along the study reach are steep and actively eroding. The sampling site is located west of highway 117 next to 2450 Blvd. Curé Labelle in Prévost, see Figure 3-11. The bank is 4-5m high and its top is at an elevation of 160m. The southern banks is being cut at its toe, where fissured clay is exposed, see Figure 3-12.

The tributary studied is located at the southern extent of the Canadian Shield complex where the Champlain Sea extended to an elevation of 256m (Randour et al., 2020). The Champlain Sea deep water sediments in the region are characterised either as clays or silts of grey, grey-blue or red-brown color (Randour et al., 2020). In the region, Lake Lampsilis extended up to an altitude of 65m (Randour et al., 2020; Macpherson, 1966) and hence the finer sediments found on site are more likely to be Champlain Sea sediments.

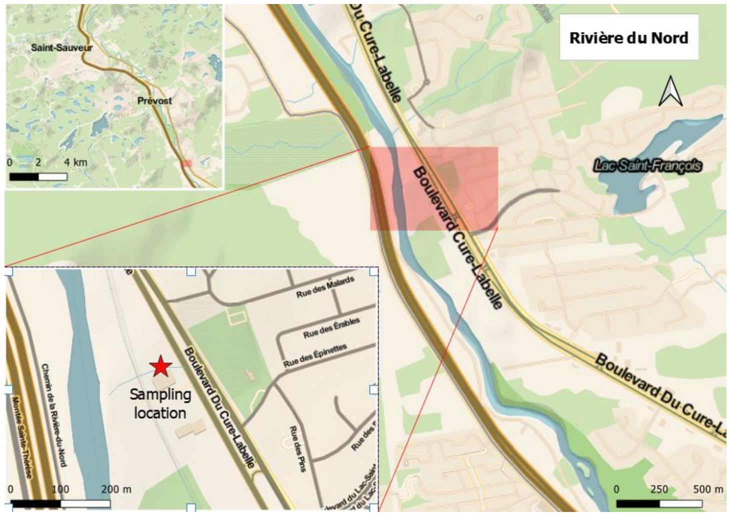

Figure 3-10. Geographic location of the Rivière du Nord tributary studied and the sampling location. Map data: Google, Stamen Design and Carto.

Figure 3-11. The sampling location is at the base of a steep bank in the Rivière du Nord tributary

Figure 3-12. Fissured clay at the base of a steep bank in the Rivière du Nord tributary

3.1.4 Site 4 and 5 – Tributaries of Chelsea Creek

Chelsea Creek is located in Chelsea, Quebec, where its headwaters are located. The creek flows into the Gatineau River at the municipal border shared by the city of Chelsea and Gatineau. Chelsea Creek runs at the base of a ravine and is surrounded by a thick forest that acts as a buffer between the creek and the surrounding sub-urban areas. The creek is meandering along most of its length as it is deeply incised in deep clay deposits. Many rotational bank failures and retrogressive landslides are observed along the upper tributary studied. This was not the case in the lower tributary, which could be explained by the mild slope of the bed as well as the milder incline of the banks. The area has an history of landslides with one major landslide that occurred in 1973 north of Chelsea village (Mitchell and Klugman, 1979).

The region has large deposits of sensitive sediments as the Champlain Sea flooded the region from 11.1 to 9.5kya (Lamarche, 2006). In the Outaouais region, these sediments can be found between 50 and 210m in altitude (Dubois Verret, 2015; Wilson, 1924). The incursion of the Champlain Sea was shorter in the Outaouais region, lasting only 1500 to 1700 years (Ochietti and Richard, 2003), with a distinct period when the western strip of the Sea became a calving bay due to the inflow of meltwaters and was relatively calm allowing for finer sediments to settle similarly to glaciolacustrine sediments (Romanelli, 1976). This episode led to the formation of rhythmites (Dubois Verret, 2015; Gadd, 1980) with low salinity (Romanelli, 1976) resembling estuary sediments (Lamothe, 1977) or lacustrine sediments (Dubois Verret, 2015). The Champlain Sea clays in the region are usually described as a thick layer of homogeneous grey silty clay with a laminated, varve-like, bottom (Dubois Verret, 2015; Romanelli, 1976). The deepest deposit found in the region is 20m-thick and the deposits contain a greater portion of silts when located in the upstream reach of valleys (Dubois Verret, 2015).

The region was also flooded by the glacial Lake Candona, from 11.6 to 11.1kya (datation corrected by Dubois Verret, 2015; Ochietti and Richard, 2003; Dyke, 2004), up to an altitude of 230-240m (Dubois Verret, 2015; Occhietti et al, 2011). These glaciolacustrine sediments are also described as fine sediment rhythmites and are hard to differentiate from the Champlain Sea sediments overlying them (Dubois Verret, 2015). Other proglacial lakes were formed in the Outaouais region during the retreat of the Champlain Sea, but their presence is mostly limited to the valley of the Rivière du Lièvre (Dubois Verret, 2015). The surficial geology of the region also includes deposits of older marine (Gadd, 1961) and glaciolacustrine sediments (Romanelli, 1976).

3.1.4.1 Site 4 – A lower tributary of Chelsea Creek

The lower tributary of Chelsea Creek studied flows into Chelsea Creek 60m upstream from a junction with Fleury Road in Chelsea, Quebec. The study reach is located 80-100m upstream from where the tributary flows into Chelsea Creek, see Figure 3-13. Block of clay are seen at the bottom of the tributary downstream from the location of the sampling site. The tributary meanders through thick deposits of exposed varved clay and is cutting the banks at their toe at several locations along the study reach, see Figure 3-14Figure 3-15, Figure 3-16 and Figure 3-17. Alluvial sediments are present on the bed at the inner corners of meanders. The thicker clay layers of the varves are of varying thicknesses, ranging from a few millimeters to 2-3cm in thickness, while the alternating layers of silt and sand are less than 1mm thick. The clay is hard and brittle along the reach. The samples were taken during a dry period allowing for the sampling of natural steps formed along the bed. The elevation of the bed at the study reach is estimated at 72m (Google Earth Pro).

Figure 3-13. Geographic location of the lower tributary of Chelsea Creek studied and the sampling location. Map data: Google, Stamen Design and Carto.

Figure 3-14. The sampling site in one of the lower tributaries of Chelsea Creek

Figure 3-15. Natural steps in the river bed in the lower tributary of Chelsea Creek

Figure 3-16. Layers of varved clay exposed in the bank of the lower tributary of Chelsea Creek

Figure 3-17. Layers of varved clay exposed in the bed of the lower tributary of Chelsea Creek

3.1.4.2 Site 5 – A upper tributary of Chelsea Creek

Another tributary upstream of the lower tributary described above was studied due to its different geomorphology and clay characteristics. The upstream tributary is at an altitude of 100m (Google Earth Pro) and flows into the lower tributary after having merged with other tributaries. The study reach is located west of the upper end of Olmstead Drive, see Figure 3-18. Numerous bank failures along the reach have exposed the clay banks and contribute to the evolution of the geomorphology of the tributary. Samples were taken from two locations along the reach: at location #1, one sample was taken in the outer edge of a meander at the bottom of a steep bank (Figure 3-19Figure 3-20Figure 3-21) while, at location #2, six other samples were taken where fluvial processes had eroded the bed into steps (Figure 3-22). The clays from the two sampling locations had different behavioural characteristics. The former was fissured clay with a much higher water content and sensitivity while the latter was laminated and brittle. The two locations are 120m apart with a difference of elevation approximately 5m. The sediments taken at location #2 are likely to be rhythmites from the early stages of the Champlain Sea with low salinity and varved structure. The sediments taken at location #1 are likely to have been deposited at a later stage of the Champlain Sea as the deposit is homogeneous and there was no apparent structure in the clay.

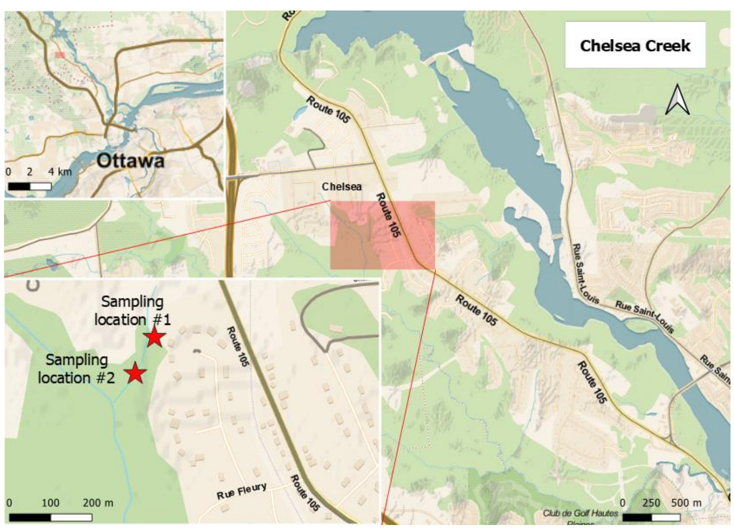

Figure 3-18. Geographic location of the upper tributary of Chelsea Creek studied and the sampling location. Map data: Google, Stamen Design and Carto.

Figure 3-19. Fissured clay at the surface of the banks of location #1 along the upper tributary of Chelsea Creek

Figure 3-20. Fissured clay at the surface of the bed of location #1 along the upper tributary of Chelsea Creek

Figure 3-21. Remoulded clay in location #1 of the upper tributary of Chelsea Creek

Figure 3-22. Quick clay landslides downstream from location #2 in the upper tributary of Chelsea Creek

3.1.5 Site 6 – Rivière St-Charles tributary

Rivière St-Charles is the main river running through Quebec City, Quebec. The river's source is Lake St-Charles and it flows into the St-Lawrence River at the municipal limit shared by Limoilou and St-Roch, where the river is restrained by concrete banks. The tributary studied has it source in a residential development in the borough of Des Rivières, east of Blvd. St-Jacques and it flows into the St-Charles River 100m downstream of the study reach, close to the entrance to the St-Charles River Linear Park south of Rue de la Rive Boisée, see Figure 3-23. At the junction with the tributary, the Rivière St-Charles is characterised by a steep slope and waterfalls are found upstream and downstream of the study location. Alluvial material is rarely found along the bed of the study reach. An over-consolidated clay loam deposit is exposed on a steep bank and across a 2m-wide bed. Samples were taken from the opposite bank where the deposit extends under 1m of organic matter, as it had a milder slope, see Figure 3-23 and

Figure 3-24. Slopes of the banks downstream and upstream from the study reach are mild. The absence of turbidity suggests there is no active of erosion along the study reach. Dropper stones as well as marine shells were found in the clay loam. The sampling site is located at an altitude of 43m.

Several Quaternary glaciations have occurred in the past two million years (Occhietti et al., 2004), which left sequences of glacial, glacio-marine, marine and fluvial deposits in the region (Filion et al., 2009). In the Quebec City region, during the last deglaciation between 11.5 to 9.8kya, the Champlain Sea extended up to an altitude of 210-235m (Laliberté, 2006; Bolduc et al., 2003; Cummings & Occhietti, 2001). The Champlain Sea sediments in the region varied in composition since the depositional environment included a coastal environment, with 5 to 10m-high tides (Ochietti et al., 2001), as well as an influx of meltwaters due to the proximity of the glacial front (Ochietti et al., 2001). Deep water Champlain Sea sediments in the region are heterogeneous, consisting of thick deposits of massive clay or loam (Parent & Occhietti, 1988). The Champlain Sea was then replaced by Lake Lampsilis once the land uplifted around 9.8kya (Ochietti, 2004; Parent & Occhietti, 1988). As the sediments sampled in this study are well consolidated, they are more likely to originate from a previous transgression of a post-glacial sea in the Quebec City region deposited in a similar environment to the Champlain Sea.

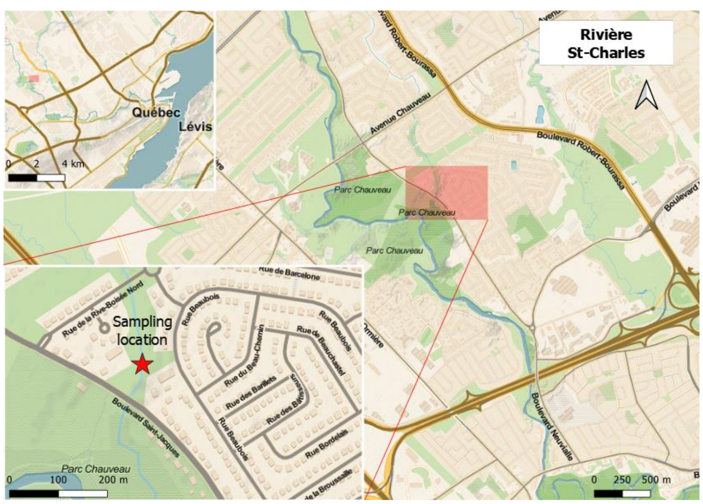

Figure 3-23. Geographic location of the Rivière St-Charles tributary studied and the sampling location. Map data: Google, Stamen Design and Carto.

Figure 3-24. The sampling site along a steep bank in one of the tributaries of Rivière St-Charles

Figure 3-25. River bed of the Rivière St-Charles tributary

3.2 Sampling methods

To collect the undisturbed or minimally disturbed samples required for representative geotechnical and fluvial erosion tests, sampling methods were developed for surficial clay deposits found in a fluvial environment through a review of the literature as well as experimentation in the field.

The following elements were considered while designing the new sampling method:

Use of light and easy to carry equipment to enable sampling in less accessible sampling sites. Fluvial environments in clay deposits can be located at the bottom of steep banks and/or far from roads or public sites.

Creation of a setup that would fit in a small make-shift cofferdam as the tributary's bed and banks might be submerged.

Collection of large samples to allow for the observation of mass erosion as well as surface erosion during the erosion tests, as well as to minimize the disturbance of the samples at their core. The smallest sample size required was determined to be approximately 150mm in diameter and thickness to observe mass erosion across the surface of the cohesive samples as blocks of 1-30mm diameter had eroded in a previous study done by Gaskin et al. (2003) on a Champlain Sea clay.

Minimization of the disturbance of the samples to minimize the impact of sampling on the erosion resistance behaviour of the cohesive sediments.

As disturbances due to sampling affect the structure and the strength of cohesive soils, and as the goal of this study was to test the *in-situ* erosion properties of undisturbed samples, a new method was developed based on the key principles underlying the Sherbrooke and the Laval sampling methods. Large samples were collected using a cylindrical stainless-steel mould (26.7cm Ø and 30cm depth) with no clearance and sharpened edges. The first trials were done using square moulds (30x30x30cm) but cylindrical moulds were more efficient for the coring of the samples. Smaller moulds were used to obtain samples dedicated to geotechnical characterisation tests (21.6cm Ø).

The new sampling method consisted of two main steps: a coring process followed by undercutting of the sample for removal, Figure 3-26. First, a reaction frame was set in place by screwing into the ground two augers at an equal distance from the sample's location, while ensuring that the clay in proximity of the samples would not be disturbed. A supporting frame was then affixed to the augers and the cylindrical mould was slowly driven into the ground with the help of hydraulic jacks. Once the mould had been driven 30cm into the ground, a trench was dug next to the sample, where a setup including another hydraulic jack, a frame and metal plate was installed. The metal plate was pushed with hydraulic jacks to undercut the sample and acted as a support during the removal of the sample once rebar handles were attached to the plate. Hydraulic jacks were preferred to any hammering tools as the slow action of the jacks induces less vibration and disturbances to the clay compared to the pounding of a hammer.

The cohesive deposits of the Rivière St-Charles tributary, the lower tributary of Chelsea Creek as well as the second sampling location along the upper tributary of Chelsea Creek were either too brittle or too hard to be sampled with the coring method developed in this study, as the augers could not be installed properly. Hence, these samples were carved by hand using a knife. The size of the samples depended on the macro fractures naturally present in the clay deposits. The samples from the Rivière St-Charles tributary were undercut using the metal plate setup while the samples taken from the two locations along the Chelsea Creek were taken at natural steps that had formed in the bed of the creeks, Figure 3-27. For a detailed list of the sampling methods used per site see Table 3-2.

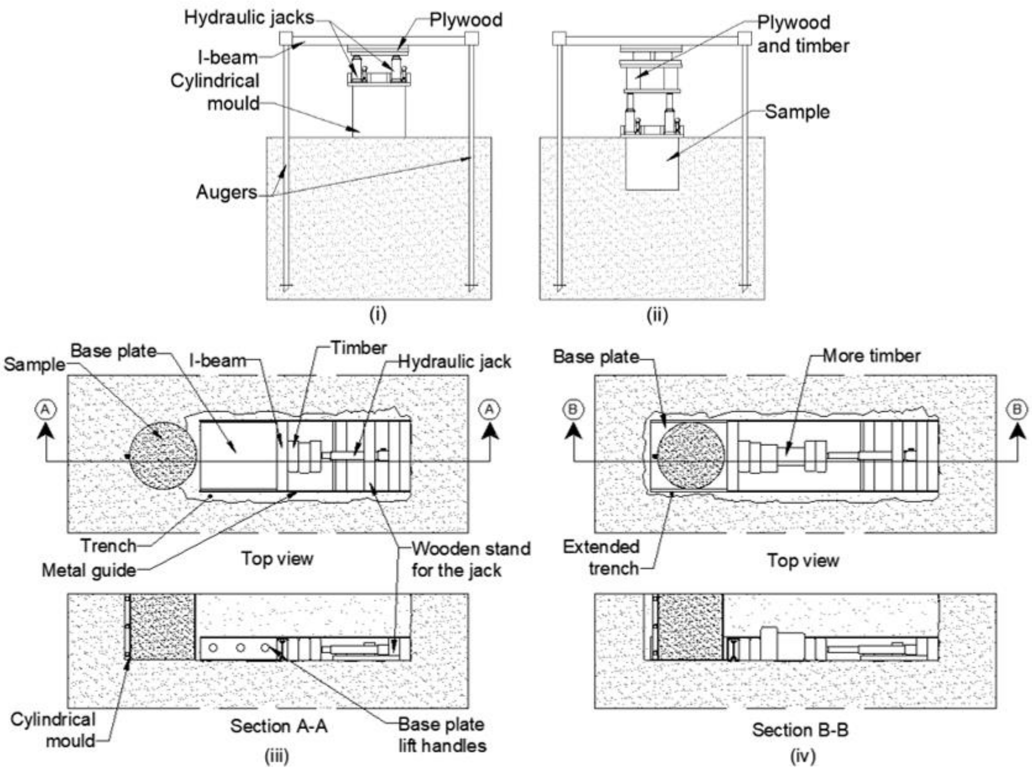

Figure 3-26. Non-consolidated clay sampling method using a cylindrical mould: (i) Augers installed to support the reaction frame and hydraulic jacks set up against mould, (ii) jacks drive the mould in the ground, (iii) a base plate setup is installed in a trench in front of the sample, (iv) jack drives the base plate under the sample

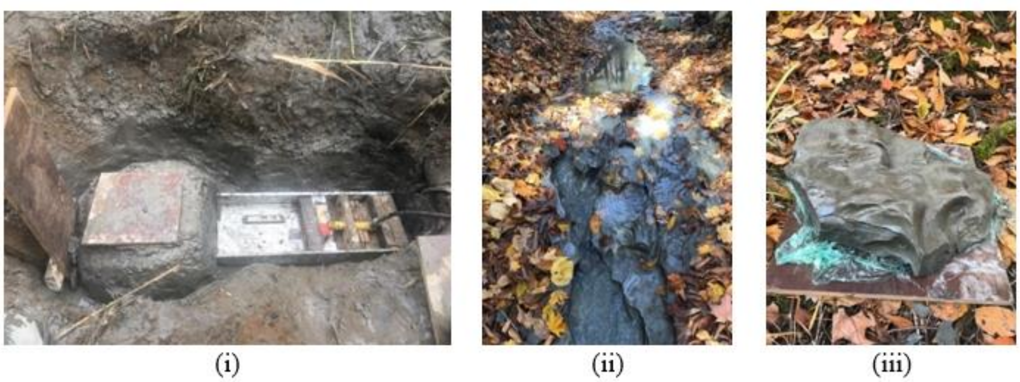

Figure 3-27. (i) Bottom plate setup at the Riviere St-Charles tributary site; the sample was then cut into a 30x30x20cm block, (ii) naturally eroded steps at the Lower Chelsea Creek site, (iii) carved out block at the Lower Chelsea Creek site.

Table 3-2. Number of samples taken at each site and sampling methods

Site	Tributary	Carved	Square mould	Circular mould, 10.5"Ø	Circular mould, 8.5"Ø	Sherbrooke sampler
1	Rivière de la Tortue		2		1	1
2	Castor River			2	1	
3	Rivière du Nord		1	3	1	
4	Chelsea Creek, lower	9				
5	Chelsea Creek, upper	6			1	
6	Rivière St-Charles	6				

At the Rivière de la Tortue tributary, the new sampling method was used in parallel with the Sherbrooke sampler to compare the disturbance caused by sampling. The samples were taken at the same location and on the same day (see Figure 3-28). The Sherbrooke sampler setup was adapted to function in a river environment; it was made more mobile by detaching, moving and reassembling the setup in the tributary. The new method proved to be more efficient than the Sherbrooke sampler in a river environment as the setup was easier to carry and the sampling was done in half the time - 1.5 hours per sample using the new method instead of 4 hours per sample for the Sherbrooke sampler. Both methods required two hours of installation and two operators. The presence of alluvial material in the creek slowed down the sampling with the Sherbrooke sampler as it was difficult to keep the surface of the clay clear as material would fill the hole made by the sampler. The new method proved to be better suited for the sampling of an exposed deposit found in a river or creek. No significant differences were observed in the results for the fall cone tests or the vane shear tests for each of the two methods (see results sections 4.1.2 and 4.1.3).

(a)

(b)

Figure 3-28. Samples taken in parallel at the Rivière de la Tortue tributary; (a) using the new sampling method; (b) using the Sherbrooke sampler.

3.2.1 Sealing, transportation and storage

Careful considerations were taken to prevent any drying or disturbances to the cohesive structure of the samples before subsequent laboratory testing. Once the samples were taken out of the deposits, they were sealed in plastic wrap and brought to a working area. They were then sealed for long-term storage using the La Rochelle sealing method (1986) which involves a layered seal of plastic film covered by a mixture of equal parts paraffin-wax and petroleum jelly. Air bubbles were removed by painting the wax film, while the plastic film was tightly held on the surface of the sample. Cheesecloth was wrapped around samples that were taken out of their mould, prior to sealing. The samples were transported using transportation boxes based on DeGroot's method (2005), in which the sample is placed in a box cushioned with foam chips. The samples were stored in refrigerators with large containers of water at a temperature of 8-9°C and 90-95% humidity to prevent any drying before testing (La Rochelle, 1986).

3.3 Clay characterisation

To identify and compare the clays from the different deposits sampled in this study, standard geotechnical tests were conducted. The basic physical properties of the clays such as grain size distribution (hydrometer analysis), phase composition of the clays (in-situ, saturated) and the Atterberg limits were determined. The clay from the Rivière St-Charles tributary was too hard and brittle to properly carry out the Atterberg limits tests or any shear/consolidation tests. Therefore, only the specific gravity, the hydrometer test and the moisture content tests (in-situ, saturated) were performed on this clay. The shear behaviour of the clays was determined using the fall cone test and the vane shear test, which were performed in undrained conditions to best represent short-term events occurring along a river reach. The geotechnical tests, summarized in Table 3-3, were conducted at the Geomechanics laboratory of the Civil Engineering Department of Université de Sherbrooke under the supervision of Professor Mourad Karray. Table 3-4 lists the tests conducted at each site.

Table 3-3. Summary of geotechnical properties obtained during the characterisation tests

Test	Properties
Hydrometer	Silt content, clay content, median grain size d_{50}
Specific gravity	Specific gravity Gs and density ρ_s of the grains
Atterberg limits	Liquid Limit *L.L*, Plastic Limit *P.L.*, Plasticity Index *P.I.* and Liquidity Index *L.I.*
Fall cone	Undrained shear strength C_u, Remoulded shear strength C_{ur}, sensitivity
Vane shear	Undrained shear strength C_u
Other properties obtained: moisture content *m* Derived properties: USDA and USCS classification, activity a_c, bulk density ρ_b, $\chi = \frac{L.I.}{G_s - 1}$ (Mostafa et al., 2008)	

Table 3-4. Tests conducted on samples of each site

Site	Tributary	Hydrometer	Specific gravity	Atterberg limits	Falling cone	Vane shear
1	Rivière de la Tortue	X	X	X	X	X
2	Castor River	X	X	X	X	X
3	Rivière du Nord	X	X	X	X	X
4	Chelsea Creek, lower	X	X	X	X	X
5	Chelsea Creek, upper	X	X	X	X	X
6	Rivière St-Charles	X	X			

To determine the disturbance of the clay due to sampling, transportation and storing, a standard oedometer test was carried out in parallel with a piezoelectric cone apparatus (P-RAT) on the samples taken at a tributary of Rivière de la Tortue in St-Mathieu, Quebec. Three samples were obtained at this location using three different sampling techniques: a sample using our sampling technique with a square mould (see section 3.2), a sample using our sampling technique with a circular mould (see section 3.2) and a sample using the Sherbrooke sampler.

At two of the sample sites, the upper and lower tributaries of Chelsea Creek, two sets of tests were performed to determine the variability in the material properties. At the upper tributary, samples were obtained at two locations having different elevations representing deposition at different points in time. At the lower tributary the clay was varved with layers of clay separated by a layer of sand and larger sized silts and tests were performed on two different layers of clay with the same varve. The results were used to plan the erosion tests.

3.3.1 Specific gravity and density

The density of the clay particles, and thus also the specific gravity of the clay particles, were obtained for each clay deposit and its subsamples. These values are required for the hydrometer test (see section 3.3.2) and to assess the mass erosion rate of the samples (see section 3.4.5).

The density test was performed in accordance with the CAN/BNQ 2501-070 norm (BNQ, 2014a). The method compares the weight of dry sediment to the weight of water occupying the same volume. The mass of water filling a pycnometer to a set volume, a dry mass of sediments and the total mass of the same pycnometer filled with sediments and topped up with water to the same set volume are measured. The pycnometer containing the sediments and the water is connected to a vacuum line to remove the air. The temperature of the water is measured in the calibration pycnometer when filled with water only (T_1) and when filled with the sediment and water (T_2). The specific gravity of the clay particles G_s is determined as:

$$G_s = \frac{m_s \cdot \rho_w(T_2)}{\rho_w(T_1) \cdot (m_s - m_{s+w} - m_w)} \qquad 3.1$$

where m_s is the dry mass of the clay particles, $\rho_w(T_1)$ is the density of water and m_w is the mass of the calibration pycnometer while $\rho_w(T_2)$ is the density of water and m_{s+w} is the mass of the pycnometer filled with sediments and water.

3.3.2 Hydrometer analysis

The hydrometer analysis provides the grain size distribution for fine sediments: the silt and clay content. The clay content is of particular importance for comparison of clays as it is an important determinant of their behaviour as clays are cohesive. The fines distributions were used to classify the clays using the USDA Classification System (USDA, 2012) and the USCS Classification System (ASTM).

The hydrometer tests were conducted in accordance with the BNQ2501-025 norm (BNQ, 2013). The method is based on Stokes' Law; the settling of particles in a viscous fluid, after different periods of elapsed time, is recorded. First, a piece of clay is fully dried, crushed and mixed with 1000mL of water and 5.00g of hexametaphosphate - a dispersing agent that helps break apart the clay particles - in a graduated cylinder. Then, a hydrometer is gently released at the free surface of the graduated cylinder at set time intervals to record the change in density in the solution as particles start to settle. In parallel, the hydrometer readings are made in a graduated cylinder containing only water and hexametaphosphate acting as a calibration reading. The temperature of the solutions is taken at the time of each reading. The mass of the dried clay M_S is taken prior to the mixing and the specific gravity S_G of the sample is obtained through the specific gravity test.

The diameter of the particles D at different time intervals is taken as:

$$D = K\sqrt{\bar{P}/t} \cdot 10^3 \tag{3.2}$$

where $\bar{P}$ is the average depth of submersion of the hydrometer, t is the time of settling and K is a function of the forces acting on the particles such as drag and gravitational acceleration. P is a function of the reading taken on the hydrometer gage R and the depth of the hydrometer is then calculated based on calibrated parameters A and B:

$$P = AR + B \tag{3.3}$$

K follows the following relationship:

$$K = \sqrt{\frac{3\eta}{g(G_s - 1)}} \tag{3.4}$$

where η is the dynamic viscosity of water (P) and g is gravitational acceleration. The viscosity η is a function of the temperature T and can be expressed by the following relationship.

$$\eta = 0.0016e^{-0.024T} \tag{3.5}$$

The percentage of particles remaining in suspension, which is equal to the percent passing, at each time interval is considered as:

$$\%\,passing = \frac{G_s}{(G_s - 1)}\frac{(R - R')F}{M_s} \times 100 \tag{3.6}$$

where R' is the reading taken in the calibration cylinder and F is a correction factor based on the use of a hydrometer 151H.

3.3.3 Liquid and plastic limits

The liquid and plastic limits tests were conducted on remoulded pieces of clay from each site, and each sublayer of clay. All sites were tested except for the Riviere St-Charles tributary clay because of its low clay content and absence of cohesion in its remoulded form. The liquid and plastic limits define the boundaries between the states of consistency (liquid, plastic, solid) of a clay, which explains the strength and resistance to deformation once remoulded (Wagner, 2013).

The liquid limit (L.L.) indicates above what moisture content the clay starts to behave as a liquid. It is defined as the moisture state at which the shear strength of the clay decreases to 25g/cm^2 (Seed et al., 1964). The plastic limit (P.L.) indicates below what moisture content the clay can no longer be remoulded without cracking, that is it stops being plastic, thus applied forces on the clay result in permanent deformations.

The two tests were conducted in accordance with the CAN/BNQ 2501-092 norm (BNQ, 2014b) which uses the fall cone penetrometer to determine the liquid limit, except for four (4) samples for which the plastic limit was tested in accordance to the ASTMD4318-00 norm (ASTM, 2000). The clay is remoulded into a homogeneous paste, a 60g stainless-steel cone is released into the paste and the penetration of the cone in the clay paste is measured (further description in 3.3.4). See the fall cone section for a more detailed procedure. The samples were tested using the multiple points method except for the samples from a lower tributary of Chelsea Creek and the Castor River tributary that were tested using the one-point method. The liquid limit for the one-point method is determined as follows:

$$L.L. = \frac{20\ (100m - 15)}{p + 10} + 15 \qquad 3.7$$

where m is the water content (%) and p is the penetration depth (mm). For the multiple point method, the penetration depth is determined for three or more remoulded clay pastes at different water contents and the liquid limit is interpolated at a penetration of 10mm as shown on the graph below.

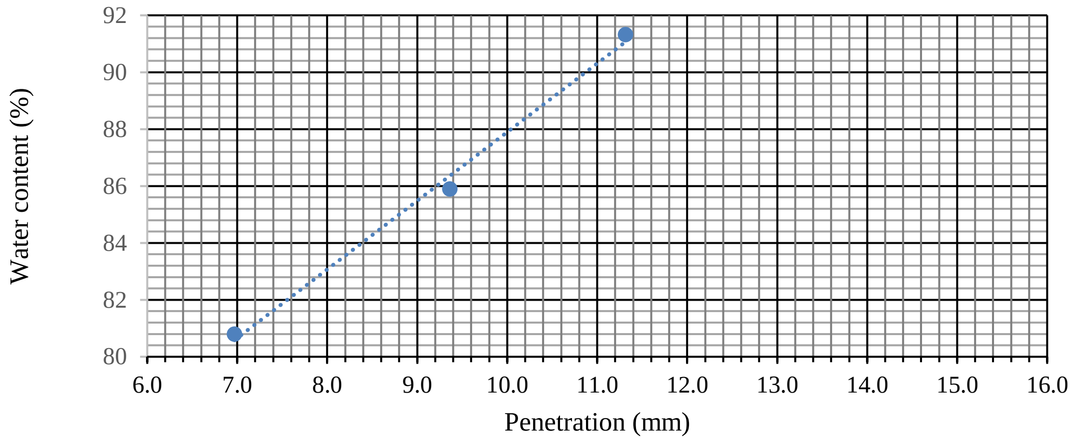

Figure 3-29. Interpolation of the water content corresponding to a 10mm penetration, to find the liquid limit of the upper tributary of the Chelsea Creek clay at location #1

The liquid and plastic limits tests define the Plasticity Index (P.I), the range of water contents at which the clay behaves plastically, and the Liquidity Index (L.I.), which defines where the current given water content w lies within the plasticity range. The Plasticity Index is defined as:

$$P.I. = L.L. - P.L. \tag{3.8}$$

The Liquidity Index is defined as:

$$L.I. = \frac{m - P.L.}{P.I.} \tag{3.9}$$

The liquid limit and the plastic limit are used to classify the clays according to the Casagrande Plasticity Chart. As the plasticity depends not only on the water content, but also on the types of clay mineral present in the clay, the plasticity index defines the activity (a function of the type of clay mineral) of the clay (Skempton, 1953). The activity of the clay samples was compared to those in the literature (Mitchell and Soga, 2005; Seed et al., 1964; compiled by Wagner, 2013). The activity a_c is defined as:

$$a_c = \frac{P.I.}{clay\ content\ (\%)} \tag{3.10}$$

3.3.4 Fall cone

The fall cone penetrometer test was used to determine the undrained shear strength of the clay specimen as well as the sensitivity of the clays. The sensitivity of the clay yields information on the stability of the clays' internal structure – or how easily the structure of an undisturbed clay shifts to a dispersed state which results in a considerable loss in shear strength (Wagner, 2013).

The tests were conducted in accordance with the CAN\BNQ 2501-110 norm. An intact block of clay is placed under the fall cone penetrometer, and after the cone is released its depth of penetration into the block of clay is measured, Figure 3-30. This is repeated at least 5 times to obtain representative penetration depths. The clay is then remoulded into a paste without adding any water. A set of measurements is made on the remoulded paste applied in three layers in a special container as seen in Figure 3-31 below. The set is deemed appropriate when the difference between the measurements of the depth of penetration on the surface of the paste is less than 0.3mm. The paste is remoulded once more and the same protocol is followed. When the difference in the average of the two sets is less than 0.3mm, the average of the two averages is recorded as the depth of penetration for the remoulded state.

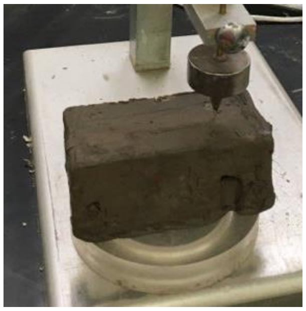

Figure 3-30. Fall cone penetrometer test conducted on an undisturbed clay sample

Figure 3-31. Fall cone penetrometer test conducted on a remoulded clay sample

The undrained shear strength c_u (kPa) obtained through the fall cone penetrometer test is obtained as follows:

$$c_u = \frac{kQ}{h^2} \qquad 3.11$$

where k is a constant associated with the geometry of the cone used, Q is the weight of the cone (10^{-3} N) and h is the penetration depth (mm). The same formula was used for the remoulded shear strength c_{ur} (kPa).

The sensitivity of the clay S_{tv} is determined using the following principle first proposed by Terzaghi (1944):

$$S_{tv} = \frac{c_u}{c_{ur}} \qquad 3.12$$

3.3.5 Vane shear test

The vane shear test provides a second set of values for the undrained shear strength of the clays. When possible, the test was repeated several times per site to quantify the variability found in the clay surface layer (i.e., crust). The undrained shear strength of the clays obtained through the vane shear test were compared to the fall cone penetrometer results.

The tests were conducted in accordance with the ASTM D4648-00 norm. A block of clay is trimmed to fit a constraining ring. The ring is then tightly mounted in the shear vane apparatus to prevent any rotation or displacement during the test, Figure 3-33. No vertical load was applied to represent river bank or bed conditions. The vane is then slowly lowered to the center of the clay block with top of the vane being 10 millimetres under the surface. The angle at which the blades are initially positioned is noted. Then a motor, that rotates the vanes at a uniform rate of 0.1°/s, is turned on until the clay specimen fails. The final angle is recorded. After removing the vanes from the sample, the ring is disassembled and the defects in the specimen are visually inspected and noted, Figure 3-33 and Figure 3-34.

Figure 3-32. The vane shear apparatus

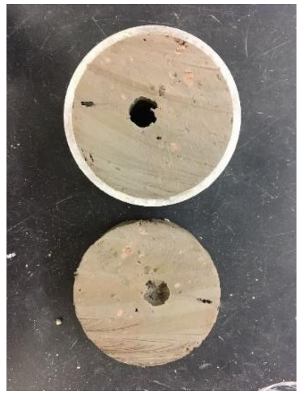

Figure 3-33. Clay specimen after failure

Figure 3-34. Other clay specimen after failure

The undrained shear strength c_u (kPa) obtained through the vane shear test is defined as follow:

$$c_u = \frac{1000T}{K} \tag{3.13}$$

where K is:

$$K = \pi D^2 \left(\frac{H}{2} + \frac{D}{6}\right) \tag{3.14}$$

where H is the height (mm) and D is the diameter (mm) of the vane blades. T is the torque of the vane calculated as:

$$T = F\left(R_{init} - R_{final}\right) \tag{3.15}$$

where F is the spring constant, R_{init} is the initial angle and R_{final} is the final angle of the vane rotation.

3.4 Fluvial erosion tests

To study and compare the shear behaviour of the clays in a fluvial-like environment, erosion tests were performed in a straight-channel flume. Particle erosion as well as mass erosion were observed, while the flume slope was gradually increased to increase the bed shear stress acting on the samples. The samples were subjected to a constant flow for two hours at each shear stress level (slope) and the erosion, if any, observed. This process was repeated at increasing shear stress levels until erosion occurred. Several measurements were taken during the erosion tests: the change in water depth along the flume used to calculate bed shear stress, the size of the eroded blocks captured in a collection basin at the outlet of the flume, the change in mass of the samples and the change in surface roughness at 1-hour intervals during the tests. A setup with sensors was designed to provide a direct measurement of the shear stress acting on the samples but proved to be ineffective as background noise was greater than the shear stress signal.

3.4.1 Flume setup for fluvial erosion tests

The erosion tests were performed in a straight-channel recirculating flume (with dimensions of 0.30x0.45x9.14m), whose slope could be varied over the range of 0 to 0.0665. The flume had a built-in false floor (0.15m from the true bed) having a cut-out into which the sample was placed (at a distance of 3.65m from the upstream inlet), so that its surface was flush with the bed (see Figure 3-35 for reference). A pool pump (‘Waterway’ spa & pool pump, model HP-20–2N22F, serial #HP050505-1282, 7.1hp, 230V, 60hz, 20amp, 11:00 discharge) was used to recirculate water from a downstream reservoir (2080L) to an upstream reservoir (1200L) integrated into the structure of the flume at the inlet. A weir located at the outlet of the flume set the minimum water depth and was used to fill up the flume and start the erosion tests in a submerged condition.

The pump could be operated either at a low setting of 0.0038m^3/s or at a higher setting of 0.019m^3/s. The flow rate was monitored using a paddle wheel flow meter (‘Midwest Instruments and Control’, 3” schedule - 80 pipe mounted flow meter, PN# PT-P-80-3.0, 40-400 GPM). When testing on a flat bed ($S_0=0$), a butterfly valve located at the outlet of the pump was partially closed to set the flow rate in the range between 0.006 and 0.019m^3/s. Bed shear stress values between 0.3 Pa to 11.6 Pa were possible with the available range of bed slope and discharge as detailed in Table 3-5. The samples were subject to erosion at a constant bed shear stress for two hours, erosion was detected visually or by a noticeable weight loss from weighing of the sample at one hour intervals. The bed slope S_0 was measured using a ruler attached to the flume. The cosine law was used to calculate the bed slope as shown in Figure 3-35.

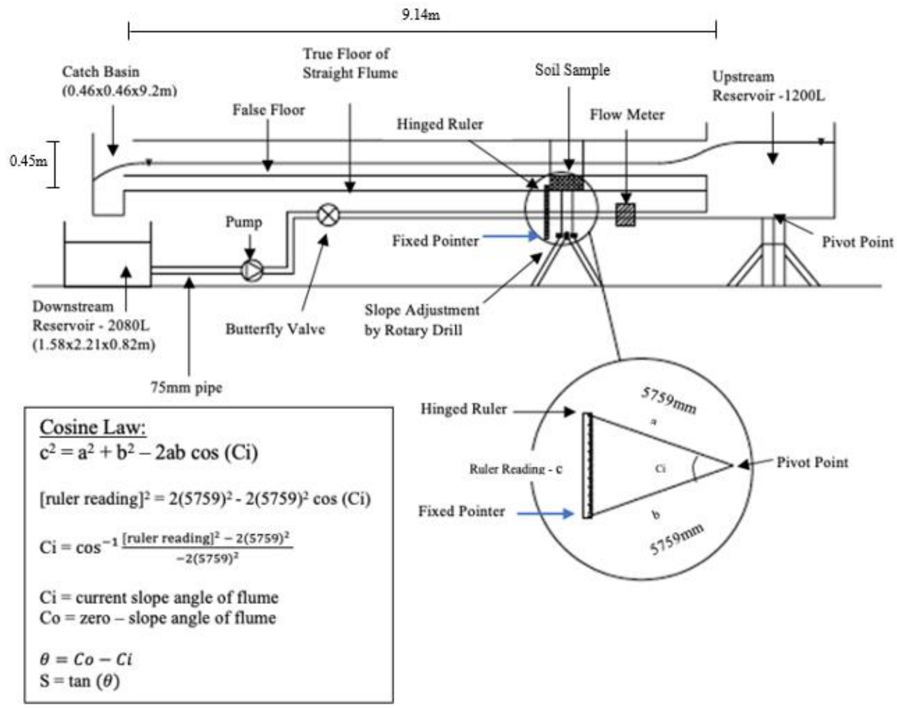

Figure 3-35. Straight-channel flume setup (adapted from Yeats, 2021)

To facilitate the installation and removal of the samples in the flume, a box setup was designed to hold the samples in place while keeping their surface flush with the false floor of the flume as shown in

Figure 3-38. To ensure the sample surface was flush with the flume false floor as the sample eroded, the sample was placed in a box containing a lifting mechanism, on which the sample sits, as shown in Figure 3-36. The samples were placed into a mould to ensure they were constrained during the erosion procedure (see section 3.4.4 for more details on the preparation of the samples prior to testing) and sit on a PVC disk. The mould lip was slightly beveled (<0.5mm) which allowed for a small clearance at the edge of the samples and could have induced small local disruptions of the bed shear stress over the sample. The disk is sits on a metal plate that can be raised or lowered and hence can lift the sample as it erodes. The box setup is versatile as different sizes of moulds can be installed simply by changing the lid of the box to one with a different hole size and changing the PVC disk to one of the appropriate size. Moulds of 4”, 8 5/16” and 10” diameter were used to maximize the cylindrical test core from the collected samples in order to maximize the surface area on which shear stress could act. The box containing a sample is shown Figure 3-37. The box setup was initially designed to be used with sensors in an attempt to record a direct measurement of the bed shear stress acting on the sample. The sensors setup is discussed further in section 3.4.6.

Table 3-5. Shear stress increments used in this study (data taken from Yeats, 2021). R is defined in section 3.4.3

		With *R* above sample			With interpolated *R*		
Slope S_0	Flow Q	Shear stress τ	Energy slope S_f	Hydraulic Radius R	Shear stress τ	Energy slope S_f	Hydraulic Radius R
	m^3/s	Pa		m	Pa		m
0	0.0035	0.3 ± 0.01	0.0011 ± 0.0000	0.029 ± 0.0003	0.3 ± 0.01	0.0011 ± 0.0000	0.029 ± 0.0002
0	0.0129	0.7 ± 0.03	0.0015 ± 0.0004	0.050 ± 0.001	--	--	--
0	0.0191	1.1 ± 0.05	0.0018 ± 0.0001	0.059 ± 0.0004	1.0 ± 0.04	0.0018 ± 0.0001	0.057 ± 0.006
0.010	0.0191	2.9 ± 0.2	0.0085 ± 0.0005	0.035 ± 0.001	3.2 ± 0.2	0.0085 ± 0.001	0.039 ± 0.002
0.019	0.0191	4.2 ± 0.2	0.014 ± 0.001	0.030 ± 0.001	4.7 ± 0.3	0.014 ± 0.001	0.034 ± 0.003
0.027	0.0191	5.4 ± 0.2	0.021 ± 0.001	0.026 ± 0.001	6.4 ± 0.2	0.021 ± 0.001	0.031 ± 0.003
0.036	0.0191	5.9 ± 0.5	0.025 ± 0.002	0.024 ± 0.0004	6.9 ± 0.6	0.025 ± 0.002	0.029 ± 0.003
0.046	0.0191	7.4 ± 0.5	0.034 ± 0.003	0.023 ± 0.0004	9.1 ± 0.6	0.034 ± 0.003	0.028 ± 0.003
0.053	0.0191	7.4 ± 0.4	0.035 ± 0.003	0.021 ± 0.0004	8.8 ± 0.5	0.035 ± 0.003	0.026 ± 0.003
0.067	0.0191	8.6 ± 0.6	0.046 ± 0.004	0.019 ± 0.0004	11.6 ± 0.8	0.048 ± 0.004	0.025 ± 0.003

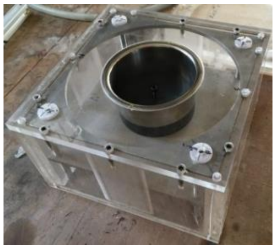

Figure 3-36. Empty box

Figure 3-37. Box containing the sample

Figure 3-38. Box setup in the flume

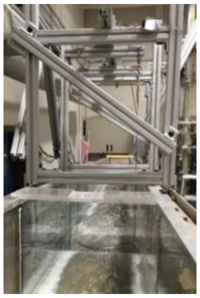

Figure 3-39. Built-in frame and cables lifting the box

The box is hooked to a frame attached to flume walls to ensure that the box is hanging and not resting on the flume's bottom, as shown in Figure 3-39. Four cables (1.2mm Ø) placed at each corner of the box were fastened to hooks pinned on load cells attached to the frame. Once the box was placed in the opening in the false floor and hanging so that its top surface was flush with the false floor, a U-shaped insert with a plastic flap was put in place to ensure that there were no gaps around the box while allowing free movement of the box as shown in dark grey in Figure 3-38.

To assess the occurrence of mass erosion and to measure the sizes of the eroded blocks, a collection basin with a net bottom was placed under the flume outlet, Figure 3-39. At 1-hour intervals, when the samples were weighed and their surface scanned to measure roughness, the discharge in the flume was reduced to lower turbidity at the outlet and the eroded material captured by the net visually inspected, Figure 3-40. If blocks were present, they were carefully removed and placed in a container. The size of the blocks were measured by placing them on a grid of ¼" to roughly measure their dimensions. As critical shear stress was determined to occur when blocks of 2-5mm started to erode (Mostafa et al., 2008), the method offered a qualitative indicator of the critical shear stress threshold as well as quantitative estimation of the size of the blocks eroding during mass erosion.

Figure 3-40. Outlet of the flume discharging into the collection basin

Figure 3-41. Net placed at the bottom of the collection basin

3.4.2 Definition and calculation of critical shear stress

The definition of critical shear stress for mass erosion used in this study is based on that established by Mostafa et al. (2008). The critical shear stress for mass erosion of the clays was determined to occur when blocks of 2-mm diameter or larger start to erode uniformly across the surface of the sample. The threshold for critical shear stress was determined by measuring the size of the blocks eroded and collected, and by measuring the loss of mass of the sample at hourly intervals (see section 3.4.5).

The boundary shear stress along the straight flume was calculated using the non-uniform flow resistance equation 2.2. The error in the shear stress measurements was mainly due to the error caused by surface waves on the water surface in the supercritical flow resulting in a ±2mm error at each measurement. The resulting error in the energy slope (± 0.0004) was used to estimate the error in the shear stress (± 0.1 to ± 1.3 Pa as the shear stress increases from 0.3 Pa to 11.6 Pa), as shown in Table 3-5.

3.4.3 Calibration of the flume to determine bed shear stress

The bed shear stress acting on the surface of the clay was estimated by observing the gradually varied water surface profile along the flume. The use of a probe to measure a velocity profile was not possible as the flume's flow is shallow and supercritical. Two calibration experiments were completed prior to the erosion tests to obtain a benchmark value for shear stress acting along the flume. A test was also performed to determine the impact of the cables of the box setup on the flow and the calculated value of the bed shear stress. A backwater analysis was performed as well to establish the difference between experimental values and the corresponding theoretical water surface profile (Yeats, 2021).

The benchmark tests were performed with the box setup in place; the top surface of the box being covered by a flat plexiglass plate. Two methods were used to analyse the results : one where the shear stress was calculated using equation 2.2 with the hydraulic radius observed above the center of the box (at x = 5.42m) and the second in which the shear stress at the same location was calculated using an average hydraulic radius for the reach, centered on the box, from x = 1.76m to x = 9.08 m along the flume. The difference between the two methods and their impact on the resulting calculated bed shear stress will be discussed.

As shown below in Figure 3-42, the flow along the flume is non-uniform and there are two regions of gradually varying flow: one extending downstream from the outlet of the inlet reservoir at the upstream end of the channel and one near the free overfall at the outlet of the flume. At all slopes used in this experiment, the flow is supercritical, except at zero slope where the flow is subcritical.

The extent and location of the gradually varied flow regions depend on the bed slope and is affected by any protrusion in the straight flume walls and floor. The profile shown in Figure 3-42 is that for a bed slope of half of the maximum possible slope of the flume. In this case the hydraulic radius at the centre of the sample is 0.023m, while that using the reach average value is 0.028m.

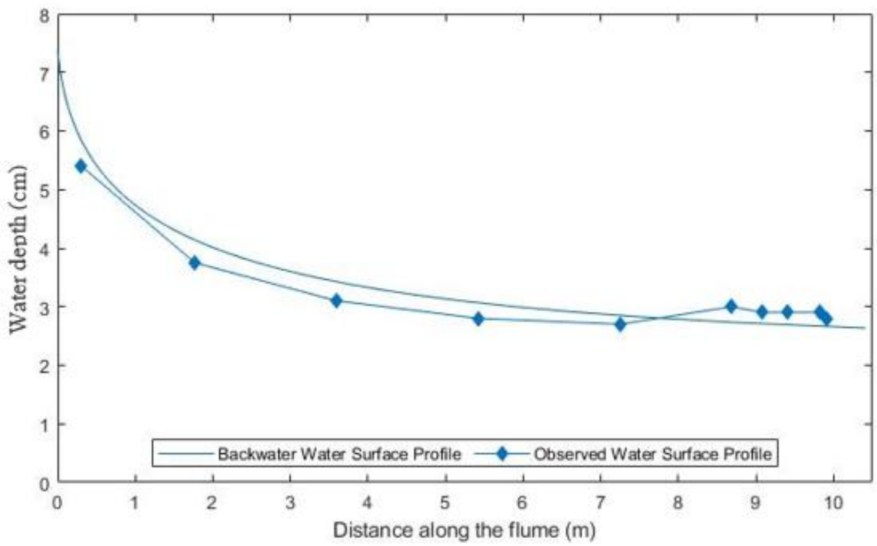

Figure 3-42. Water surface profile at a slope of 0.0456 along the flume in the upstream to downstream direction (data taken from Yeats, 2021)

The bed shear stress calculated with a hydraulic radius above the sample gave results with a lower average difference between the theoretical backwater profile and the experiment values, see Figure 3-43. The measured hydraulic radius above the sample resulted in calculated bed shear stress values that were between 9 and 44% larger than those calculated with the best-fit backwater profile. Using the average hydraulic radius in the flume reach (x = 1.76 m to 9.08 m) to calculate the bed shear stress resulted in a milder water surface slope, overestimation of the hydraulic radius above the sample and calculated bed shear stress levels that were -7% to 36% higher than those calculated with the best-fit backwater profile depending on the slope, as presented in Figure 3-44. The shear stress obtained through the backwater profile was also calculated either by using the hydraulic radius above the sample (Figure 3-43) or using the hydraulic radius interpolated above the sample (Figure 3-44).

Uniform flow assumption was not used in this study as a gradually varied profile developed resulting is an energy slope that was greater that the bed slope, as shown in Table 3-5. Therefore, the results for the critical shear stress shown in the following sections was obtained using the energy slope and the observed hydraulic radius above the sample, while qualitatively comparing the results to the benchmark values and the reach average values.

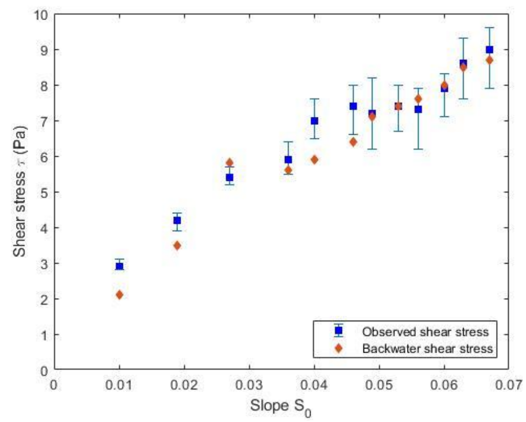

Figure 3-43. Theoretical shear stress vs observed shear stress using the hydraulic radius observed above the sample

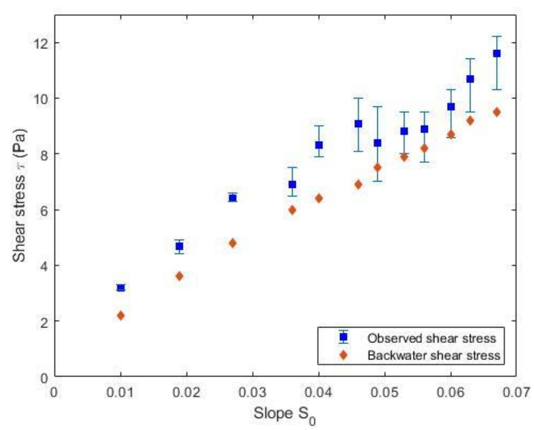

Figure 3-44. Theoretical shear stress vs observed shear stress using the hydraulic radius interpolated above the sample

A test was performed to assess the effect the cables of the box setup on the water surface profile and the overall estimate of shear stress along the flume. The water surface profile in the flume both with and without the cables in place was measured to assess the difference the calculated bed shear stress. The cables lowered the energy grade line slope across the flume by less than 6% for most slopes except for slopes of 0.010, 0.019 and 0.027 where the energy grade line increased by 8, 2 and 7% respectively (for details see appendix B; data taken from Yeats, 2021).

3.4.4 Preparation of the clay samples for fluvial erosion tests

The procedure for sample preparation was based on standard methods used in the preparation of clay samples for oedometer testing for which a piece of clay is trimmed to fit an oedometer ring (ASTM D2435). First, each stored sample was opened and a small piece (>10g) was taken to obtain the moisture content of the samples prior to erosion tests. The steps described in section 3.2.1 ensured that the samples were kept at their field moisture content. The samples were cut and trimmed with a sharp knife and a wire saw to roughly the shape of the mould. The selected mould (x, y, z) (open top and bottom) was placed on top of the sample and slowly pushed into the material, trimming as required for the sample to fit into the mould reducing to a minimum the disturbance of the clay. A PVC disk, fitting inside the mould, was then placed under the sample. Any sample protruding above the top of the mould rim was trimmed to create a flat surface. These steps are shown below in Figure 3-45 to Figure 3-47. To consider the surface irregularities created while trimming, initial entrainment was ignored when the samples were placed in the flume – at a bed slope of zero and low flow with a shear stress of 0.3Pa.

Figure 3-45. Trimming of the samples to fit in a mould

Figure 3-46. Sample in the mould before final shave

Figure 3-47. Final product

3.4.5 Erosion rate measurement

The erosion rate was measured by measuring the change in mass of the sample occurring during the fluvial erosion testing. The mass of the samples was measured, using a calibrated scale as shown in Figure 3-60, before being placed in the flume and at a regular 1h intervals during the erosion testing. The erosion rate was initially calculated as mass lost (g) per hour of erosion and was then divided by the surface area of the sample to obtain mass lost (g) per surface area (cm^2) per hour of shear action as shown in Eq. 3.16 and 3.17.

$$\dot{Z}\ \left(\frac{g}{h}\right) = \frac{dM_{loss}}{dt} = \frac{M_f - M_i}{\Delta t} \tag{3.16}$$

$$\dot{Z}\ (g/cm^2/h) = \frac{M_f - M_i}{A_s * \Delta t} \tag{3.17}$$

where M_i is the initial mass (g) of the sample, M_f is the mass (g) of the sample after a duration t (h) of erosion and A_s is the surface area of the sample (cm^2).

The standard scour rate of mm/hr could be determined assuming the clay to be fully saturated to obtain the bulk density. The bulk density of the clay ρ_b (kg/m^3) for a saturated clay is determined using the specific gravity of the grains, S_G, obtained through the specific gravity and density tests (see section 3.3.1) and the moisture content m before testing as:

$$\rho_b = \frac{(1+m)G_S\rho}{1+mG_S} \tag{3.18}$$

The scour rate, or erosion rate, was determined to be:

$$\dot{Z}\ (mm/h) = \frac{M_f - M_i}{\rho_b A_s \Delta t} \tag{3.19}$$

The standard measure for scour was then determined to compare the erosion rate of the samples to the scour rates found in other erosion studies (Shan et al., 2015).

3.4.6 Wet/Dry cycle procedure for erosion tests

To assess the impact of changing water levels in a river and hence of wetting/drying cycles experienced by the clay bank material on their erosion, samples were subject to a wetting/drying cycle before erosion testing. After the samples were tested in their intact condition at *in-situ* moisture content, they were placed on a shelf and allowed to dry at ambient air temperature and humidity for 48 hours (range of temperature: 21-23°C). The samples were then replaced into the mould and subject to a second fluvial erosion test. Before placing the samples in the flume, a thin layer of clay (>10g) was shaved off the top of the sample to measure the moisture content of the surface of the clay after 48 hours of air-drying. The fluvial erosion testing procedure was similar to that performed on the samples in the intact in-situ moisture content condition. However, 30-minute intervals between increases in the applied shear stress were used instead of 2 hours, if there was no significant difference with previous observations in the intact condition and longer time intervals if the behaviour deviated from the previous observations.

3.4.7 Direct measurement of bed shear stress

To directly measure the shear stress applied to the surface of the clay samples, as well as to monitor the change in shear stress over time, a direct shear stress measurements setup using a suspended box and six load cells was developed, as shown in Figure 3-50.

As described in section 3.4.1, the box, in which the samples are mounted, is suspended in a cut-out in the false floor of the flume using four metal cables of 1.2mm diameter, each at a corner of the box, which are attached to four load cells. The cut-out is slightly larger than the box resulting in 2mm gaps on all sides. The cables are adjusted to ensure that the top of the box is flush with the false floor of the flume. The box is thereby hanging 2-5mm above the true floor of the flume allowing the box to move freely in the lateral direction. Two load cells, mounted on plate placed across the downstream side of the cut-out measure the horizontal load from the box using the two bolts which are attached to the load cells, see Figure 3-48 and Figure 3-49.

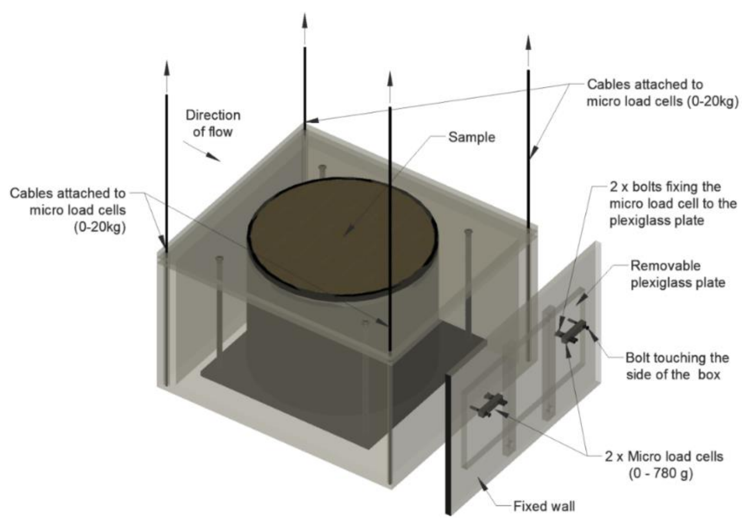

Figure 3-48. Side view of the direct measurement setup

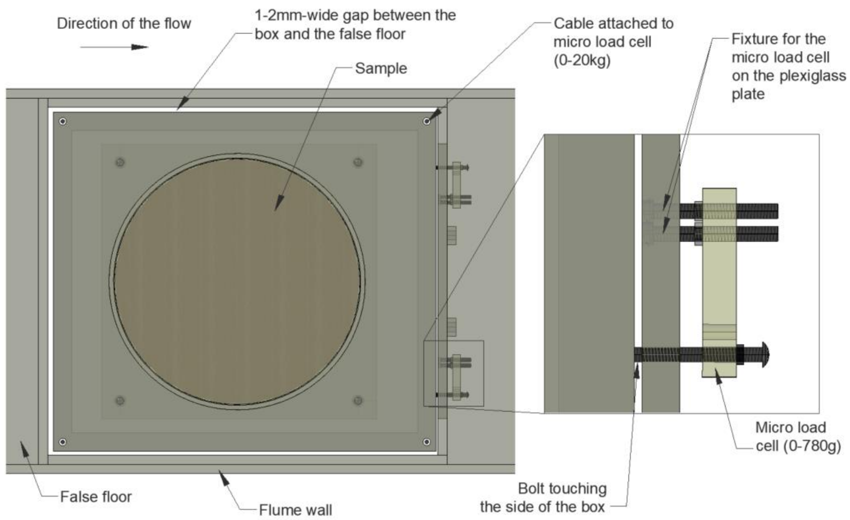

Figure 3-49. Top view of the direct measurement setup

3.4.7.1 Software and hardware of the direct shear stress measurement rig

Real time monitoring of the sample mass was the aim of the four load cells connected to the four cables from which the box hangs. These are micro load cells with a capacity of 0-20kg (Phidgets, 2021a). The two load cells measuring the horizontal forces on the downstream side of the box are micro load cells with a capacity of 0-780g (Phidgets, 2021b). The two load cells located on the downstream side of the box have been waterproofed and are left to dry in between experiments to prevent corrosion. All six micro load cells are connected to Wheatstone bridges (Phidgets, 2021c), which are, in turn, connected to an analog-to-digital converter to relay the signal via a USB connection to a computer (Phidgets, 2021d). Since the erosion test is long and the precision required for the output is in the range of 1g, creep is factored in when considering the output of the sensors. For the micro load cells that are located on top of the box, creep at maximum capacity is around 20g/hour (Phidgets, 2021a) and for the micro load cells mounted downstream from the box creep at maximum capacity is around 1.6g/hour (Phidgets, 2021b). The load cells are calibrated each day before each experiments to avoid any gross errors related to creep.

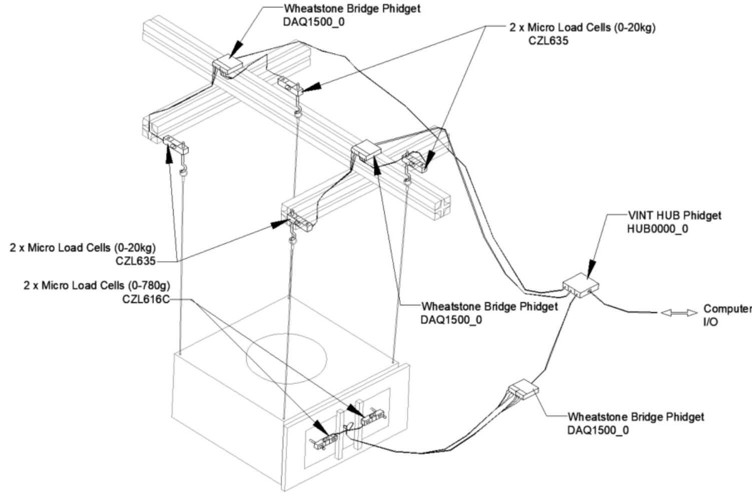

Figure 3-50. General assembly of the sensors used to record lateral and vertical loads in this study

3.4.7.2 Calibration of load cells on direct shear stress measurement rig

The output of the load cells is a voltage, which is calibrated with a standard set of calibrated weights to convert the signal to a mass. The top load cells are calibrated by suspending a known mass from the cables, see Figure 3-53. The side load cells are either calibrated in a dry environment or in a water tank to simulate as closely as possible the conditions in the flume, as shown in Figure 3-51 and 3-52.

The sensors were calibrated daily for each experiment. First the sensors were warmed up for 30 minutes to reach a stable temperature (such that it did not affect the behaviour of the strain gauges). To reduce the time spent calibrating and to ensure that the sensors are always at their running temperature, the sensors are run in parallel, while their outputs are diverted to different channels. The load cells signals were plotted in real-time on the computer with one plot for all sensors as they warmed up, and one plot per sensor for calibration.

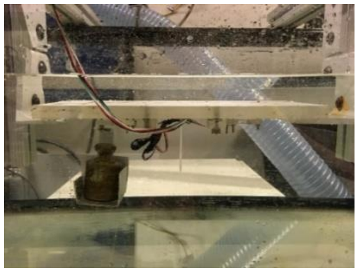

Figure 3-51. Side view of calibration setup of micro load cells (0-780g)

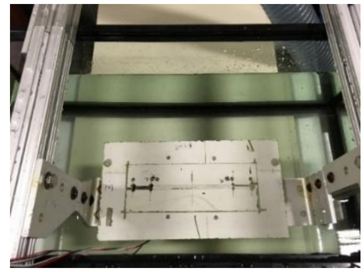

Figure 3-52. Top view of calibration setup of micro load cells (0-780g)

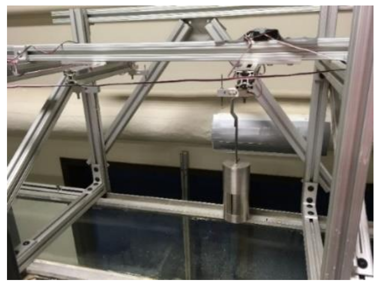

Figure 3-53. Calibration setup of micro load cells (0-20kg)

3.4.7.3 Preliminary tests to calibrate the direct shear stress measurement rig.

To define the error and the precision of the outputs of the sensors, the forces acting on the box setup were assessed in a series of tests. The results of the tests, as load cell outputs, were used to assess the main sources of error/bias, which were the weight of the box and the location of its center of gravity, the skewness of the setup, the ambient temperature and the effect of drag on the cables and forces on the surfaces on the box that are normal to the flow. The free body diagram of the setup in a dry flume is shown in Figure 3-54, in a flume filled up is shown in Figure 3-55 and when water is circulating is shown in Figure 3-56.

In most cases, the component of the weight of the box *W* in the downstream flume direction rapidly exceeded the maximum capacity of the side load cells as the box with a sample weighted between 5 and 9 kg. Therefore, the use of the sensors was limited to zero slope and a slope of 0.010 for samples trimmed down to 4” diameter cores. The issue with measuring shear stresses at slopes as mild as 0-0.010 is that the shear stresses applied on the sediment surface is relatively small compared to the other forces acting on the sensors. For example, the estimated shear stress applied on the sediment surface based on the shear stress obtained from the energy slope for a core of 4”-diameter at low flow (0.0035m^3/s) and high flow (0.0191m^3/s) at zero slope is 0.0024 and 0.008N respectively while at a slope of 0.010 it is 0.024N. Hence, the measurement of shear stress requires a highly sensitive set of sensors and a measurement error at a smaller scale than 0.001N.

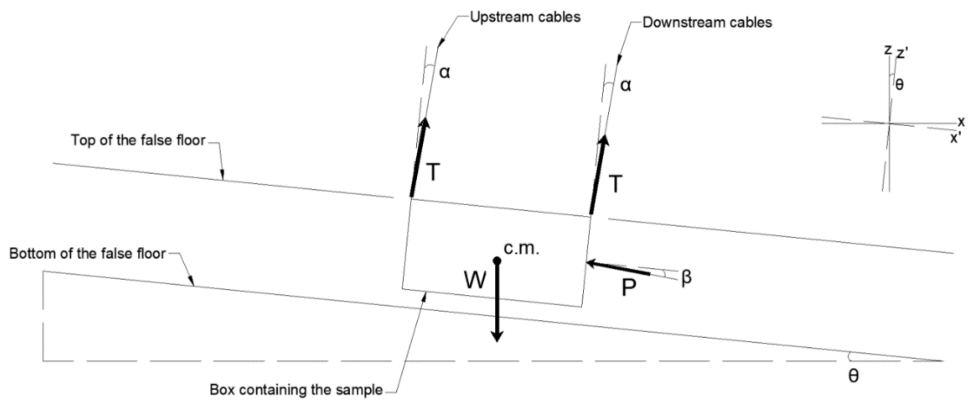

Figure 3-54. Free body diagram of the box setup when the channel is dry

Several forces are introduced in the setup once the flume is filled with water: a buoyancy force F_B acting at the center of mass of the box containing the sample and drag forces D acting on the cables supporting the box once water circulates in the flume. During the installation of the setup, when the box is attached to the load cells and lowered in its hole in the false floor of the flume, the angles of the cables α and the angle at which the box is laid on the side load cells β are unique to each experiment/installation of the box. The effect of the skewness introduced to the box setup during installation is shown in Figure 3-57 and Figure 3-58.

Since the current sensors and box arrangement is underdetermined, a metal plate was mounted on top of the samples to obtain a relative shear stress. This assumes that mounting the plate on the box does not change any of the angles and forces acting on the cables connected to the top load cells. Unfortunately, the difference between the shear stress measured with a clear sediment surface and a metal plate was smaller than the error related to the forces involved in the system and the resolution of the sensors currently used.

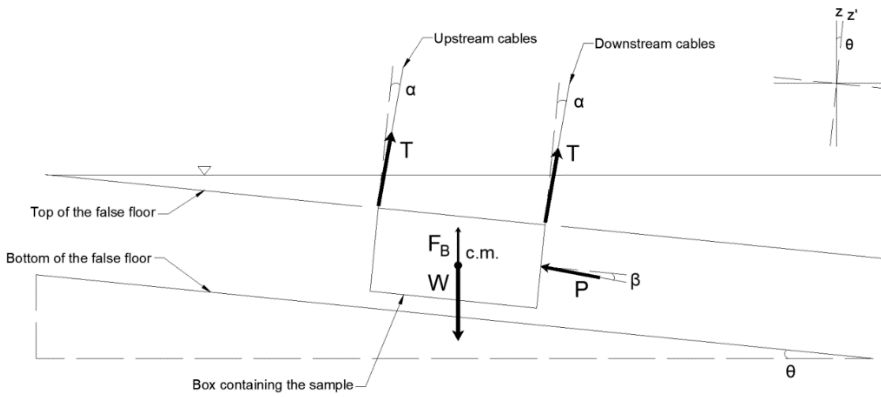

Figure 3-55. Free body diagram of the box setup when the flume acts as a reservoir

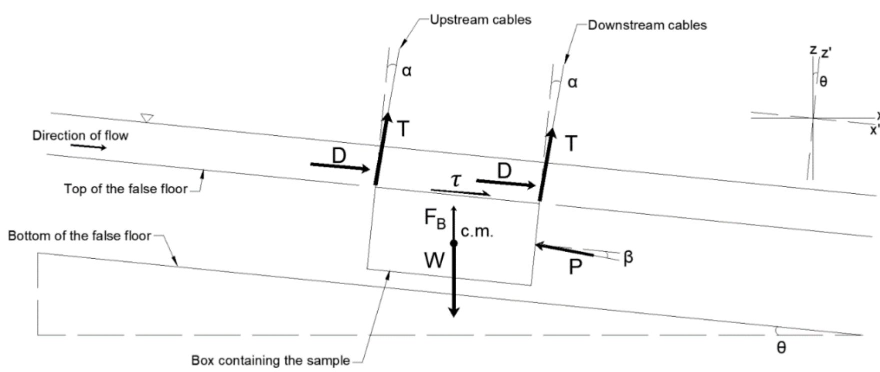

Figure 3-56. Free body diagram of the box setup when water is running in the flume

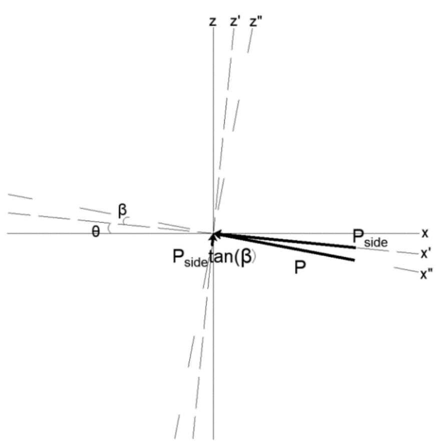

Figure 3-57. Relationship between the point loads applied on the bolts attached to the side micro load cells and the readings of the micro load cells (0-780g)

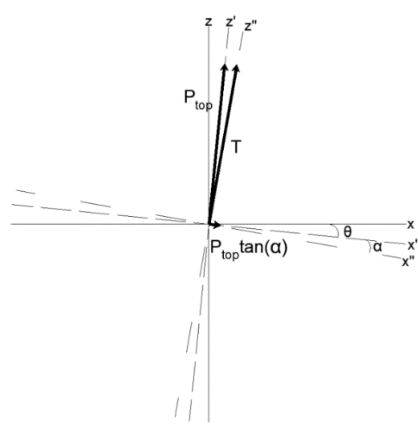

Figure 3-58. Relationship between the tension in the cables and top micro load cells (0-20kg) readings

Temperature also needs to be considered as it affects the voltage output of the side load cells. Temperature biases are only significant on the output readings of the side load cells as they are mounted underneath the false floor of the flume and are submerged, which leads to a greater heat exchange between the sensors and their surrounding medium unlike the load cells located on the top frame. The volume of water located underneath the false floor is not circulating and thus reaches a thermal state of equilibrium after a set amount of time depending on the initial temperature of the water. The error related to the temperature changes on the voltage ratio output of the load cells leads to a greater relative error at low capacity (86% error for an applied load of 0.02N between 8.5°C and 22°C) and an insignificant error at greater capacity (1% error for an applied load of 4.5N between 8.5°C and 22°C). The sensors should be paired with a temperature probe to account for the change in temperature and reduce the error related to temperature fluctuations.

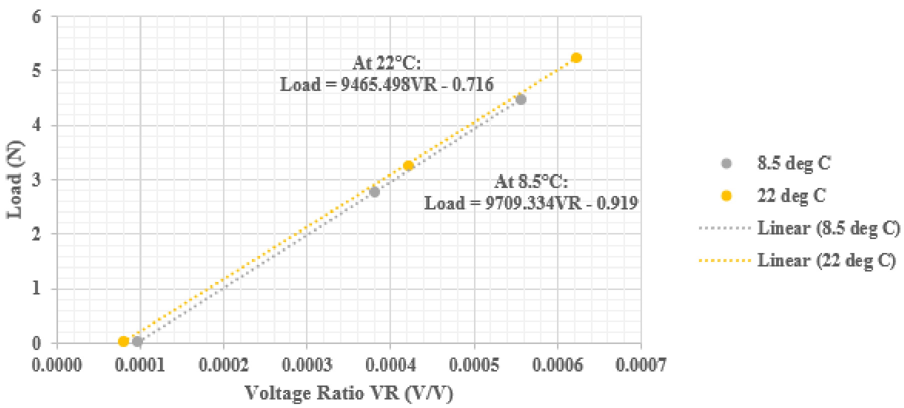

(a)

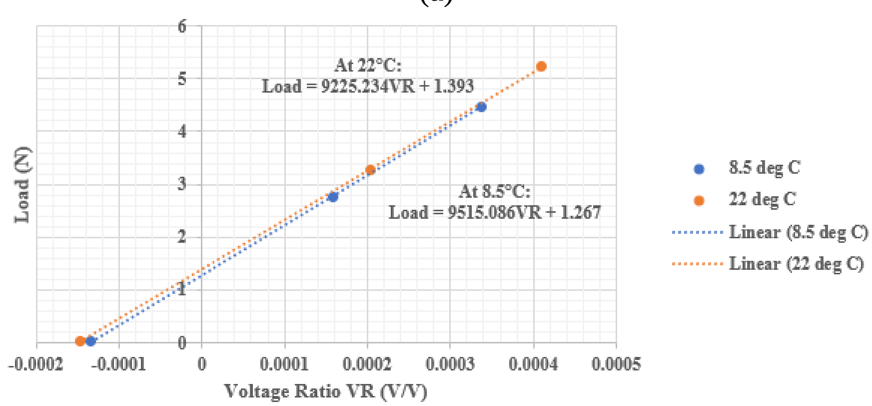

(b)

Figure 3-59. Voltage Ratio and Load relationship based on two different ambient temperatures; (a) Side micro load cell located on the left, (b) Side micro load cell located on the right

3.4.8 Rig to assess the roughness of the eroded sample surface

The roughness of the sample as it underwent erosion was measured using a roughness assessment rig. The roughness was measured before placing the samples in the flume and at a regular intervals of one hour during testing. For each roughness measurement, the samples were weighed and then placed under a Kinect v2 sensor (see Table 3-6 for the technical specifications) to capture a point cloud of the position of their surface, see Figure 3-60 (the description of the sensor is below). The point clouds were used to determine the geometric roughness of the surface of the samples.

The roughness analysis was performed on the surface of each sample at (1) the initial condition after trimming, (2) before reaching critical shear stress, (3) during the first and second hour of erosion at critical shear stress, and (4) at each interval where the shear stress exerted by the eroding fluid was greater than critical shear stress.

Figure 3-60. Weighting setup and Kinect sensor setup

The Kinect v2 sensor is motion sensing device with integrated RGB cameras and depth sensors. Its use is growing in research as it is relatively cheap compared to other depth sensing devices and as Microsoft provides a software development kit (SDK) with PC-compatible drivers for its Kinect devices. The Kinect sensor needs to be calibrated to account for distortions when the data points cover a large area or when there is a range of colors distorting the reflection (Lachat et al, 2015). The distortion was negligible in this application as all the data points where within a 10cm radius from the center of the focus of the sensor. A frame was built to position the sensor 60cm above the surface of the sample, an optimal distance used to obtain a point cloud with a 1.5mm resolution (Roy, 2019).

Table 3-6. Technical specifications of the Microsoft Kinect V2 Sensor (taken from Roy, 2019)

Infrared (IR) Camera Resolution	512 x 424 pixels
RGB Camera Resolution	1920 x 1080 pixels
Field of View	70 x 60 degrees
Framerate	30 frames/second
Operative Measuring Range	From 0.5 to 4.5m
Object Pixel Size (GSD)	Between 1.4mm (at a 0.5m range) and 12mm (at a 4.5m range)

Using Cloud Compare, a 3D point cloud processing software, the surface of each sample was defined and saved for post-processing. The point clouds were then reimported into MATLAB where the *planefit* function (Schmidt, 2021) was used to obtain a fitted 3D plane. The fitted plane was then shifted back to the original X and Y values of the initial point cloud by interpolating the points across the fitted surface to obtain a difference in elevation between the real surface and the fitted surface. An example of the point clouds of the initial surface, the plane fit and the superimposed surfaces are shown Figure 3-61.

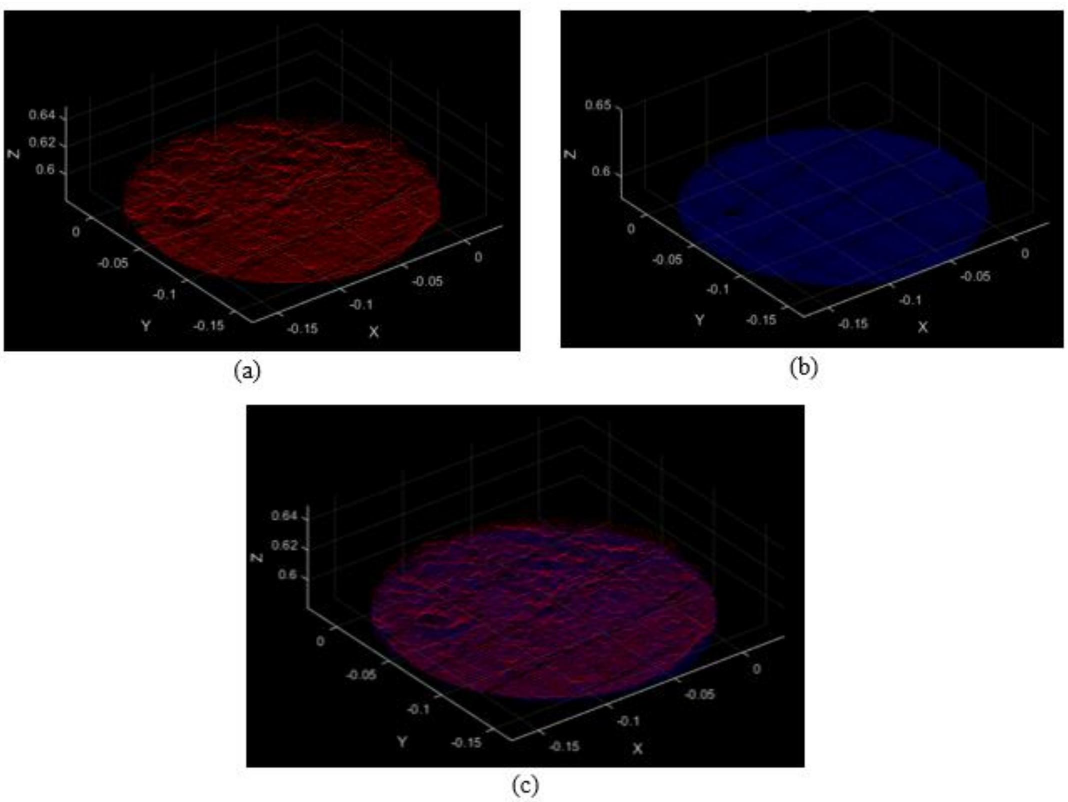

Figure 3-61. Plane fitting over a rough surface; (a) the captured surface, (b) the plane fit, (c) the two layers superimposed

The standard deviation of the difference in elevation (Z values) between the captured surface and the fitted plane then calculated to obtain the geometric roughness across the surface of the samples d_z:

$$d_z = \sqrt{\frac{\sum_{i=1}^{n}(z_{i,captured\,surface} - z_{i,fitted\,plane})^2}{n}} \quad 3.20$$

4 Results

4.1 Geotechnical properties

Standard geotechnical tests were preformed to obtain the physical properties as well as the phase composition of the clays, to determine the sensitivity of the clays and to test their shear resistance to rotation of a blade in a vane shear test. A summary of the results is shown in Table 4-2.

4.1.1 Physical properties

The cohesive sediments sampled displayed a wide range of physical properties in terms of the properties of the clay minerals, density of the clay particles, grain size distribution, plasticity and degree of compaction.

In order to compare the cohesive sediments to each other and to clays studied in previous research, the sediments were classified based (1) on their plasticity index, as defined by Burmister (1949; cited in Wagner, 2013), (2) on their firmness, based on the four stages of compaction distinguished by Van Rijn (2020), (3) on the soil consistencies defined by Dhams and Fritz (1998; cited in Wagner, 2013) and (4) on the type of clay minerals present in the deposits, based on the consistency limits of clay minerals observed by Mitchell and Soga (2005; cited by Wagner, 2013) as well as the activity of the clay minerals defined for pure clays and mixtures (Mitchell and Soga, 2005; Seed et al., 1964; cited in Wagner, 2013).

Table 4-1. Summary of plastic properties of the clays studied

Tributary	Location	Plasticity	Firmness	Consistency	Minerals
Rivière de la Tortue	#1	High plasticity	Firm	Clay, high plasticity	Kaolinite
	#2				

Castor River		High plasticity	Stiff	Clay, medium plasticity	Illite – Kaolinite
Rivière du Nord		High plasticity	Stiff	Clay, high plasticity	Kaolinite/Bentonite
Chelsea Creek, lower		Medium plasticity	Stiff to very stiff	Clay, low plasticity	Kaolinite
Chelsea Creek, upper	#1	Very high plasticity	Medium to firm	Clay, high plasticity	Kaolinite/Bentonite
	#2				
Rivière St-Charles		--	Very stiff	--	--

The clays taken from the upper tributary of Chelsea Creek had a mineral activity corresponding to a mixture of 19:1 kaolinite to bentonite (Seed et al., 1964). Bentonites are expandable minerals with a high plasticity while kaolinites are low plasticity minerals (Wagner, 2013). They were the only clays with a mineral activity categorised as normal while the other clays fell into the low-active or inactive category. None of the clays were deemed to contain significant amounts of active and swelling minerals as they did not behave in an expandable manner.

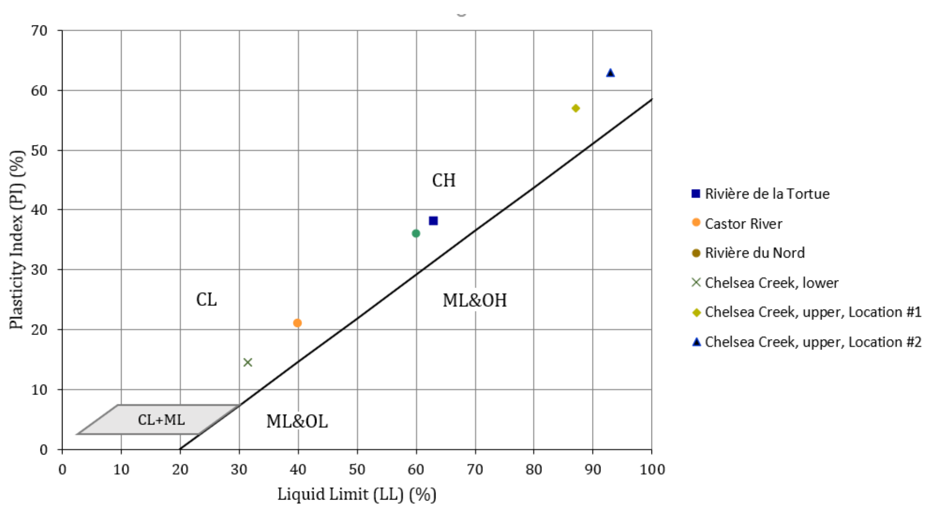

Figure 4-1. Clay classification according to USCS (2012)

The cohesive sediments were also classified according to the Unified Soil Classification System (USCS), which is the classification system most commonly used in soil mechanics, and according to the soil classification of the United States Department of Agriculture (USDA). The classification all the samples (clays), except for the loam (SC) taken at the Rivière St-Charles tributary is shown below in Figure 4-1.

Table 4-2. Summary of results of characterisation tests

Tributary	Sampling technique	Sublayer	G_s	Silt content %	Clay content %	m	L.L.	P.L.	P.I.	L.I.	a_c	USDA	USCS	Fall cone C_u (kPa)	Vane Shear C_u (kPa)	Sensitivity
Rivière de la Tortue	Square mould	Location #1	2.687	18	76	48	60	24	36	67	47	Clay	CH	47	43.0 - 46.2	4.1
	Circular mould	Location #2	2.718	16	74		63	24	39	59	52	Clay / Silty clay	CH	37	47.2 - 49.4	3.8
	Sherbrooke sampler	Location #2	2.668			47	63	26	37	57	50	Clay / Silty clay	CH	44	30.2 - 57.8	2.7
Castor River	Circular mould		2.704	44	52	26	40	19	21	33	40	Silty clay	CL	125	85.2 - 122.2	0.1
Rivière du Nord	Circular mould		2.666	35	56	42	60	24	36	50	65	Silty clay	CH	270	84.8 - 128.2	15.8
Chelsea Creek, lower	Carved	top layer	2.742	39	39	25	33	17	16	50	41	Clay loam	CL	146	154.6	23.3
	Carved	bottom layer	2.748	40	45	29	30	17	13	92	29	Silty clay	CL	106		14.7
Chelsea Creek, upper	Circular mould	Location #1	2.732	31	63	80	87	30	57	88	91	Silty clay	CH	60		13.2
	Carved	Location #2	2.712	36	58	73	93	30	63	68	109	Silty clay	CH	47	18.1 - 41.8	10.6
Rivière St-Charles	Carved		2.724	40	24	17						Loam	SC			

Most sediments were classified as inorganic clays of high plasticity (CH), also called fat clays, which have swelling minerals present in their matrix (Holtz et al., 1956). The cohesive sediments found at the Castor River tributary and the lower tributary of Chelsea Creek were classified as inorganic clays of low to medium plasticity (CL) which is owed to their relatively high silt or sand content. The USDA classification of the cohesive sediments is found in Table 4-2.

4.1.2 Fall cone tests and sensitivity

Fall cone tests were performed on intact and remoulded samples to obtain an estimate of the undrained shear strength of the clays in both states as well as their sensitivity. None of the clays were sensitive enough to be categorised as quick clays, defined by Osterman (1963) as having a sensitivity between 30 and 50. Clays from all sites, except the Rivière de la Tortue tributary and the Rivière St-Charles tributary, were very hard to remould as breaking the clay into blocks and then working into a paste required extensive work. As the cohesive sediments were well cemented, sensitivity could simply be explained by the loss of strength caused by breaking of the crystalline cement bridges formed between the clay grains.

The undrained shear strength of the intact and remoulded clays varied significantly between sites (see Table 4-3). The clays taken at the Rivière de la Tortue had a medium sensitivity with an undrained shear strength varying from 37.4 to 47.2kPa and a remoulded shear strength varying from 9.7 to 16.0kPa. The clay taken at the tributary of Castor River was insensitive as well as having a much lower average penetration rate while being remoulded. This means the clay was more compacted in the remoulded state than in its original form. The clays taken at the Rivière du Nord and a lower tributary of Chelsea Creek had a higher sensitivity ratio ranging from 15.8 and 14.7 to 23.3 respectively. Both sediments had a high undrained shear strength in the undisturbed state, 270.3kPa and 105.9-146.5kPa respectively, and a much weaker remoulded shear strength. The undrained shear strength of the clays taken at the upper tributary of Chelsea Creek varied between 59.9 at location #1 and 46.8kPa at location #2 . Both clays had a similar remoulded strength of 4.4-4.5kPa.

Table 4-3. Sensitivity of the clays as well as undisturbed and remoulded undrained shear strength of the clays

Site	Sampling method	Sublayer	Average penetration (mm) Intact	Average penetration (mm) Remoulded	C_u (kPa)	C_{ur} (kPa)	Sensitivity
Tributary of Rivière de la Tortue	Square mould		9.11	3.92	47.24	11.5	4.11
	Circular mould		5.12	4.26	37.4	9.7	3.84
	Sherbrooke sampler		9.47	3.32	43.7	16.0	2.73
Tributary of Castor River	Circular mould		5.61	0.36	124.6	1401	0.09
Tributary of Rivière du Nord	Circular mould		3.81	3.21	270.3	17.1	15.8
Lower tributary of Chelsea Creek	Carved	bottom layer	6.09	4.96	105.9	7.2	14.7
	Carved	top layer	5.18	5.30	146.5	6.3	23.3
Upper tributary of Chelsea Creek	Circular mould	Location #1	8.09	6.24	59.9	4.5	13.2
	Carved	Location #2	9.15	6.32	46.8	4.4	10.6

4.1.3 Vane shear tests

The vane shear tests were performed on samples from all sites except for the Rivière St-Charles tributary as it was too firm. The undrained shear resistance of all sites varied from 24.2kPa to 154.6kPa. The tests were performed on as many samples as possible for each site to determine a range of shear resistance as variation along the surface crust, the upper most layer of a clay, was to be expected.

Table 4-4. Undrained shear strength of the clays obtained through vane shear tests

Site	Sampling method	Sublayer	# of test(s)	Undrained shear strength S_u (kPa) Mean	Range
Tributary of Rivière de la Tortue	Square mould		4	44.7	43.0 - 46.2
	Circular mould		2	48.3	47.2 - 49.4
	Sherbrooke sampler		5	38.1	30.2 - 57.8
Tributary of Castor River	Circular mould		2	102.0	85.2 - 122.2
Tributary of Rivière du Nord	Circular mould		4	103.3	84.8 - 128.2

Lower tributary of Chelsea Creek	Carved	N/A	1	154.6	
Upper tributary of Chelsea Creek	Circular mould	Location #1	1	41.8	
	Carved	Location #2	2	24.2	18.1 - 41.8

4.1.3.1 Site 1 – Rivière de la Tortue

A total of 11 vane shear tests were performed on blocks of clay taken from three different samples taken from the Rivière de la Tortue tributary. The undrained shear strength proved to be consistent across the three samples as shown in Table 4-4 with a mean varying from 38.1kPa to 48.3kPa. A majority of the specimens failed in clear manner as the clay in proximity to the vane remoulded, as shown in Figure 4-2 but several specimens exhibited slight cracking outside the vane perimeter as shown in Figure 4-4. The difference in failure mode could be explained by the presence of pockets of red silts and sands in the core creating a non-uniform matrix with weaker planes.

Figure 4-2. Clear vane shear failure in a homogeneous clay sample taken at site 1

Figure 4-3. Heterogeneous specimen taken at site 1; presence of pockets of silts and sand

Figure 4-4. Vane shear failure of heterogeneous specimen taken at site 1; presence of cracks across the core after failure

4.1.3.2 Site 2 – Castor River tributary

Two vane shear tests were performed on samples taken at the Castor River tributary. The undrained shear strength ranged from 85.2 to 122.2kPa. The specimen failed in a brittle manner as shown in Figure 4-5, in which several cracks propagated outside the vane perimeter. The clay failed as small blocks failed close to the outer perimeter of the vane.

Figure 4-5. Vane shear failure of a sample taken at site 2

4.1.3.3 Site 3 – Rivière du Nord tributary

Four vane shear tests were performed on samples taken at the Rivière du Nord tributary. The undrained shear strength obtained through the vane shear test differed substantially from the fall cone test as the resistance to vane shear was half that of to the fall cone. The undrained shear strength of the clays varied from 84.8 to 128.2kPa. The clay was brittle and the vane shear test revealed the presence of fissures in the specimen as shown in Figure 4-6 and Figure 4-7. The fissures appear to be cutting the clay in small cubes and the blocks around the perimeter of the vane were broken down into smaller blocks.

Figure 4-6. Vane shear failure

Figure 4-7. Vane shear failure

4.1.3.4 Site 4 – A lower tributary of Chelsea Creek

One vane shear test was performed on the bottom varve of a sample taken at the lower tributary of Chelsea Creek. The undrained shear strength of the varve was the greatest of all the clays studied at 154.6kPa. The sand layer on top of the varve did not affect the undrained shear strength of the specimen. The specimen failed in a clear manner as only the clay around the vane was remoulded after failure as shown in Figure 4-8.

Figure 4-8. Vane shear failure of a thick varve taken at site 4

4.1.3.5 Site 5 – An upper tributary of Chelsea Creek

Three vane shear tests were performed on three specimens from two different locations along the upper tributary of Chelsea Creek. The vane shear test revealed the presence of fissures of random shapes and directions in the clay sample from location #1 as shown in Figure 4-9 to Figure 4-11.

The clay from location #2 had a layered structure and was less sensitive than the clay from location #1. The undrained shear strength of the clays found at both locations was in the same range; one sample obtained at each location had the same undrained shear strength of 41.8kPa. Another sample from location #2 had a much lower undrained shear strength of 18.1kPa as it failed in a more brittle manner as shown in Figure 4-12 where cracks are seen separating the clay layers.

Figure 4-9. Vane shear failure of clay from location #1

Figure 4-10. Complete failure during testing of clay from location #1

Figure 4-11. Vane shear failure of clay from location #1

Figure 4-12. Vane shear failure of clay from location #2

4.2 Fluvial erosion tests

The fluvial erosion tests test two sample conditions: one in which the samples tested are at in-situ moisture content and one in which the samples tested are first left to air-dry in the laboratory for 48 hours. To provide an estimate of the range in values of shear stress and erosion rate from a given site, three samples were tested per site, except for the St-Charles River tributary site for which one sample was tested as it proved more resistant to shear than the upper shear threshold possible in the current flume system and the Rivière de la Tortue tributary site where only two samples were tested from as one sample was retested to validate the results.

Table 4-5. Average critical shear stress and erosion rate for all sites

		Condition: Intact, in-situ moisture content			*Condition: Air-dried for 48 hours*		
Site	Location	Average moisture content *m*	Average critical shear stress τ_{cr}	Average erosion rate at τ_{cr}	Moisture content *m*	Critical shear stress τ_{cr}	Erosion rate at τ_{cr}
		%	Pa	mm/h	%	Pa	mm/h
Rivière de la Tortue tributary	#1	48	4.3	0.07	44	4.2	--
	#2	47	2.6	0.04	--	--	--
Castor River tributary	--	25	2.7	1.42	27	1.9	0.59
Rivière du Nord tributary	--	42	0.8	0.64	43	0.9	0.34
Lower tributary of Chelsea Creek	--	30	0.4 -6.9*	0.16	30	5.4	1.06
Upper tributary of Chelsea Creek	#1	80	0.2	1.3	72	0.2	0.3
	#2	68	>10.4	--	70	>10.9	--
Rivière St-Charles tributary	--	17	>11.5	--	11	0.9	--

* Critical shear stress was 0.4 for samples with thinner varves (<10mm) and higher for samples with thicker varves (>10mm).

4.2.1 Site 1 – Rivière de la Tortue tributary

Two samples taken at the Rivière de la Tortue tributary were tested: one sample taken in a square mould at location #1 and one sample taken with the Sherbrooke sampler at location #2. The sample taken at location #1 was tested at its in-situ moisture content and re-tested after being air-dried for 48 hours. The clay from both locations was slightly supple and heterogeneous as it contained small rocks, red patches of silts and pockets of sand. There were no significant difference in the erosion resistance or erosion mechanisms between the intact and the drier state, although it is noted that the moisture content only decreased from 48 % to 46%. As the depths were not recorded during the first test, the benchmark values were used to estimate the shear stress above the sample.

Table 4-6. Summary of critical shear stress and erosion rates for samples collected at the Rivière de la Tortue tributary

Sample	m	Critical shear stress τ_{cr}	Erosion rate at τ_{cr}		
	%	Pa	g/h	g/cm^2/h	mm/h
Condition: Intact, in-situ moisture content					
Square mould	49	4.2 ± 0.3†	6.5	0.019	0.11
Square mould (repeated)	47	4.4 ± 0.5	2.5	0.007	0.04
Sherbrooke sampler	47	2.6 ± 0.5	2.0	0.024	0.14
Condition: Air dried for 48 hours					
Square mould	44	4.2 ± 0.6	--	--	--

†Missing values; Shear stress obtained through benchmark tests

The sample collected at location #1 was the first sample to be tested in the flume. The sample was exposed to a minimum of two hours of flow at the eight standard bed shear stresses used in this study. Mass erosion (blocks >2mm) started to occur at 4.2Pa and continued at a constant rate of 0.019g/cm^2/h. The erosion rate increased to 0.027g/cm^2/h once a shear stress of 7.4Pa was reached at slope of 0.046. Blocks of 12-18mm diameter were eroding from the surface but were more likely to detach from the edges. The size of the blocks eroding remained the same even as the shear stress increased. At the maximum shear stress possible in the flume of 9.0Pa and the erosion rate reached a peak of 0.029g/cm^2/h.

As this was the first fluvial erosion trial in the flume, the sample was tested a second time to check for repeatability. Under 2.8Pa of shear stress (a lower slope than the previous threshold for critical shear stress), large blocks (>6mm) eroded during the first hour, but no significant erosion occurred in the second hour. Once the flume setup reached 4.4Pa, blocks started eroding uniformly across the surface at lower rate of 0.007g/cm^2/h. The blocks were of a similar size to those previously eroded during the first erosion test. This (4.4Pa) was determined as the critical shear stress.

(a) (b) (c) (d)

Figure 4-13. Erosion test with sample collected in a square mould at the Rivière de la Tortue tributary, at location #1; (a) Sample before erosion tests; (b) Sample after 2 hours of mass erosion; (c) Sample after 13.6 hours of mass erosion; (d) Eroded blocks due to mass erosion

(a) (b) (c)

Figure 4-14. Second erosion test with sample collected in a square mould at the Rivière de la Tortue tributary, at location #1; (a) Sample before erosion tests; (b) Sample after 2 hours of mass erosion; (c) Eroded blocks due to mass erosion

The sample collected at location #2 with the Sherbrooke sampler had a more uniform and smoother surface. It also behaved in a more brittle manner during erosion. Mass erosion started to occur at a shear stress of 2.6Pa (slope of 0.010) at a rate of 0.024g/cm^2/h. A network of cracks started to propagate visible at the surface. The erosion rate increased significantly as the shear stress was increased, reaching a rate of 0.185g/cm^2/h at a shear stress of 4.6Pa. The erosion test was stopped at this point. Erosion had occurred from the entire the surface, but to a greater extent near one of the sides where a layer of coarser sediments was exposed, as shown in Figure 4-15 below.

(a) (b) (c)

Figure 4-15. Erosion test with sample collected with the Sherbrooke sample at the Rivière de la Tortue tributary, at location #2; (a) Sample before erosion tests; (b) Sample after 2 hours of mass erosion; (c) Eroded blocks due to mass erosion

There was no significant change in the erosion behaviour of the sample taken at location #1 after it was allowed to dry for 48 hours, likely due to the small decrease in moisture content at its surface from 47 to 44%. Critical shear stress was reached at 4.2Pa when blocks of 6-12mm diameter started to erode. The weight of the sample slightly increased as recorded at a regular 30-minute intervals, which suggests absorption of water by the sample. Erosion was visually observed and blocks were collected at each time interval to follow the progression of the erosion.

(a) (b) (c)

Figure 4-16. Erosion test with sample collected in a square mould at the Rivière de la Tortue tributary, at location #1, after being air dried for 48 hours; (a) Sample before erosion tests; (b) Sample after 2 hours of mass erosion; (c) Sample after 13.6 hours of mass erosion; (d) Eroded blocks due to mass erosion

4.2.2 Site 2 – Castor River tributary

Three samples from the Castor River tributary were tested at in-situ moisture content, while one sample was tested after being air-dried for 48 hours. Unlike the other samples, preservation of the in-situ properties was imperfect for this site as the samples contained pockets of sand resulting in unevenly distributed moisture loss during storage. The drier clay parts were discarded during sample preparation. The sample used for geotechnical testing was the least disturbed of all the three samples as it contained only small pockets of sand. All three samples had a critical shear stress of 2.5-3.0Pa, and erosion was observed. The erosion resistance of the sample with pockets of sand decreased after being air-dried, as shown by the critical shear stress reducing from 3.0 to 1.9Pa.

Table 4-7. Summary of critical shear stress and erosion rates for samples collected at the Castor River tributary

Sample	m	Critical shear stress τ_{cr}	Erosion rate at τ_{cr}		
	%	Pa	g/h	g/cm^2/h	mm/h
Condition: Intact, in-situ moisture content					
#1	24	2.5 ± 0.5	22.5	0.275	1.36
#2 used also for geotechnical tests	27	3.0 ± 0.6	23.7	0.290	1.47
#3	25	2.7 ± 0.6	117.6	1.439	7.16
Condition: Air dried for 48 hours					
#2 used also for geotechnical tests	27	1.9 ± 0.5	9.6	0.118	0.59

Sample #1 exhibited different phases of erosion, initially small plates detached from the surface at 0.3Pa, while a constant rate of mass erosion started at 2.5Pa. The erosion of material started at the sample edges and progressed inwards and, by a shear stress of 5.2Pa, the core of the sample had split into three larger pieces. One of these loose pieces eroded at that point, as there was enough lift forces in the flow to erode it as an alluvial particle.

Sample #3 had cracks throughout, but erosion started at a similar shear stress as for the other two samples. As shown in Figure 4-18, larger blocks remained intact before the sample was placed in the flume. At a shear stress of 2.7Pa, smaller (<12mm) and larger blocks (>60mm), originating from a larger piece, were lifted away from the sample by the flow.

(a) (b) (c) (d)

Figure 4-17. Erosion test with sample #1 collected at the Castor River tributary; (a) Sample before erosion tests; (b) Sample after 2 hours of mass erosion; (c) Sample after 6 hours of mass erosion; (d) Eroded blocks due to mass erosion

(a) (b) (c)

Figure 4-18. Erosion test with sample #3 collected at the Castor River tributary; (a) Sample before erosion tests; (b) Sample after 2 hours of mass erosion; (c) Eroded blocks due to mass erosion

Sample #2 (also used for the geotechnical tests) eroded at a shear stress under 3.0Pa at a similar rate as sample #1 (0.290g/cm^2/h). As shown in Figure 4-19, the surface of the sample was intact and smooth before being placed in the flume. At the critical shear stress, mass erosion (smaller blocks <12mm) occurred across the entire surface, but at a greater rate in the center of the sample, away from the edges. The erosion mechanism differed as blocks were not already delineated by cracks unlike other samples.

(a) (b) (c)

Figure 4-19. Erosion test sample #2 (also used for geotechnical tests) collected at the Castor River tributary; (a) Sample before erosion tests; (b) Sample after 2 hours of mass erosion; (c) Eroded blocks due to mass erosion

After testing at in-situ moisture content, sample #2 was left to dry for 48 hours and re-tested. Even though the moisture content measured at the surface of the sample remained the same, the clay started to erode at a constant rate under the lower shear stress of 1.9Pa. The eroded blocks were roughly the same size as in the previous test. As erosion had already occurred and left sharper edges at the center, it is possible that the uneven surface had a greater effect on the erosion resistance of the clay than the drying. As shown in Figure 4-20, the center troughs deepened during the second test on the sample.

(a) (b) (c)

Figure 4-20. Erosion test with the geotechnical sample collected at the Castor River tributary after being air dried for 48 hours; (a) Sample before erosion tests; (b) Sample after 2 hours of mass erosion; (c) Eroded blocks due to mass erosion

4.2.3 Site 3 – Rivière du Nord tributary

Two samples collected at the Rivière du Nord tributary were subject to fluvial erosion tests. One sample was cut into two halves to provide an additional sample. Three tests were performed on intact samples at in-situ moisture content, while only one was used to observe the effect of air-drying. The samples had a low critical shear stress of 0.8-0.9Pa. As observed during sample preparation, all the samples appeared to be fissured. There was no significant difference between the erosion mechanisms and critical shear stress of the in-situ moisture content sample and that exposed to the air for 48 hours.

Table 4-8. Summary of critical shear stress and erosion rates for samples collected at the Rivière du Nord tributary

Sample	m	Critical shear stress τ_{cr}	Erosion rate at τ_{cr}		
	%	Pa	g/h	g/cm^2/h	mm/h
Condition: Intact, in-situ moisture content					
#1	42	0.8 ± 0.4	13.7	0.167	0.94
# 2 top (used geotechnical tests)	42	0.9 ± 0.3	9.6	0.118	0.66
#2 bottom	41	0.8 ± 0.4	4.7	0.058	0.32
Condition: Air dried for 48 hours					
#2 bottom	43	0.8 ± 0.3	4.9	0.060	0.34

Sample #1 was the most fissured sample of the two samples used in the erosion tests. Sample preparation was challenging as cutting the sample to size by shaving it broke the surface of the sample into smaller blocks. The core of the sample appeared to be intact and was deemed appropriate for testing. Particle erosion occurred at the lowest shear stress (0.2Pa) removing the loose material from the surface and leaving an irregular surface of blocks, while mass erosion occurred at 0.8Pa when the flow forces were large enough to erode blocks of roughly 12mm in diameter, which was identified as the critical shear stress.

(a) (b) (c) (d)

Figure 4-21. Erosion test with sample #1 collected at the Rivière du Nord tributary; (a) Sample before erosion tests; (b) Sample after 2 hours at 0.7Pa; (c) Sample after 2 hours at 0.8Pa; (d) Eroded blocks due to mass erosion

The two halves of sample #2 eroded in a similar manner with a critical shear stress of 0.8-0.9Pa. The core of the samples appeared to be more intact than sample #1. Erosion occurred uniformly across the surface of the top half at a rate of 0.118g/cm^2/h with the erosion of blocks of 2-6mm in thickness. However, erosion occurred mainly at the edge of the sample in the bottom half, as a large region remained intact, at half the rate of that of the top half (0.058g/cm^2/h), but with slightly larger blocks eroded. Cracks started to form at 0.2Pa. Lastly, air-drying for 48 hours did not affect the erosion behaviour of the bottom half sample. Under the same conditions, the sample eroded at the same rate ($0.060 g/cm^2/h$).

(a) (b) (c)

Figure 4-22. Erosion test with the top half of the geotechnical sample collected at the Rivière du Nord; (a) Sample before erosion tests; (b) Sample after 2 hours of mass erosion; (c) Eroded blocks due to mass erosion

(a) (b) (c)

Figure 4-23. Erosion test with the bottom half of the geotechnical sample collected at the Rivière du Nord; (a) Sample before erosion tests; (b) Sample after 2 hours of mass erosion; (c) Eroded blocks due to mass erosion

(a) (b) (c)

Figure 4-24. Erosion test with the bottom half of the geotechnical sample collected at the Rivière du Nord tributary after being air dried for 48 hours; (a) Sample before erosion tests; (b) Sample after 2 hours of mass erosion; (c) Eroded blocks due to mass erosion

4.2.4 Site 4 – A lower tributary of Chelsea Creek

Three samples collected at a lower tributary of Chelsea Creek were tested intact at in-situ moisture content, two of which were tested again after being air-dried for 48 hours. All the samples were carved from natural steps in the tributary and consisted of varying thicknesses of varves of clay interlaid with sands or silts. The main factor affecting the erosion resistance of the varved clays was the thickness of the layers; the thinner layers of 1-2mm thickness, eroded at a shear stress of 0.2Pa, while the thicker layers of 22-28mm thickness, eroded at 5.8 and 8Pa. The moisture contents of all three samples were between 27 to 32%. There was no observable difference between the erosion behaviour of the intact in-situ moisture content samples and the samples that were allowed to dry, noting that drying did not reduce the moisture content.

Table 4-9. Summary of critical shear stress and erosion rates for samples collected at a lower tributary of Chelsea Creek

Sample	m	Critical shear stress τ_{cr}	Erosion rate at τ_{cr}		
	%	Pa	g/h	g/cm^2/h	mm/h
Condition: Intact, in-situ moisture content					
#6	27	5.8 ± 0.9	3.0	0.009	0.04
#7	30	8.0 ± 1.3	5.4	0.016	0.08
#9	32	0.4 ± 0.2	24.0	0.069	0.36
Condition: Air dried for 48 hours					
#6	30	<7.8 ± 1.5	28.0	0.080	0.41
#9	29	2.9 ± 0.4	117.0	0.334	1.7

Sample #6 had the thickest varves of all the samples tested with a top layer of 28mm sitting on another 22mm-thick layer. As shown in Figure 4-25, blocks of <6mm diameter detached from the top layer at approximately 5.8Pa in a consistent but slow erosion rate of 0.009g/cm^2/h. With increasing shear stress increments at intervals of 2 hours up to a maximum level of 10.1Pa, the erosion patterns remained similar. The main core of the sample remained intact and there were no sign of separation between the varves.

(a) (b) (c)

Figure 4-25. Erosion test with sample #6 collected at lower tributary of Chelsea Creek; (a) Sample before erosion tests; (b) Sample after 2 hours of mass erosion; (c) Eroded blocks due to mass erosion

Sample #7 contained two thicker varves separated by a thin layer of sand (<1mm) with a 22mm-thick varve on top of a 26mm-thick varve. Subject to fluvial erosion, the edge of the top layer started to erode at 6.6Pa, but general mass erosion only started to occur at 8.8Pa. As shown in Figure 4-26, large pieces ranging from 6 to 24mm diameter were detached from the surface and were eroded away, while a very large piece was detached from the clay but was not carried away by the flow. Sample #7 eroded in a more brittle manner than sample #6 at the same shear stress.

(a) (b) (c)

Figure 4-26. Erosion test with sample #7 collected at lower tributary of Chelsea Creek; (a) Sample before erosion tests; (b) Sample after 2 hours of mass erosion; (c) Eroded blocks due to mass erosion

Sample #9 contained thinner layers of clay tightly overlaid that eroded at a low shear stress of 0.4Pa. Samples eroded at the trimmed edges and progressed inwards; plates, instead of blocks, first in the outer layer eroded and subsequently in the layers located near the surface were eroded. The top layer shown in picture (a) in Figure 4-27 was first broke into pieces, which were then washed away after 2 hours of erosion at 0.4Pa. The detached plates ranged between 2mm and 6mm in a diameter, while the erosion rate was constant at 0.069g/cm^2/h.

(a) (b) (c)

Figure 4-27. Erosion test with sample #9 collected at a lower tributary of Chelsea Creek; (a) Sample before erosion tests; (b) Sample after 2 hours of mass erosion; (c) Eroded blocks due to mass erosion

Samples #6 and #9 were air-dried for 48 hours and re-tested. These two samples were more resistant to erosion in the second trial. As the moisture content on the surface of the samples did not decrease significantly, other factors such as the thickness of the varves, a reduced exposure to environmental damage could be the cause of an increase in erosion resistance.

For sample #6, some erosion (<2mm) occurred at 2.9Pa, no visible erosion occurred at 5.4Pa and constant mass erosion (>2mm) occurred at 7.8Pa with a mass erosion rate of 0.334g/cm^2/h. The mass erosion occurred closer to the edges of the top layer and larger blocks eroded as shown in Figure 4-28.

(a) (b) (c)

Figure 4-28. Erosion test with sample #6 collected at a lower tributary of Chelsea Creek after being air dried for 48 hours; (a) Sample before erosion tests; (b) Sample after 2 hours of mass erosion; (c) Eroded blocks due to mass erosion

The thinner layers of sample #9 eroded at 0.9Pa as shown in picture (c) in Figure 4-29, while a thicker mass eroded at 2.9Pa as shown in picture (d). Cracks appeared at 2.9Pa and while some pieces were broken off from the sample at 0.9Pa, there were only carried away by the flow at 2.9Pa.

(a) (b) (c) (d)

Figure 4-29. Erosion test with sample #9 collected at lower tributary of Chelsea Creek after being air dried for 48 hours;; (a) Sample before erosion tests; (b) Sample after 2 hours of mass erosion; (c) Eroded blocks after 1 hour of mass erosion at 0.9Pa ; (d) Eroded blocks after 40 minutes of mass erosion at 2.9Pa

Three samples from two locations were tested from the lower tributary of Chelsea Creek. At one location, one sample was tested only in the intact in-situ moisture content condition, while one was tested only after leaving the sample to dry for 48 hours. At a second location, a third sample was tested under both conditions. There was no significant change in erosion resistance behaviour before and after allowing the samples to dry.

Table 4-10. Summary of critical shear stress and erosion rates for samples collected at an upper tributary of Chelsea Creek, Location #1

Sample	m	Critical shear stress τ_{cr}	Erosion rate at τ_{cr}		
	%	Pa	g/h	$g/cm^2/h$	mm/h
Condition: Intact, in-situ moisture content					
#7	80	0.2 ± <0.1	16.3	0.200	1.3
Condition: Air dried for 48 hours					
#7	72	0.2 ± <0.1	4.2	0.051	0.3

Table 4-11. Summary of critical shear stress and erosion rates for samples collected at an upper tributary of Chelsea Creek, Location #2

Sample	m	Critical shear stress τ_{cr}	Erosion rate at τ_{cr}		
	%	Pa	g/h	$g/cm^2/h$	mm/h
Condition: Intact, in-situ moisture content					
#2	68	> 10.4*	--	--	--
Condition: Air dried for 48 hours					
#4	70	>10.9*	--	--	--

* Critical shear stress was higher than the maximum bed shear stress possible in the flume.

Sample #7, collected at location #1, showed signs of fissuration at its surface during sample preparation; the outer perimeter of the sample was desiccated with small blocks detaching from the main core. Small roots were also present in the sample. The sample eroded at a shear stress of 0.2Pa with large blocks, as large as 30x18x2mm, eroding in a random manner across the entire surface as shown in Figure 4-30. The blocks seemed to be detaching from the core from irregular, larger and smaller, failure planes as shown in (d) in Figure 4-30. The fissuration was irregular than the desiccation found on the outer edges of the untrimmed sample after the wax was removed.

There was no significant difference between the erosion behaviour of the intact in situ moisture content sample and the sample after being air-dried for 48 hours, although the moisture content at the surface of the sample dropped from 80 to 72%. Mass erosion occurred at 0.2Pa in both cases. Overall smaller blocks eroded during the second test ranging in size between 6 and 12mm in diameter.

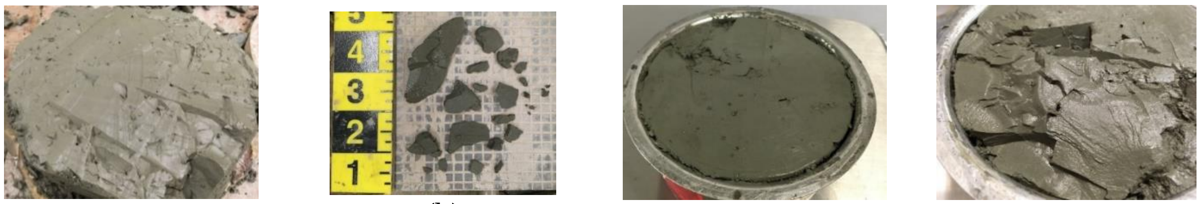

(a) (b) (c) (d)

Figure 4-30. Erosion test with sample #7 of an upper tributary of Chelsea Creek, collected at location #1; (a) Sample during sample preparation; (b) Eroded blocks from mass erosion; (c) Sample before erosion tests; (d) Sample after 2 hours of mass erosion

(a) (b) (c)

Figure 4-31. Erosion test with sample #7 of an upper tributary of Chelsea Creek after being air-dried for 48 hours; (a) Sample before erosion tests; (b) Sample after 2 hours of mass erosion; (c) Eroded blocks due to mass erosion

Sample #2, collected from location #2, did not erode after having been subject to fluvial erosion at 10 intervals of two hours at increasing shear stress up to the maximum possible in the flume of 10.4Pa. The sample did not change during testing, no cracks or any form of erosion was present on the surface of the sample. The clay was homogeneous and there were no signs of any weaker planes while trimming the clay during sample preparation as shown in Figure 4-32.

(a) (b) (c) (d)

Figure 4-32. Sample #2 of an upper tributary of Chelsea Creek, collected at location #2; (a) Sample during sample preparation; (b) Block detached from core during sample preparation; (c) Sample before erosion tests; (d) Sample after 15.4h of erosion tests with no visible erosion

During removal of sample #2 from the mould at the end of the first experiment, the clay was accidently damaged. Another sample from the second location was used to perform the erosion test on an air-dried sample. There was no significant decrease in moisture content between sample #2 at in-situ moisture content and sample #4 after being air-dried. Sample #4 behaved in a similar manner to sample #2 during the erosion test as no general erosion occurred from the surface up to the maximum shear stress of 10.9Pa. The trimming of the sample created edges close to the rim of the mould. At a shear stress of 7.6Pa, one large block detached (42x36x36mm) from the sample as shown in Figure 4-33. As this was an isolated event and no other erosion occurred, it is assumed that a weaker plane in the sample allow the block to detach, and thus, it was not representative of the general erosion behaviour. This was confirmed as when the shear stress was increased to 10.9Pa, there as no other visible sign of erosion on the surface or in the hole left by the detached block.

(a) (b) (c)

Figure 4-33. Erosion test with sample #4 of an upper tributary of Chelsea Creek after being air-dried for 48 hours; (a) Sample before erosion tests; (b) Sample after 2 hours of mass erosion; (c) Eroded blocks due to mass erosion

4.2.5 Site 6 – Rivière St-Charles tributary

Only one sample collected at the Rivière St-Charles tributary was tested as there were no signs of erosion after a cumulative period of two hours under incrementally increasing bed shear stress up to maximum of 11.5Pa. The sample contained black turbidites within a coarser brown matrix. Sea shells were present in the matrix of the clay loam. As shown in Figure 4-34 below, no visible erosion or changes occurred throughout the erosion tests.

Table 4-12. Summary of critical shear stress and erosion rates for samples collected at the Rivière St-Charles tributary

Sample	m	Critical shear stress τ_{cr}	Erosion rate at τ_{cr}		
	%	Pa	g/h	g/cm^2/h	mm/h
Condition: Intact, in situ moisture content					
#1	17	> 11.5*	--	--	--
Condition: Air dried for 48 hours					
#1	11	0.9 ± 0.3	--	--	--

* Critical shear stress was higher than the maximum bed shear stress possible in the flume.

(a) (b)

Figure 4-34. Erosion test with a sample from the tributary of Rivière St-Charles; (a) Sample before erosion tests; (b) Sample with no visible erosion after reaching the maximum bed shear stress of the flume

The air-dried sample had a similar texture, while dry, before being placed in the flume and the moisture content had decreased from 17% to 11%. Once the sample was re-wetted by being placed in the flume most of its surface particles behaved in a cohesionless manner due to slaking of the material. Particle erosion occurred homogeneously across the surface of the sample at 0.2Pa while mass erosion started to occur at 0.9Pa. Even though there were clear signs of erosion due to the turbidity of the water downstream from the sample and the evidence of eroded blocks (of 2-6mm diameter), the mass of the sample increased over time when weighed at 60-minute intervals. This indicates that the sample was reabsorbing water during the test. As shown in Figure 4-35, the sample had heaved during the test and cracks had formed across the surface. The heaved sample had softer consistency and applying pressure to the surface resulted in it releasing water similarly to a sponge. The decreased in erosion resistance seen with air-drying was the greatest with this sample as compared to other samples.

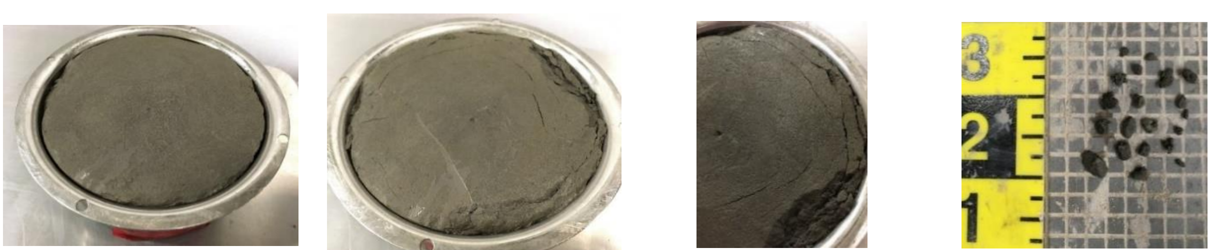

(a) (b) (c) (d)

Figure 4-35. Erosion test with a sample from the tributary of Rivière St-Charles after being air dried for 48 hours; (a) Sample before erosion tests; (b) and (c) Sample after 2 hours of mass erosion ; (d) Eroded blocks after 2 hours of mass erosion

4.3 Surface roughness of the samples after fluvial erosion

Surface roughness measurements of the sample surfaces were taken at a one-hour interval during the erosion tests to capture the change in roughness at a shear stress lower than the critical shear stress, at critical shear stress and at a shear stress greater than critical shear stress (see Appendix B). The change over time was observed and analysed for clay samples from all sites. The geometric roughness was plotted against a normalised shear stress, the ratio of acting shear stress over the critical shear stress, to observe the change in roughness as the shear stress was incrementally increased (see Figure 4-36 to Figure 4-39). As the samples from site 5 and site 6 either did not erode or eroded at a very low shear stress, the results are not displayed below but in Table 9-20, Table 9-23, Table 9-24 and Table 9-25 in Appendix B. It is important to note that roughness was taken as the standard deviation between the surface of the sample and a plane best fitted to that surface over time which means that as particles and blocks eroded the best fitted plane followed the average elevation change. In other words, the roughness represents the overall difference in elevation across the sample and not the difference in elevation between the initial surface and the current surface of the sample.

The general trend is an increase in roughness over time as the shear reached critical shear stress. For the case of the Rivière du Nord tributary where the clay was fissured and the critical shear stress was reached at 0.8-0.9Pa, surface erosion smoothed the surface either before or as the shear stress reached the critical threshold. Particles had eroded at 0.4Pa leaving blocks exposed but the force of the fluid flow was not sufficient to transport the blocks away. Hence, once the critical threshold was reached, blocks eroded resulting in a reduced roughness of the surface occurring during the first hour of erosion followed by a roughening occurring during the second hour of erosion as shown in Table 4-13. Roughening and smoothening also occurred on samples from a lower tributary of Chelsea Creek as the varves of clay eroded in a plate-like manner leaving parts of the varves intact until the entire layer eroded. The samples from the Rivière de la Tortue tributary increased their surface roughness during the first hour of erosion under critical shear stress, which was followed by a reduction in surface during the second hour of erosion. Lastly, the samples from the Castor River tributary increased their surface roughness as shear stress increased as blocks detached from the surface of the clay.

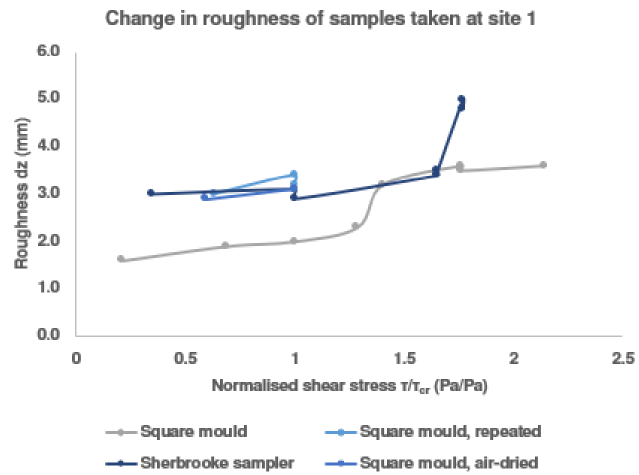

Figure 4-36. Change in surface roughness of samples taken at site 1 – Rivière de la Tortue tributary

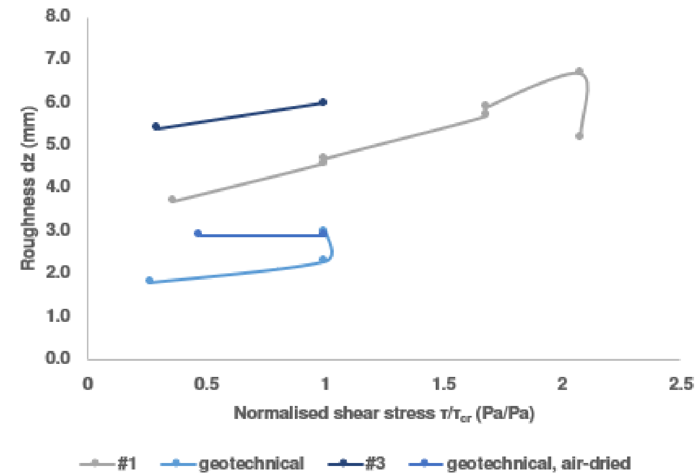

Figure 4-37. Change in surface roughness of samples taken at site 2 – Castor River tributary

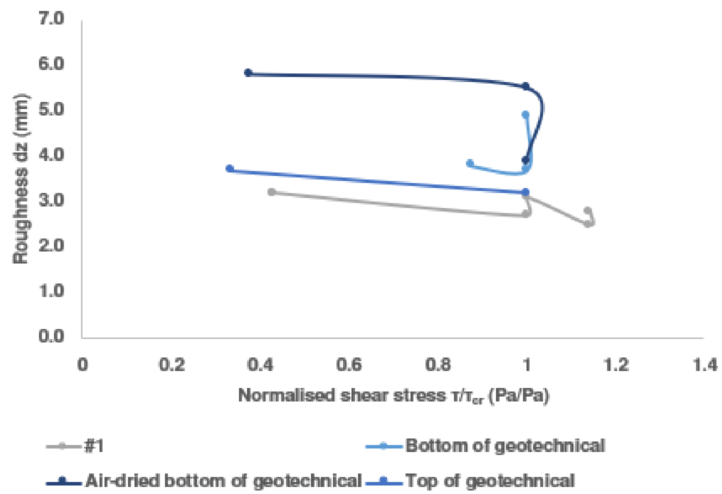

Figure 4-38. Change in surface roughness of samples taken at site 3 – Rivière du Nord tributary

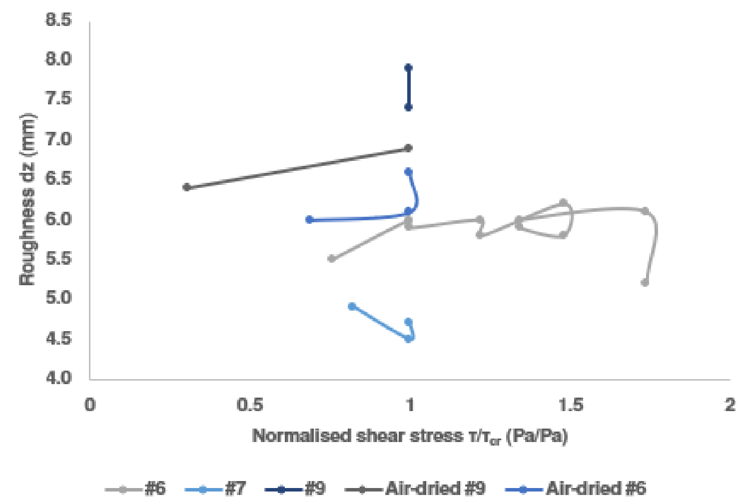

Figure 4-39. Change in surface roughness of samples taken at site 4 – a lower tributary of Chelsea Creek

Table 4-13. Change in roughness under critical shear stress after one and two hours of erosion

Site	Sample	Location	Δdz (mm) at τ_{cr}	
			1 hour	2 hours
Rivière de la Tortue	Square mould	#1	--	0.1
	Square mould	#1	0.4	-0.2
	Sherbrooke sampler	#2	0.1	-0.2
Castor River	#1		0.9	0.1
	Geotechnical		0.5	0.7
	#3		0.6	--
Rivière du Nord	#1		-0.5	0.4
	Geotechnical bottom		-0.1	1.2
	Geotechnical top		-0.5	--
Lower tributary of Chelsea Creek	#6		0.5	-0.1
	#7		-0.4	0.2
	#9		1.1	-0.5
Upper tributary of Chelsea Creek	#7		-0.2	0.2

Another important observation to note is that the rate at which the roughness changed over time did not change as the shear stress increased above the critical threshold. Also, as shown in Figure 4-36 to Figure 4-39 for the samples that were tested for excess shear stress, the roughness of the samples seems to have a reached a plateau after several hours of erosion, which suggests that an equilibrium is reached between smoothening and roughening of the samples.

5 Discussion

Post-glacial clays commonly form the banks and beds of rivers in the region, but literature on the erosion properties of local deposits is almost non-existent. The main objective of this research was, therefore, to provide more details on the spatial distribution of different post-glacial clays found in the St-Lawrence and the Ottawa River valleys and the range in their properties. To achieve this, six undisturbed samples of cohesive river deposits of different geologic origins were obtained to compare and assess the erosion resistance of the clays and to determine if there were any correlations between geotechnical properties and erosion resistance that could help in the design of erosion mitigation measures. The erosion mechanisms, critical shear stress and erosion rate of six cohesive sediment deposits (five clays, one clay loam) with distinct characteristics were successfully observed and compared. No general trends were discernable to predict the erosion behaviour of post glacial clays from the St-Lawrence and the Ottawa River valleys.

The most interesting results from this research concern the two key features of the clays found in the region: the internal structure of the clays and the presence of cementation. Cementation is a common characteristic found in older glacial deposits found in Northern climates (Mitchell and Klugman, 1979; Torrance, 1975), and it impacts not only the erosion mechanisms, but also the erodibility of a clay. The results from the erosion studies suggest that internal structure is a key characteristic controlling the size of particles eroded during surface erosion and during mass erosion, the critical shear stress and the erosion rate. The five clays and one loam studied had a critical shear stress ranging from 0.2 to more than 11.5Pa and the erosion rate varied from 0.04 to 7.16mm/h. A comparison of the results to previous studies on cohesive sediments found in the United States (Briaud et al., 2017; Shafii et al., 2016) indicates that the presence of cementation in the clays had a significant impact as it reduces their plasticity, and increases the size of mass erosion. The erosion rates, critical shear stress and erosion mechanisms of cemented clays cannot be predicted from the behaviour of non-cemented clays. The results of the erosion studies of samples (of this study) subjected to a wet-dry cycle suggest that a certain threshold of clay content could act as a controlling parameter of the erosion behaviour of weathered cohesive sediments as it affects the timescale of the drying.

An important contribution of this study is the interpretation of different factors affecting the erosion behavior of post-glacial clays, the characterization of the geotechnical properties of the sediments and the number (six) and spatial distribution of different post-glacial deposits investigated. These results significantly increase the body of literature on the fluvial erosion behaviour of deposits of post-glacial clays of the St-Lawrence and the Ottawa River valleys. The wide range of sediments tested allowed for the observation of the influence of unique structures present in well consolidated and cemented glaciolacustrine, glaciomarine and marine cohesive deposits.

Lastly, a coring method was developed to sample post-glacial clay deposits, which facilitates the sampling process. This is an important contribution for future erosion studies as it is important to obtain samples in a process causing as little disturbance to the sample as possible, and because geotechnical sampling methods (Lefebvre, 1979; LaRochelle et al., 1981) were resource intensive when used in a fluvial environment.

5.1 Influence of internal structure

The post glacial clay deposits sampled had different depositional and consolidation histories. They were glaciolacustrine sediments, several different Champlain Sea sediments and older glaciomarine sediments. Spatial and temporal variations in the deposition environment of the Champlain Sea have led to the deposition of a wide range of grain sizes and the presence of stratification in the deposits of certain regions, as described in more detail in the site descriptions in section 3.1. All deposits were well-consolidated except for the remoulded Champlain Sea deposit obtained at site 1 (Riviere de la Tortue, a tributary of the St. Lawrence River), which is a firm silty clay with pockets of silts and sands. The origin of the sediments determined if the internal structure consisted of planes of weakness, or varves, which, as indicated by the results is a determining factor controlling the erosion mechanisms of the sediment.

The resistance to erosion of stratified clays (two deposits) is highly influenced by the thickness of the stratification as well as the properties of the material between the layers. This was apparent for the varved silty clay collected at the lower tributary of Chelsea Creek (site 4) for which erosion occurred at 0.4Pa and at an erosion rate of 0.36mm/h for varves of less than 10-mm thickness while for varves of more than 10-mm thickness erosion occurred between a range of 5.8 and 8.0Pa at the erosion rate of 0.04 and 0.08mm/h, respectively. The stratified clay taken at location #2 at site 5 (upper Chelsea Creek) also contained large strata, larger than 40mm, and the critical shear stress of the samples exceeded the maximum bed shear stress of the flume of approximately 10.4Pa. The thickness of the clay layers not only affected the erodibility of the clays, but also determined the erosion mechanisms occurring at different shear stresses. For thinner varves, surface erosion, the removal of a few layers of clays, was first observed, then, as the shear stress was increased mass erosion was observed as entire blocks of a varve were detached from the less cohesive interbed layer and carried away by the flow. In the case of a thicker varve, surface erosion was not observed, which suggests a variation in the varve properties. Mass erosion occurred when the flow's shear stress overcame the undisturbed strength of the weaker inter-varve layer, and a large block eroded from the specimen core. Hence, the erosion results suggest that the presence of varves in the clay and the varve thickness has a significant influence on the critical shear stress and the erosion rate of stratified clays, as blocks eroded are defined by the thickness of the varve and the resulting size determines the shear stress at which these blocks are carried away by the flow. The effect of the varves on the erosion cannot be accounted for with other standard geotechnical properties.

The sporadic presence of pockets of sands and silts also impacted the erosion resistance of the different clays tested. The erosion test results for samples taken at site 1 (Riviere de la Tortue), a remoulded Champlain Sea clay, as well as observations made during preparation of samples taken at site 2 (Castor River), a Champlain Sea silty clay, suggest that the presence of larger aggregates of coarser and non-cohesive material reduces the critical shear stress of the cohesive soil. The erosion initiated around these larger aggregates resulted in a lowered critical shear stress in their vicinity and in larger blocks eroding relative to the observed mass erosion occurring at locations without larger aggregates. Their influence is hard to quantify as they appear randomly in the clay matrix and can only be seen once a layer has eroded. These results are in accordance with observations made by Kamphuis et al. (1990) and Lefebvre and Rohan (1986) on the influence of zones of weaknesses such as pockets of silts on the erodibility of clays.

Furthermore, another important factor influencing the internal structure of the clays tested is the influence of weathering on the surface deposit sampled (Gaskin et al. 2003, Kamphuis et al. 1990 and Lefebvre and Rohan 1986). The presence of fissures increases erodibility and lowers the critical shear stress. Desiccation results in fissures in the clay material as the moisture content in the material is lowered and the volume of the clay decreases. The clays from three sites (site 2: Castor River, site 3: Riviere du Nord, site 5: upper tributary of Chelsea Creek) were affected by desiccation as the specimens collected from these sites had fissures at their surface (see Figures Figure 3-9, Figure 3-12 and Figure 3-19). The samples had undergone different degrees of desiccation, which was evident *in-situ* due to spalling at the surface, the surface being a layer of small blocks of less than 5mm diameter, while for other samples (geotechnical samples taken at the Castor River tributary and at the Rivière du Nord tributary) the effect of desiccation could only be seen during erosion. For very desiccated samples (sample #1 taken at the Rivière du Nord tributary; samples #1 and #3 taken at the Castor River tributary), mass erosion occurred at very low shear stresses, around 0.2Pa, as the loose material in between blocks dispersed into the flow and the lift and drag forces of the flow overcame the weight of the blocks. The erosion of these blocks, once they had separated from the parent material, was as a cohesionless particle. For samples with less or no apparent fissures at their surface (geotechnical samples taken at the Castor

River tributary and at the Rivière du Nord tributary), the erosion occurred at low shear stresses, varying from 0.2 to 3.0Pa depending on the site, and in a more brittle manner as large blocks broke off and were transported away, revealing the presence of fissures. The critical shear stress of samples taken at site 2 (Castor River), a fissured Champlain Sea silty clay, was constant across samples, but the erosion rate increased 7-fold when fissures were visible at the surface.

5.2 Influence of cementation

Most cohesive sediments tested were well cemented as they were moderately sensitive, but difficult to remould except for the remoulded Champlain Sea silty clay taken at site 1(Riviere de la Tortue) and the Champlain Sea silty clay taken at site 2 (Castor River). Cementation in a well consolidated cohesive sediment affects its plasticity, by making it more brittle, and increases its strength (Mitchell and Klugman, 1979; Torrance, 1974).

As the plasticity of the samples was determined using standard Atterberg limits tests, in which the clays are remoulded, the relationships, or the lack of trends, based on the results from the erosion tests and the geotechnical assessment are different from that reported to date in the literature for non-cemented clays. The multivariate assessments of the St. Lawrence Lowlands clays diverge from previous results obtained by Briaud et al. (2017), Shafii et al. (2016) and Mostafa et al. (2008), who studied the fluvial erosion of a large number of sediments including some non-cemented clays. The predicted critical shear stress obtained for the cemented post-glacial clays with the regression relationships defined by Briaud et al. (2017) were either overestimations by a factor of 10 or underestimations by a factor 10^{10} (see Appendix C for comparison). The predicted critical shear stress obtained using the regression curve defined for fine grained soil by Shafii et al. (2016), was reasonably close for the less cemented samples, but not close for the cemented sediments as shown in Figure 5-1. Based on the work of Shafii et al. (2016), the value of critical shear stress for a given fine grained soil should increase with plasticity, undrained shear strength (from the vane shear test), moisture content and mean grain size. The relative error between Shafii et al. (2016) regression value for shear stress (calculated based on equation 2.10) and the observed value is on average 17% for site 1 (Riviere de la Tortue) and 27% for site 2 (Castor River).

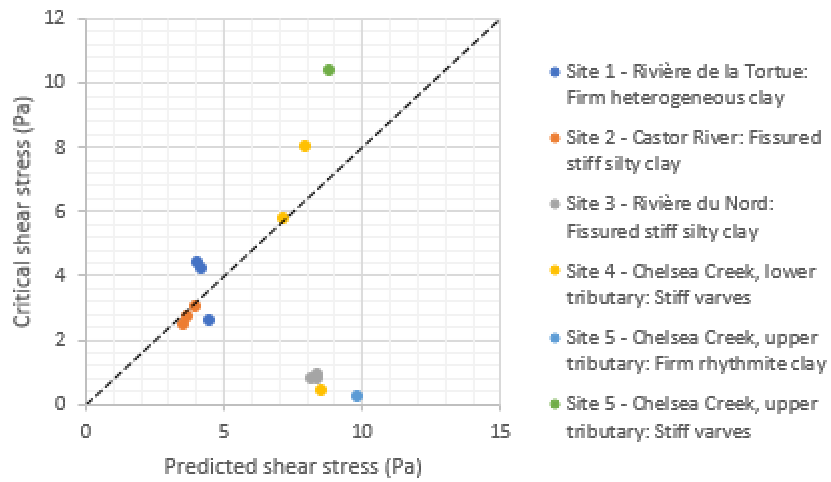

Figure 5-1. Critical shear stress obtained from the erosion tests versus the predicted shear stress based on Shafii et al. (2016) for fine grained sediments

No general trend could be established based on the dimensional analysis proposed by Mostafa et al. (2008) as shown in Figure 5-2 , in which an inversely proportional linear relationship was found between the critical shear stress and a dimensionless number χ ($= \frac{LI}{S_g - 1}$, equation 2.6). Note that both the values of χ and dimensionless shear stress τ* obtained in this study are much greater than the range of values observed by Mostafa et al. (2008) in their work, as the maximum dimensionless shear stress observed in their study was around 43 while χ varied between 0.25 and 0.61 in their study.

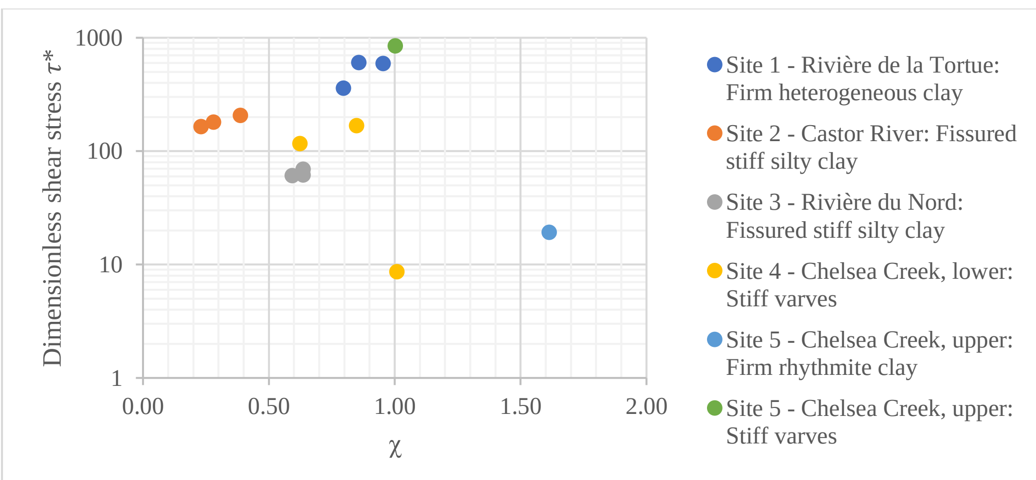

Figure 5-2. Dimensionless shear stress in relation to χ (method proposed by Mostafa et al., 2008)

5.3 Influence of clay content on the critical shear stress due to a wet-dry cycle

The results from the erosion tests performed on samples that were allowed to air-dry for 48 hours (one or two samples per site) show that for the samples containing at least 39% clay (all the samples except for the ones taken at the Rivière St-Charles tributary), there is no significant impact on the erosion rate nor the critical shear stress. The decrease in moisture content over the 48 hours drying period for these samples was minimal at the surface of the clays (<10% change in moisture content) likely due to the very slow hydraulic conductivity of clays (Wagner, 2013) resulting in very slow/small reductions in moisture content. However, the clay loam (Site 6: Riviere St. Charles), with a clay content of 24% and percent fines (silts and clays) of 63%, underwent a significant loss of cohesion during the wet-dry cycle, which reduced the moisture content by 35%. The clay loam was well cemented and its undrained shear strength exceeded the maximum bed shear stress of the flume of 11.5Pa, in its field condition or *in-situ* moisture content. The moisture content of the surface of the sample decreased from 17% to 11% in 48 hours and the sample heaved (slaked) when re-wetted (see Figure 4-36 b)). The erodibility of the clay loam increased considerably as the critical shear stress decreased from > 11.5 Pa to 0.9Pa. The main erosion mechanisms was particle erosion of the surface material and mass erosion of small blocks (2 – 6 mm) due to slaking of the soil. The results show that cohesive sediments containing a smaller fraction of clay sizes, or equivalently sufficient fraction of silt sizes and greater, are much more vulnerable to shorter wet-dry cycles, likely due to their higher hydraulic conductivity (Wagner, 2013), which is in accordance with the previous findings on desiccation of cohesive soils (Gaskin et al. 2003, Lim, 2006; Shaikh et al., 1988).

5.4 General trends in critical shear stress of the samples

All but one of the specimens tested lay within the predicted range of critical shear stress for fine grained (non-cemented) sediments of Briaud et al. (2017) as shown in Figure 2-1. There was considerable variability in the critical shear stress observed between samples from the same site and an individual sample might not be representative of site conditions due to particular characteristics of a sample. This is more apparent when the presence of vulnerabilities to erosion in the clays is not uniform in the deposit found along a river bank or bed. The vulnerabilities observed include thin stratification, such as thin varves, the presence of pockets of non-cohesive sediments and the presence of fissures.

The spatial variability of the sediments in a deposit (seen in the variability of different samples from a given site) affects the range of critical shear stresses at a site, which means that it is more difficult (or more samples would be required) to identify trends based on individual soil properties. Two trends based on soil properties were observed in this study. The dimensionless critical shear stress generally increases with an increase of field moisture content and an increase in clay content as shown in Figure 5-4 and Figure 5-5, respectively. The firm rhythmite clay taken at site 5 (upper tributary of Chelsea Creek) has a much lower critical shear stress to moisture content than the rest of the clays tested. Also, the two varved clays taken at the two tributaries of Chelsea Creek had a lower dimensionless shear stress for a given clay content and for a given moisture content (Chelsea Creek, lower) and a higher dimensionless shear stress for a given clay content (Chelsea Creek, upper). However, no trend could be observed for the critical shear stress of the samples and any other the soil properties tested in this study of bulk density, liquid limit, plastic limit, plasticity index, liquid index, percent fine and vane shear strength. In the literature, it has been reported that critical shear stress increases with field moisture content, clay content and plasticity for non-cemented clays (e.g., Briaud et al., 2017, Le Hir, 2008). The results agree with the observation made by Zreik et al. (1998) for undisturbed cohesive sediments that there is no correlation with the undrained shear strength of clays obtained in vane shear tests as an individual parameter and the critical shear stress. Kamphuis (1983) results of a linear relationship between vane shear strength and critical shear strength of remoulded and re-compacted cohesive sediments shows the importance of testing clays in as near to *in-situ* conditions as possible to replicate the *in-situ* behaviour.

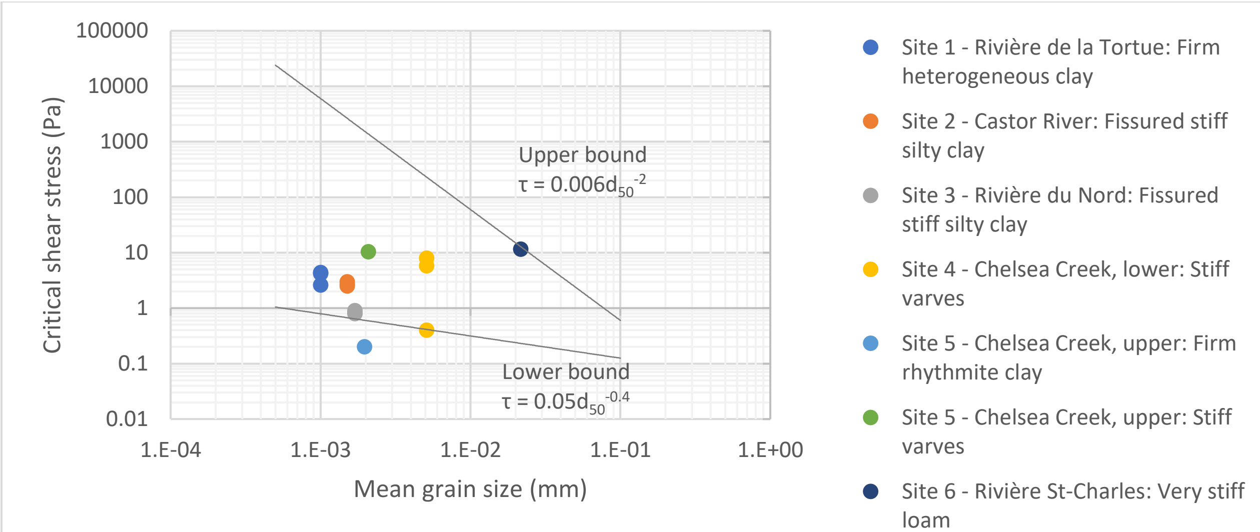

Figure 5-3. Critical shear stress in relation to the mean grain size; with the lower and upper bound of fine-grained sediment data compiled by Briaud et al. (2017)

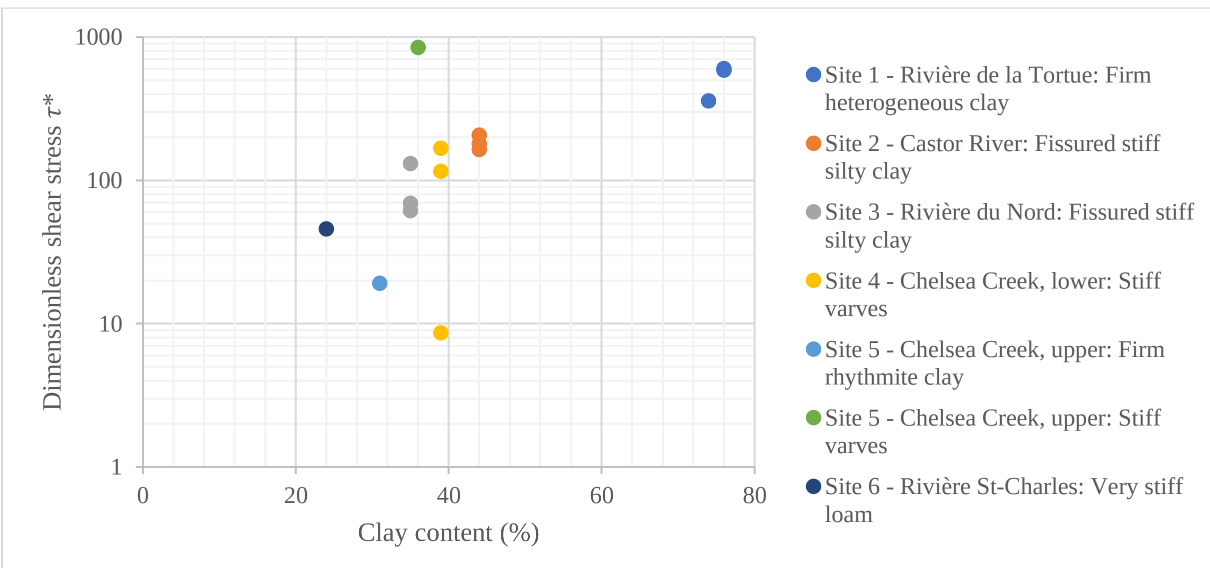

Figure 5-4. Dimensionless critical shear stress in relation to the clay content

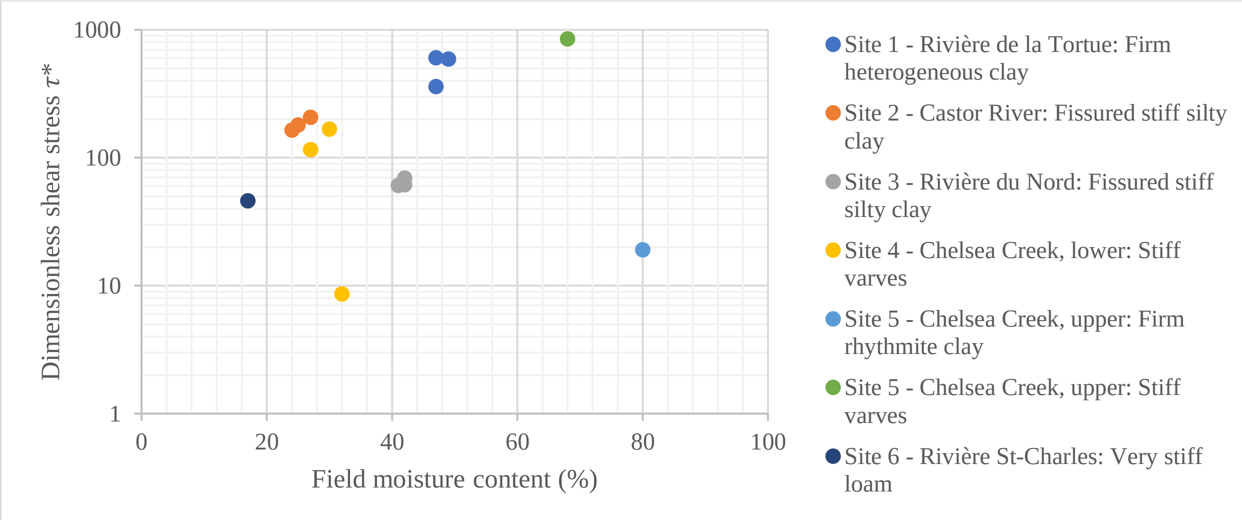

Figure 5-5. Dimensionless critical shear stress in relation to the field moisture content

5.5 Recommendations

As no clear trends were observed between the erosion properties of the clays studied and standard geotechnical properties, site investigation is recommended to assess the erosion behavior of clay deposits found in the St-Lawrence and the Ottawa River valleys. For well consolidated and cemented clays, commonly found in the region, field observers should pay particular attention to the following vulnerabilities that decrease the critical shear strength and increase the erodibility of the clays: presence of stratification and thinner layers, presence of pockets of non-cohesive geomaterial within the cohesive matrix as well as the presence of fissures. The structure of the clays should first be defined and then compared to other clays with a similar internal structure.

The predictions based on the relationship between soil properties and erodibility of estuarine clays and other fluvial clays found in warmer climates are not relevant to the deposits found in the St-Lawrence and Ottawa River valleys as they are post-glacial deposits. Hence, a database for glaciomarine and glaciolacustrine clays should be built similarly to one developed by Shafii et al. (2016) et Briaud et al. (2017) as a large number of specimens is required to report on the erosion characteristics of deposits with a wide range in the geologic history of deposition. Smaller samples could be taken to facilitate the sampling process and allow a large number of tests to be performed on undisturbed clay sediments. This would also allow for the sampling at several locations in a river reach to quantify the spatial variability of geotechnical properties (i.e., in the bed and banks of a river).

The method used to measure surface roughness of the samples could be used in similar applications as in the work done by Beckers et al. (2020) and could be used to measure erosion volumes ΔV, erosion areas A_e, specific deepening Δz_s and the number of disconnected areas m. This would allow for the measurement of the progression of the erosion at a relatively low cost compared to that currently available on the market.

5.6 Study limitations

The study limitations include the error in the measurements made with the available testing methods and the ability of the sampling methods to obtain undisturbed sediment samples. Given the scarcity of previous studies on the erosion mechanisms of clays found in post-glacial environments with which to compare the results the magnitude of these errors are difficult to quantify.

The measurement of bed shear stress used in the straight flume setup designed for this study assumed a gradually varied flow to estimate bed shear stress ($S = S_f$), which was verified by comparison to bed shear stress estimated using a uniform flow assumption ($S = S_0$) (Yeats 2021). A more precise measurement of bed shear stress was attempted using direct measurement of the shear stress applied to the sample using a system in which the sediment sample was placed in a suspended box, so that both vertical loads and horizonal loads could be measured using a time series from load cells. The vertical measurements were planned to assess real time erosion rates from measurements of sample weight, while the horizontal load cells were planned to measure the bed shear stress exerted on the sample. However, the errors in the measured loads was greater that the magnitude of the weight loss and shear loads rendering the measurements unusable. Direct measurement of shear stress could improve the accuracy of the critical shear stress estimates using a method similar Crowley et al. (2014) and Shan et al. (2015). To improve measurements of water depth to estimate bed shear stress estimations pressure gages could be installed upstream and downstream of the sample in the flume bed.

The maximum bed shear stress possible to achieve in the flume was lower than the critical shear stress of three of the sediment samples tested, which, therefore, also did not allow the erosion mechanisms to be observed. The limitation in bed shear stress is due to the relatively low discharge and hence low depth possible in the flume and the low maximum slope. Other flume apparatus have reached higher bed shear stress values and this is required in order to determine the critical shear stress of consolidated glacial clays. In addition, the flow condition in the flume was supercritical (resulting in relatively larger errors in bed shear stress from absolute errors in depths measured), while most river flows are sub-critical.

The test designed to assess the effect of weathering was a preliminary quantification of the impact of on wet-dry cycle, as it was only one air-drying period of 48 hours. This test did, however, provide insight for the design of future studies that might want to test undisturbed samples at different field moisture contents.

Furthermore, it was not possible to quantify the disturbance caused during sampling on the fissured clays and sampling might have affected the erosion resistance of clays with minimal strength and planes of weaknesses. Surface deposits are not as confined as deeper deposits and are more likely to exhibit weaknesses caused by environmental and hydrological weathering. The comparison of the sample obtained using the coring sampling method developed in this study to the sample from the Sherbrooke sampler, lead to the conclusion that Sherbrooke sampler, although it obtains high-quality samples, is costly, time consuming and difficult to use in a river environment.

This study is limited in its range as the sites sampled only represent a small subset of glacial and interglacial cohesive sediment deposits in the St. Lawrence and Ottawa River valleys. However, it is the first study to assess the erosion properties of as wide of a range of local deposits of the St-Lawrence and Ottawa River valleys. Many soil properties were determined in order to draw a better general portrait of the variability in geotechnical properties of the sediments.

6 Conclusion

This study aimed to increase the knowledge of the erosion behaviour, critical shear stress and mechanisms of erosion of post-glacial clay deposits of the St-Lawrence and Ottawa River valleys, and to determine if the erosion behaviour is correlated with any of the geotechnical properties of the sediments. A new sampling method was designed to provide large undisturbed (or minimally disturbed) clay samples using a coring process for surface sediments. Six sites were sampled in the St. Lawrence and Ottawa River valleys in five deposits of Champlain Sea clays and one lacustrine or glaciolacustrine deposit. A summary of the geologic and geotechnical characteristics and a summary of the critical shear stress of the clays studied are shown in Table 6-1 and Table 6-2 respectively. Key characteristics of the clays at each study sites are also summarized below.

Table 6-1. Summary of geologic and geotechnical characteristics of clays sampled

Tributary	Type of deposit	Characteristics	% Silt	% Clay	ρ_b (10^3 kg/m^3)	m	P.I.	L.I.	C_u (kPa)	Sensitivity
Rivière de la Tortue	Remoulded Champlain Sea clay	Firm heterogeneous clay	18	76	1.73	48	36	67	43.0 - 46.2	4.1
			16	74			39	59	47.2 - 49.4	3.8
					1.73	47	37	57	30.2 - 57.8	2.7
Castor River	Champlain Sea sediments	Stiff rhythmite silty clay	44	52	1.99	26	21	33	85.2 - 122.2	0.1
Rivière du Nord	Champlain Sea sediments	Stiff rhythmite silty clay	35	56	1.78	42	36	50	84.8 - 128.2	15.8
Chelsea Creek, lower	Lacustrine or glaciolacustrine sediments	Stiff varves of clay and sand	39	39	2.03	25	16	50	154.6	23.3
			40	45	1.97	29	13	92		14.7
Chelsea Creek, upper	Champlain Sea clay	Firm rhythmite clay	31	63	1.54	80	57	88		13.2
		Stiff rhythmite silty clay	36	58	1.57	73	63	68	18.1 - 41.8	10.6
Rivière St-Charles	Glaciomarine sediments	Very stiff loam	40	24	2.17	17				

Table 6-2. Average critical shear stress and erosion rate for all sites

		Condition: Intact, in-situ moisture content			*Condition: Air-dried for 48 hours*		
Tributary	Characteristics	Average moisture content *m*	Average critical shear stress τ_{cr}	Average erosion rate at τ_{cr}	Moisture content *m*	Critical shear stress τ_{cr}	Erosion rate at τ_{cr}
		%	Pa	mm/h	%	Pa	mm/h
Rivière de la Tortue	Firm heterogeneous clay	48	4.3	0.07	44	4.2	--
		47	2.6	0.04	--	--	--
Castor River	Stiff rhythmite silty clay	25	2.7	1.42	27	1.9	0.59
Rivière du Nord	Stiff rhythmite silty clay	42	0.8	0.64	43	0.9	0.34
Chelsea Creek, lower	Stiff varves of clay and sand	30	0.4 -6.9*	0.16	30	5.4	1.06

Chelsea Creek, upper	Firm rhythmite clay	80	0.2	1.3	72	0.2	0.3
	Stiff rhythmite silty clay	68	>10.4	--	70	>10.9	--
Rivière St-Charles	Very stiff loam	17	>11.5	--	11	0.9	--

* Critical shear stress was 0.4 for samples with thinner varves (<10mm) and higher for samples with thicker varves (>10mm).

The shear resistance behavior of the remoulded Champlain Sea clay, obtained at site 1 (Rivière de la Tortue), was influenced by the presence of pockets of sand and silts as well as its high clay content (74-76%). The clay was non-sensitive, non-cemented and firm. Samples were collected along the river bank which resulted in a degree of variability in the clay strength in the vane shear tests, varying from 43.0 to 49.4kPa and from 30.2 to 57.8kPa at the first location and second location, respectively. While in the erosion tests, critical shear stress of 4.2-4.4Pa and 2.6Pa were observed at the first and second location, respectively. Surface erosion as well as mass erosion of blocks of 6-18mm diameter was observed at critical shear stress and remained constant as the shear stress was increased above the critical threshold. The results suggest a relatively larger spatial variability of remoulded surface deposits, thus requiring careful consideration to properly assess the erosion behavior of the bed and banks in such cases.

The stiff rhythmite silty clay obtained at site 2 (Castor River) behaved in a much more brittle manner eroding at a critical shear stress of 2.5-3.0Pa and having a vane shear strength of 85.2-122.2kPa.The silty clay was well cemented and had medium plasticity due to its high silt content. The silty clay was also more compacted and with higher undrained shear strength in its remoulded form (layered in a dish for the fall cone test) than in its undisturbed state. The presence of pockets of sand in the larger samples resulted in uneven moisture loss in the silty clay during storing, but which had little impact on the critical shear stress threshold as samples with visible disturbances (cracks) eroded at the same shear stress as a sample with no visible signs of disturbance.

The stiff rhythmite silty clay obtained at site 3 (Rivière du Nord) had a weak resistance to erosion as the banks sampled were desiccated, exhibiting generalized weathering resulting is failure in the form of the surface being composed of small blocks. The silty clay was well cemented with a sensitivity of 15.8. The samples had a vane shear strength of 84.8 to 128.2kPa and failed outside of the vane perimeter in small blocks. Constant mass erosion was observed at a critical shear stress of 0.8-0.9Pa. Blocks were already dislodged at 0.3Pa but the drag and lift forces of the eroding fluid were too small to carry them away as in the process of the erosion of non-cohesive alluvial material.

The erosion resistance of a varved silty clay obtained at site 4 (lower tributary of Chelsea Creek) depended highly on the thickness of the varves, as varves of 1-2mm thickness eroded at a critical shear stress of 0.2Pa, while thicker varves of 22-28mm eroded at 5.8-8.0Pa. The silty clay was well cemented having a sensitivity of between 14.7 and 23.3. Two varves were characterized, one as a clay loam and one as a silty clay, which suggests variability in the composition of different layers in the same varved deposit. The stiff silty clay vane shear strength was the greatest of all the samples studied (154.6kPa) and exhibited no signs of desiccation.

A firm rhythmite clay and a stiff rhythmite silty clay obtained at two sampling locations at site 5 (upper tributary of Chelsea Creek) exhibited similar shear resistance behavior in the remoulded state, with a vane shear strength of 4.5-4.5kPa, but very different behavior in the undisturbed state. The firm rhythmite clay was highly plastic, cemented and had a high liquidity index (91%). The clay failed along weaker planes that appeared to be random in size and direction; it had a vane shear strength of 59.9kPa and a critical shear stress of 0.2Pa. The layered stiff rhythmite silty clay appeared to have a layered structure, had a lower moisture content, was more consolidated and behaved in much more brittle manner during the vane shear test, failing at 41.8kPa. Its erosion resistance was greater than the shearing capacity of the flume apparatus used in this study (>10.9Pa).

The very stiff clay loam obtained at site 6 (Rivière St-Charles) has a high resistance to erosion when undisturbed and with in-situ moisture content having a critical shear stress greater than 11.5Pa, the maximum possible in the flume. The very stiff clay loam had 24% clay and 40 silt with a low moisture content of 17% and high bulk density of 2.17 x10^3 kg/m^3 . It was the only sample that underwent a significant loss of cohesion after being left to air-dry for 48 hours, which decreased its moisture content to 11% and its critical shear stress to 0.9Pa with heaving and slaking occurring once it was submerged in water.

Measurements of surface roughness at regular intervals during fluvial erosion showed that, once a sample had passed the critical shear stress threshold, smoothening and roughening of the samples' surface reached an equilibrium.

Based on the identification of soil properties and erosion tests performed on the five clay and one clay loam deposits in the St. Lawrence and Ottawa River valleys, it can be concluded that the factors controlling the erosion behavior of cohesive sediments found in post-glacial environments are intricate, complex and highly dependent on the sediments' origins as well as their current exposure to the elements. The research clearly illustrates that the internal structure of the clays as well as their degree of cementation determine the erosion behaviour, with cemented clay exhibiting higher critical shear stresses than non-cemented clays and mass erosion being the dominant erosion mechanism for structured clays. Several of the well cemented cohesive sediments tested exhibited properties leading to weaknesses, such as thin stratifications, the presence of pockets of non-cohesive sediments and fissures, which affected their erosion behavior by lowering the critical shear stress and resulting in mass erosion of blocks delineated by the structural weaknesses. The presence of these vulnerabilities also lead to a greater range in the critical shear stress and erosion rates found at particular sampling locations. The results confirm that fluvial erosion of cemented clays cannot be predicted by soil properties, although there was a general trend of increased critical shear stress with increased percentage clay size and increased moisture content. In addition, the behaviour of cemented post glacial clays cannot be predicted from the large database of EFA tests on non-cemented cohesive soils found in the US (Briaud et al., 2017; Shafii et al., 2016). Currently, the erosion behaviour and critical shear stress of a cemented post glacial clay cannot be predicted and must be investigated at each site. Further research is needed to provide information about the properties of post glacial clays and to provide guidelines for erosion mitigation measures suited for the Canadian environment.

7 References

Afzalimehr, H., & Rennie, C. D. (2009). Determination of bed shear stress in gravel-bed rivers using boundary-layer parameters. *Hydrological sciences journal*, *54*(1), 147-159.

Afzalimehr, H., & Anctil, F. (2000). Accelerating shear velocity in gravel-bed channels. *Hydrological sciences journal*, *45*(1), 113-124.

Al-Madhhachi, A. S. T., Hanson, G. J., Fox, G. A., Tyagi, A. K., & Bulut, R. (2013). Deriving parameters of a fundamental detachment model for cohesive soils from flume and jet erosion tests. *Transactions of the ASABE*, *56*(2), 489-504.

American Society for Testing and Materials (2000a). ASTM D4318-00, *Standard Test Methods for Liquid Limit, Plastic Limit, and Plasticity Index of Soils.*

American Society for Testing and Materials (2000b). *ASTM D4648-00, Standard Test method for Laboratory Miniature Vane Shear Test for Saturated Fine-Grained Clayey Soil.*

Amundsen, H.A., Emdal, A. & Thakur, V. (2016). Engineering characterization of a leached marine clay using Sherbrooke block samples. *Proceedings of the 5th International Conference on Geotechnical and Geophysical Site Characterisation, ISC 2016* 1: 529-534.

Arneson, L.A., Zevenbergen, L.W., Lagasse, P.F., and Clopper, P.E. (2012). *Evaluating Scour at Bridges,* 5th Ed, Hydraulic Engineering Circular 18, Publication No. FHWA-HIF-12-003.

Bariteau, L. (1988). La cartographie géomorphologique au 1 :20 000 de modelés polygéniques : un exemple des Basses-Terres du St-Laurent. Masters thesis. Geography department, Université de Montréal [geomorphologic map at 1:20,000 of the region 31G/01-200-0101].

Beckers, F., Inskeep, C., Haun, S., Schmid, G., Wieprecht, S., & Noack, M. (2020). High spatio-temporal resolution measurements of cohesive sediment erosion. *Earth Surface Processes and Landforms*, *45*(11), 2432-2449.

Bolduc, A. et al. (2003). Géologie des formations superficielles, région de Québec, Québec. Open file 3835, 1 :50,000 (rev.), Geological Survey of Canada.

Briaud, J. L., Govindasamy, A. V., & Shafii, I. (2017). Erosion charts for selected geomaterials. *Journal of Geotechnical and Geoenvironmental Engineering*, *143*(10), 040170-72.

Briaud, J. L., & Chen, H. C. (2006). Levee erosion by overtopping during the Katrina hurricane. In *Proceedings of the third international conference on scour and erosion*.

Briaud, J. L., Ting, F. C. K., Chen, H. C., Cao, Y., Han, S. W., & Kwak, K. W. (2001). Erosion function apparatus for scour rate predictions. *Journal of geotechnical and geoenvironmental engineering*, *127*(2), 105-113.

Bureau de normalisation du Québec (2013). *BNQ 2501-025. Sols – Analyse granulométrique des sols inorganiques*.

Bureau de normalisation du Québec (2014a). *CAN/BNQ 2501-070 norm. Soils – Determination of Relative Density of Solid Particles.*

Bureau de normalisation du Québec (2014b). *CAN/BNQ 2501-092 norm. Soils – Determination of the Liquid Limit by the Fall Cone Penetrometer and Determination of Plastic Limit.*

Bureau de Normalisation du Québec (2014c). *CAN\BNQ 2501-110 norm. Soils – Determination of Undrained Shear Strength and Determination of Sensitivity of Cohesive Soils Using the Fall Cone Penetrometer.*

Burmister, D. M. (1949, December). Principles and techniques of soil identification. In *Proceedings of Annual Highway Research Board Meeting. National Research Council. Washington, DC* (Vol. 29, pp. 402-434).

Carto. (2017). Carto voyager. [map tiles]. Retrieved from: https://a.basemaps.cartocdn.com/rastertiles/voyager_nolabels/{z}/{x}/{y}@2x.png (July 30, 2021).

Chapman, L.J. and Putnam, D.F. (1984). The physiography of southern Ontario. Ontario Geological Survey, Special Vol. 2.

Chapuis, R. P., & Gatien, T. (1986). An improved rotating cylinder technique for quantitative measurements of the scour resistance of clays. *Canadian geotechnical journal*, *23*(1), 83-87.

Chow, V. T. (1959). *Open-channel hydraulics*. New York: McGraw-Hill.

Christensen, R. W., Das, P. E., AS, F., & Braja, M. (1973). Hydraulic erosion of remolded cohesive soils. *Highway Research Board Special Report*, (135).

Crowley, R. W., Robeck, C., & Thieke, R. J. (2014). Computational modeling of bed material shear stresses in piston-type erosion rate testing devices. *Journal of Hydraulic Engineering*, *140*(1), 24-34.

Cummings, D. & Occhietti, S. (2001). Late Wisconsinan sedimentation in the Québec City region: evidence for energetic subaqueous fan deposition during initial deglaciation. Géologie Physique Quaternaire. *55*, 257-273.

DeGroot, D.J., Poirier, S.E., & Landon, M.M. (2005). Sample disturbance–soft clays. *Studia Geotechnica et* Mechanica 27(3-4).

Delage, M. (1997). Façonnement et métamorphose du modelé drumlinoïde par deux écoulements glaciaires successifs dans la région de Huntingdon (sud du Québec). Doctoral thesis, Université de Montréal, Québec.

Dubois Verret, M. (2015). Géomorphologie quaternaire de l'Outaouais (Québec) : écoulements glaciaires et paléogéographie de la déglaciation. (Master's thesis). Université du Québec à Montréal

Dietrich, H. G., Dahms, E., Fritz, L., Kohler, E. E., Heimerl, H., Rösch, H., ... & Weinberg, R. (1998). Meßparameter. In *Handbuch zur Erkundung des Untergrundes von Deponien und Altlasten* (pp. 67-253). Springer, Berlin, Heidelberg.

Elbeggo, D., Hussien, M. N., Ethier, Y., & Karray, M. (2019). Robustness of the P-RAT in the shear-wave velocity measurement of soft clays. *Journal of Geotechnical and Geoenvironmental Engineering*, *145*(5), 04019014.

Evans, S.G. and Brooks, G.R. (1993). An earthflow in sensitive Champlain Sea sediments at Lemieux, Ontario, June 20, 1993, and its impact on the South Nation River. *Canadian Geotechnical Journal*. **31**(3): 384-394. https://doi.org/10.1139/t94-046

Ewane, M. S., Silvestri, V., & James, M. (2020). The Use of Laboratory Indentation Testing to Characterize Champlain Sea Clay. *Geotechnical and Geological Engineering*, *38*(6), 6365-6383.

Filion, L., Lavoie, M. & Querrec, L. (2009). The natural environment of the Québec City region during the Holocene, Post-Medieval Archaelogy, 43(1), 13-29. DOI: 10.1179/007942309X12457508843847

Gadd, N.R. (1980). Late-glacial regional ice-flow patterns in eastern Ontario. Canadian Journal of Earth Sciences, *17*, 1439-1453.

Gadd, N. (1976). Surficial geology and landslides of Thurso-Russell map area, Ontario. Geological Survey of Canada, Paper 75-35.

Gadd, N.R. (1961). Surficial geology of the Ottawa area, report of progress. Geological Survey of Canada, Paper 61-19.

Gaskin, S., Pieterse, J., Al Shafie, A. and Lepage, S. (2003). Erosion of undisturbed clay samples from the banks of the St-Lawrence River. Canadian Journal of Civil Engineering. *30*, 585-595.

Geological Survey of Canada (2014). Surficial geology of Canada/ Géologie des formations superficielles du Canada. *Canadian Geoscience Map 195 (ed. Prelim., Surficial Data Model V.2.0 Conversion).*

Google. (n.d. https://mt1.google.com/vt/lyrs=p&x={x}&y={y}&z={z}). Google terrain. [map tiles]. Retrieved from: https://mt1.google.com/vt/lyrs=p&x={x}&y={y}&z={z} (July 30, 2021).

Grass, A. J. (1970), Initial instability of fine bed sand. J. Hydr. Div., ASCE, 96, No. HY3, 619.

Hanson, G. J., & Cook, K. R. (2004). Apparatus, test procedures, and analytical methods to measure soil erodibility in situ. *Applied engineering in agriculture*, *20*(4), 455.

Hanson, G. J., & Robinson, K. M. (1993). The influence of soil moisture and compaction on spillway erosion. *Transactions of the ASAE*, *36*(5), 1349-1352.

Heinzen, R. T., & Arulanandan, K. (1977). Factors influencing dispersive clays and methods of identification. In *Dispersive clays, related piping, and erosion in geotechnical projects*. ASTM International.

Hjulström, F. (1935). Studies of the morphological activity of rivers as illustrated by the river fyris, bulletin. *Geological Institute Upsalsa*, *25*, 221-527.

Holtz, W. G., & Gibbs, H. J. (1956). Engineering properties of expansive clays. *Transactions of the American Society of Civil Engineers*, *121*(1), 641-663.

Jepsen, R. A., ROBERTS, J. D., Gailani, J. Z., & Smith, S. J. (2002). *The SEAWOLF flume: Sediment erosion actuated by wave oscillations and linear flow* (No. SAND2002-0100). Sandia National Labs., Albuquerque, NM (US); Sandia National Labs., Livermore, CA (US).

Jobin, B., Latendresse, C., Grenier, M. et al. (2010). Recent landscape change at the ecoregion scale in Southern Québec (Canada), 1993–2001. *Environ Monit Assess* **164,** 631–647. https://doi.org/10.1007/s10661-009-0918-5

Kamphuis, J.W., Gaskin, P.N. & Hoogendoorn, E. (1990). Erosion tests on four intact Ontario Clays. *Canadian Geotechnical Journal* 27: 692-696.

Kamphuis, J. W., & Hall, K. R. (1983). Cohesive material erosion by unidirectional current. *Journal of Hydraulic Engineering*, *109*(1), 49-61.

Karlsrud, K. & Hernandez-Martinez, F.G. (2013). Strength and deformation properties of Norwegian clays from laboratory tests on high-quality block samples. *Canadian Geotechnical Journal* 50(12): 1273-1293.

Karray, M., M. Ben Romdhan, M. N. Hussien, and Y. Ethier. 2015. Measuring shear wave velocity of granular material using the piezoelectric ring-actuator technique (P-RAT). *Can. Geotech. J.* 52 (9): 1302–1317. https://doi.org/10.1139/cgj-2014-0306.

Kuelegan, G. H. (1938). Laws of turbulent flow in open channels. *J. Res. Natl. Bur. Stand.*, *21*, 707–741.

Kironoto, B. A., Graf, W. H., & Reynolds (1995). Turbulence characteristics in rough non-uniform open-channel flow. *Proceedings of the institution of civil engineers-water maritime and energy*, *112*(4), 336-348.

Kironoto, B. A., Graf, W. H., & Reynolds. (1994). Turbulence characteristics in rough uniform open-channel flow. *Proceedings of the Institution of Civil Engineers-Water Maritime and Energy*, *106*(4), 333-344.

Krone, R. B. (1999). Effects of bed structure on erosion of cohesive sediments. *Journal of Hydraulic Engineering*, *125*(12), 1297-1301.

Monin, A. S. & Yaglom, A. M. (1971). Statistical Fluid Mechanics: Mechanics of Turbulence, Vol. 1, MIT Press, Cambridge, MA, 769 pp.

Lachat, E., Macher, H., Landes, T., & Grussenmeyer, P. (2015). Assessment and calibration of a RGB-D camera (Kinect v2 Sensor) towards a potential use for close-range 3D modeling. *Remote Sensing*, *7*(10), 13070-13097.

Laflen, J. M., & Beasley, R. P. (1960). *Effects of compaction on critical tractive forces in cohesive soils*. University of Missouri, College of Agriculture, Agricultural Experiment Station.

Laliberté, S. (2006). Sédimentologie et stratigraphie d'un delta édifié dans un contexte de régression forcée : exemple du delta de la rivière Sainte-Anne, Québec, Canada. (Master's thesis). Université Laval.

Lamarche, L. (2006). Reconstitution géologique du lac Saint-Pierre et de ses ancêtres à l'Holocène. Dans L. Lamarche et al. (dir.), Histoire Holocène de la région de Lamoraie-lac St-Pierre (p.4-20). Association québécoise pour l'étude du Quaternaire (AQQUA).

Lamontagne, L., Martin, A., Cossette, J.M. & Grenon, L. (2000). Étude pédologique dans le comté de Laprairie (Québec), Agriculture et agroalimentaire Canada.

Lamothe, M. (1989). A New Framework for the Pleistocene Stratigraphy of the Central St-Lawrence Lowlands, Southern Québec. *Géographie physique et Quaternaire*, 43(2) : 119-129.

Lamothe, M. (1977). Les dépôts meubles de la région de Saint-Faustin-Saint-Jovite, Québec : cartographie, sédimentologie et stratigraphie. (Master's thesis). Université du Québec à Montréal.

La Rochelle, P., Sarrailh, J., Tavenas, F., Roy, M. & Leroueil., S. (1981). Causes of sampling disturbance and design of a new sampler for sensitive soils. *Canadian Geotechnical Journal* 18 : 52-66.

La Rochelle, P., Leroueil, S. & Tavenas, F. (1986). A technique for long-term storage of clay samples. *Canadian Geotechnical Journal* 1(23): 602-605.

Lavelle, J. W., Mofjeld, H. O., & Baker, E. T. (1984). An in situ erosion rate for a fine-grained marine sediment. *Journal of Geophysical Research: Oceans*, *89*(C4), 6543-6552.

Le Bissonnais, Y. L. (1996). Aggregate stability and assessment of soil crustability and erodibility: I. Theory and methodology. *European Journal of soil science*, *47*(4), 425-437.

Lee, C., Wu, C. H., & Hoopes, J. A. (2004). Automated sediment erosion testing system using digital imaging. *Journal of Hydraulic Engineering*, *130*(8), 771-782.

Lefebvre, G., & Poulin, C. (1979). A new method of sampling in sensitive clay. *Canadian Geotechnical Journal* 16: 226-233.

Lefebvre, G., Rohan, K., and Douville, S. (1985). Erosivity of natural intact structured clay: Evaluation. *Canadian Geotechnical Journal* 22: 508–517.

Lim, S. (2006). *Experimental investigation of erosion in variably saturated clay soils*. University of New South Wales. Doctoral thesis.

Liu, J., Afroz, M., & Ahmad, A. (2021). Experimental investigation of the impact of salinity on Champlain Sea clay. *Marine Georesources & Geotechnology*, *39*(4), 494-504.

Lunne, T., Berre, T. & Strandvik, S. (1999). Sample disturbance effects in soft low plastic Norwegian clay. *Norges Geotekniske Institutt* 204: 81-102.

Mazurek, K.A., Rajaratnam, N. & Sego, D.C. (1999). The characteristics of erosion of a consolidated clay. *Canadian Society for Civil Engineering* 2: 207-216.

McNeil, J., Taylor, C., & Lick, W. (1996). Measurements of erosion of undisturbed bottom sediments with depth. *Journal of Hydraulic Engineering*, *122*(6), 316-324.

Miller, M. C., McCave, I. N., & Komar, P. (1977). Threshold of sediment motion under unidirectional currents. *Sedimentology*, *24*(4), 507-527.

Mitchell, J. K., & Soga, K. (2005). *Fundamentals of soil behavior* (Vol. 3). New York: John Wiley & Sons.

Mitchell, R.J. & Klugman, M.A. (1979). Mass instabilities in sensitive Canadian soils. Engineering Geology, 14. 109-134.

Mitchell, R.J. (1978). Earthflow terrain evaluation in Ontario. Ontario Ministry of Transportation and Communications, Research Report 213.

Mobley, J., Melville, J., & Parker, F. (2009). *Evaluation of scour potential of cohesive soils* (No. Project 930-644).

Montgomery, D. R., & Buffington, J. M. (1997). Channel-reach morphology in mountain drainage basins. *Geological Society of America Bulletin*, *109*(5), 596-611.

Moore, W. L., & Masch Jr, F. D. (1962). Experiments on the scour resistance of cohesive sediments. *Journal of Geophysical Research*, *67*(4), 1437-1446.

Moore, W. L., & MASCH, F. (1961). Experiments on scour resistance of cohesive sediments. Journal of geophysical research, 66(8). 2547pp.

Moriwaki, Y., & Mitchell, J. K. (1977). The role of dispersion in the slaking of intact clay. In *Dispersive clays, related piping, and erosion in geotechnical projects*. ASTM International.

Mostafa, T. S., Imran, J., Chaudhry, M. H., & Kahn, I. B. (2008). Erosion resistance of cohesive soils. *Journal of hydraulic research*, *46*(6), 777-787.

Nash, D.F.T., Sills, G.C. & Davison, L.R. (1992). One-dimensional consolidation testing of soft clay from Bothkennar. *Geotechnique* 42(2): 241-256.

Occhietti, S., Parent, M., Lajeunesse, P., Robert, F. and Govare, E. (2011). Late Pleistocene-Early Holocene Decay of the Laurentide Ice Sheet in Québec-Labrador. In J. Ehlers, P.L. Gibbard and P.D. Hughes (dir.). Developments in Quaternary Science, 15. Amsterdam, The Netherlands, 601-630.

Occhietti, S. et al. (2004). Late Wisconsinan-Early Holocene deglaciation of Québec-Labrador. Ehlers & Gibbard 2004. 243-273.

Occhietti, S. & Richard, P.J.H. (2003). Effet réservoir sur les âges ^{14}C de la Mer de Champlain à la transition Pléistocène-Holocène : révision de la chronologie de la déglaciation au Québec méridional. Géographie physique et Quaternaire, 57(2-3), 115-138.

Occhietti, S. et al. (2001). Paléoenvironnement de la Mer de Champlain dans la région de Québec, entre 11,300 et 9750 BP, le site de Saint-Nicholas. Géologie Physique Quaternaire. *55*, 23-46.

Osipov, V. I. (1975). Structural bonds and the properties of clays. *Bulletin of the International Association of Engineering Geology-Bulletin de l'Association Internationale de Géologie de l'Ingénieur*, *12*(1), 13-20.

Osterman, J. (1963). Studies on the properties and formation of quick clays. *Clays and clay minerals*, *12*(1), 87-108.

Parent, M. & Occhietti, S. (1999). Late Wisconsinan deglaciation and glacial lake development in the Appalachians of southeastern Québec. *Géographie physique et Quaternaire*, *53*(1), 117–135. https://doi.org/10.7202/004859ar

Parent, M. & Occhietti, S. (1988). Late Wisconsinan deglaciation and Champlain Sea invasion in the St. Lawrence valley, Québec. Géologie Physique Quaternaire. *42*, 215-246.

Partheniades, E. (2009). *Cohesive sediments in open channels: erosion, transport and deposition*. Butterworth-Heinemann.

Partheniades, E. (1965). Erosion and deposition of cohesive soils. *Journal of the Hydraulics Division*, *91*(1), 105-139.

Phidgets (2021a). Micro Load Cell (0-20kg) – CZL635. https://www.phidgets.com/?tier=3&catid=9&pcid=7&prodid=225

Phidgets (2021b). Micro Load Cell (0-780g) – CZL616C. https://www.phidgets.com/?tier=3&catid=9&pcid=7&prodid=223

Phidgets (2021c). Wheatstone Bridge Phidget. https://www.phidgets.com/?tier=3&catid=64&pcid=57&prodid=957

Phidgets (2021d). VINT Hub Phidget. https://www.phidgets.com/?tier=3&catid=2&pcid=1&prodid=643

Pineda, J.A. et al. (2016). Effects of tube sampling in soft clay: A microstructural insight. *Geotechnique* 66(12): 969-983.

Pokrajac, D., Finnigan, J. J., Manes, C., McEwan, I., & Nikora, V. (2006). On the definition of the shear velocity in rough bed open channel flows. In *River flow* (Vol. 1, pp. 89-98).

Prinz, H., & Strauß, R. (2006). *Abriss der Ingenieurgeologie*. Elsevier/Spectrum Akademischer Verlag.

QGIS Development Team, 2021. QGIS Geographic Information System. Open Source Geospatial Foundation Project. http://qgis.osgeo.org.

Randour, I., Daigneault, R. A., Lamothe, M., Roy, M., & Robitaille, A. (2020). Cartographie des formations superficielles de la région des Laurentides-Lanaudière, phase 2. Gouvernement du Québec, Canada.

Raudkivi, A. J., & Witte, H. H. (1990). Development of bed features. *Journal of Hydraulic Engineering*, *116*(9), 1063-1079.

Reddi, L. N., Lee, I. M., & Bonala, M. V. (2000). Comparison of internal and surface erosion using flow pump tests on a sand-kaolinite mixture. *Geotechnical testing journal*, *23*(1), 116-122.

Regazzoni, P., Marot, D., Courivaud, J., Hanson, G., & Wahl, T. O. N. Y. (2008, May). Soil erodibility: A comparison between the jet erosion test and the hole erosion test. In *Proceeding of the inaugural international conference of the engineering mechanics institute, Minneapolis, Minnesota* (pp. 1-7).

Richard, S.H. (1982). Surficial geology, Russell, Ontario. Geological Survey of Canada, Map 1507A.

Roberts, J. D., Jepsen, R. A., & James, S. C. (2003). Measurements of sediment erosion and transport with the adjustable shear stress erosion and transport flume. *Journal of Hydraulic Engineering*, *129*(11), 862-871.

Rodrigues, C. G., & Vilks, G. (1994). The impact of glacial lake runoff on the Goldthwait and Champlain Seas: The relationship between Glacial Lake Agassiz runoff and the Younger Dryas. *Quaternary Science Reviews*, *13*(9-10), 923-944.

Rodrigues, C. G. (1992). Successions of invertebrate microfossils and the late Quaternary deglaciation of the central St Lawrence Lowland, Canada and United States. *Quaternary Science Reviews*, *11*(5), 503-534.

Rohan, K., Lefebvre, G., Douville, S., & Milette, J. P. (1986). A new technique to evaluate erosivity of cohesive material. *Geotechnical Testing Journal*, *9*(2), 87-92.

Rohan, K., Lefebvre, G., & Douville, S. (1980). Erosion mechanisms of intact clay (in French). In *Proc., of the Canadian Coastal Conf* (pp. 200-219).

Romanelli, R. (1976). The Champlain Sea episode in the Gatineau River Valley and Ottawa Area. (Doctoral thesis). McGill University.

Roy, J. (2019). Use of an RGB-D Sensor as a Depth Data Acquisition Device for Erosion Tests Conducted in Transparent Flumes. Undergraduate research paper. McGill University, Montreal, Canada.

Schmertmann, J. H. (1955). The undisturbed consolidation behavior of clay. *Transactions of the American Society of Civil Engineers*, *120*(1), 1201-1227.

Val Schmidt (2021). planefit (https://www.mathworks.com/matlabcentral/fileexchange/36353-planefit), MATLAB Central File Exchange.

Seed, H. B., Woodward, R. J. and Lundgren, R. (1964). *Fundamental Aspects of the Atterberg Limits.* J. Soil Mechanics and Foundations Division, ASCE, Vol. 90, No. SM6, pp 75-105.

Shafii, I., Briaud, J., Chen, H., & Shidlovskaya, A. (2016). Relationship between soil erodibility and engineering properties.

Shaikh, A., Ruff, J. F., Charlie, W. A., & Abt, S. R. (1988). Erosion rate of dispersive and nondispersive clays. *Journal of Geotechnical Engineering*, *114*(5), 589-600.

Shan, H., Shen, J., Kilgore, R., & Kerenyi, K. (2015). *Scour in cohesive soils* (No. FHWA-HRT-15-033). United States. Federal Highway Administration. Office of Infrastructure Research and Development.

Shields, A. (1936). Anwendung der Aehnlichkeitsmechanik und der Turbulenzforschung auf die Geschiebebewegung. *PhD Thesis Technical University Berlin*.

Shogaki, T. (1996). *A method for correcting consolidation parameters for sample disturbance using volumetric strain*. Soils and foundations, Vol. 36, 3(123-131), 123-131.

Skempton AW (1953). *The colloidal activity of clays.* In: Proceedings of the third international conference on soil mechanics and foundation engineering. Zurich, Switzerland, ICOSOMEF, pp 57-61

Smart, G. M., Duncan, M. J., & Walsh, J. M. (2002). Relatively rough flow resistance equations. *Journal of Hydraulic Engineering*, *128*(6), 568-578.

Smart, G. M. (1999). Turbulent velocity profiles and boundary shear in gravel bed rivers. *Journal of Hydraulic Engineering*, *125*(2), 106-116.

Smerdon, E. T., & Beasley, R. P. (1959). *The tractive force theory applied to stability of open channels in cohesive soils*. University of Missouri, College of Agriculture, Agricultural Experiment Station.

Song, T., Graf, W. H., & Lemmin, U. (1994). Uniform flow in open channels with movable gravel bed. *Journal of Hydraulic Research*, *32*(6), 861-876.

South Nation Conservation (2014). Castor River, subwatershed report card. Accessed on: https://www.nation.on.ca/sites/default/files/Castor%20Report_0.pdf

Stamen Design. (2014). Stamen Toner Lite. [map tiles]. Map tiles by Stamen Design, under CC BY 3.0. Data by OpenStreetMap, under ODbL. Retrieved from: http://tile.stamen.com/toner-lite/{z}/{x}/{y}.png (July 30, 2021).

Tanaka, M., Tanaka, H. & Shiwatoki, D.R. (2001). Sample quality evaluation of soft clays using six types of samplers. *Proceedings of the International Offshore and Polar Engineering Conference* 2: 493-500.

Terzaghi, K. (1944). *Ends and means in soil mechanics*. Harvard University.

Tolhurst, T. J., Defew, E. C., De Brouwer, J. F. C., Wolfstein, K., Stal, L. J., & Paterson, D. M. (2006). Small-scale temporal and spatial variability in the erosion threshold and properties of cohesive intertidal sediments. *Continental Shelf Research*, *26*(3), 351-362.

Torrance, J.K. (1975). On the Role of Chemistry in the Development and Behaviour of the Sensitive Marine Clays of Canada and Scandinavia. Canadian Geotechnical Journal, 12. 326-335.

Trammell, M. A. (2004). *Laboratory apparatus and methodology for determining water erosion rates of erodible rock and cohesive sediments* (Doctoral dissertation, University of Florida).

Tremblay, T. (2008). Hydrostratigraphie et géologie du quaternaire dans le bassin-versant de la rivière Châteauguay, Québec. Masters thesis, Université du Québec à Montréal.

United States Department of Agriculture (2012). *Chapter 3 Engineering Classification of Earth Materials*. Part 631, National Engineering Handbook. 210-VI-NEH, Amend 55.

Utley, B. C., & Wynn, T. M. (2008). Cohesive soil erosion: Theory and practice. In *World Environmental and Water Resources Congress 2008: Ahupua'A* (pp. 1-10).

Vanoni, V. A. (1975). River dynamics. In *Advances in applied mechanics* (Vol. 15, pp. 1-87). Elsevier.

Vanoni, V. A. (1964). Measurements of critical shear stress for entraining fine sediments in a boundary layer.

Van Rijn, L. C. (2020). Literature review of critical bed-shear stresses for mud-sand mixtures. Retrieved from: https://www.leovanrijn-sediment.com/papers/Threshsandmud2020.pdf

Wagner, J.F. (2013). Mechanical properties of clays and clay minerals. In *Developments in Clay Science* (Vol. 5, pp. 347-381). Elsevier.

Wan, C. F., & Fell, R. (2004). Laboratory tests on the rate of piping erosion of soils in embankment dams. *Geotechnical testing journal*, *27*(3), 295-303.

Wibowo, J. L., & Robbins, B. A. (2018). Discussion of "Erosion Charts for Selected Geomaterials" by Jean-Louis Briaud, Anand V. Govindasamy, and Iman Shafii. *Journal of Geotechnical and Geoenvironmental Engineering*, *144*(10), 07018024.

Wilson, M. E. (1924). Arnprior-Quyon and Maniwaki areas, Ontario and Quebec (No. 136). FA Acland.

Winterwerp, J. C., Van Kesteren, W. G. M., Van Prooijen, B., & Jacobs, W. (2012). A conceptual framework for shear flow–induced erosion of soft cohesive sediment beds. *Journal of Geophysical Research: Oceans*, *117*(C10).

Yeats, D. (2021). Fluvial erosion of glacial tills in Ontario: erosion mechanics, critical shear stress and geotechnical properties. Master's thesis. McGill University, Montreal, Canada.

8 Appendix A – Particle Size Distribution

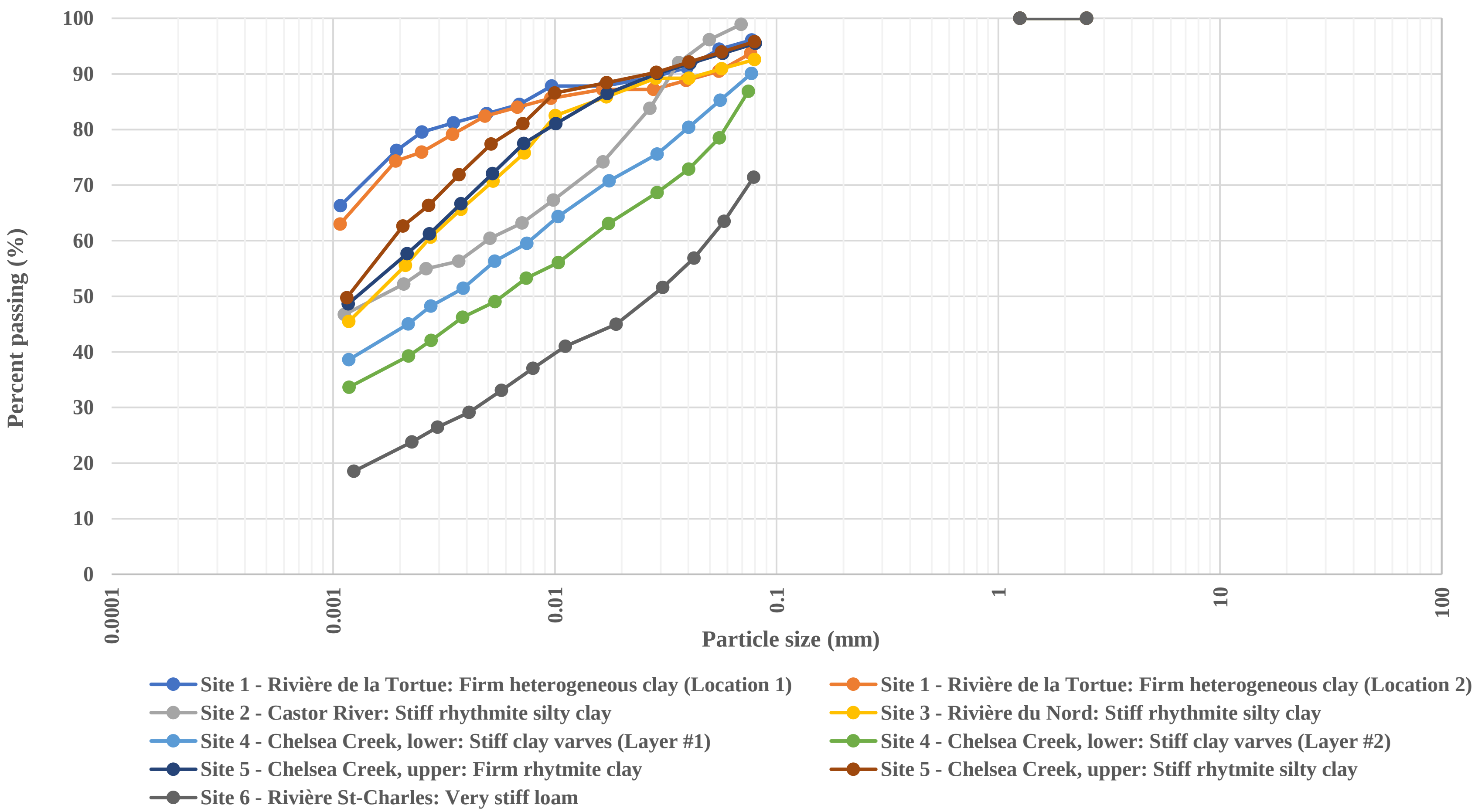

Figure 8-1. Cumulative particle size distribution (hydrometer analysis)

9 Appendix B – Erosion tests

9.1 Preliminary tests

Table 9-1. Difference between the two shear stress calculation methods and the shear stress obtained through a backwater analysis; using data from the calibration study (data taken from Yeats, 2021)

Slope	Above sample R			Interpolated R		
	Backwater shear (Pa)	Observed shear (Pa)	% Difference	Backwater shear (Pa)	Observed shear (Pa)	% Difference
0.010	2.1	2.9 ± 0.2	+ 36%	2.2	3.2 ± 0.1	+ 44%
0.019	3.5	4.2 ± 0.3	+ 19%	3.6	4.7 ± 0.3	+ 30%
0.027	5.8	5.4 ± 0.3	- 7%	4.8	6.4 ± 0.2	+ 34%
0.036	5.6	5.9 ± 0.5	+ 4%	6.0	6.9 ± 0.6	+ 15%
0.040	5.9	7.0 ± 0.6	+ 18%	6.4	8.3 ± 0.7	+ 31%
0.046	6.4	7.4 ± 0.8	+ 16%	6.9	9.1 ± 1.0	+ 32%
0.049	7.1	7.2 ± 1.0	+ 2%	7.5	8.4 ± 1.4	+ 11%
0.053	7.4	7.4 ± 0.7	0%	7.9	8.8 ± 0.8	+ 11%
0.056	7.6	7.3 ± 1.1	- 3%	8.2	8.9 ± 1.2	+ 9%
0.060	8.0	7.9 ± 0.8	- 1%	8.7	9.7 ± 1.1	+ 12%
0.063	8.5	8.6 ± 1.0	+ 1%	9.2	10.7 ± 1.2	+ 16%
0.067	8.7	9.0 ± 1.1	+ 3%	9.5	11.6 ± 1.3	+ 22%

Table 9-2. Effect of the presence of the box setup on the shear stress along the flume estimate (data taken from Yeats, 2021)

	Shear stress τ (Pa)		
Slope	With wires	No wires	% Difference
0.010	3.2	3.0	8%
0.019	4.6	4.6	2%
0.027	6.1	5.7	7%
0.036	7.1	7.4	-4%
0.040	8.1	8.1	0%
0.046	8.9	9.0	-1%
0.049	9.4	9.7	-3%
0.053	9.8	10.2	-4%

0.056	10.1	10.7	-5%
0.060	10.6	11.2	-6%
0.063	11.1	11.86	-6%
0.067	11.82	12.58	-6%

9.2 Site 1 – Rivière de la Tortue tributary

Table 9-3. Erosion rate at applied shear stress during erosion test of the sample in the square mould taken at the Rivière de la Tortue tributary

Slope	Moisture content m	Duration	Shear stress τ	Erosion rate			dz (initial: 2.2mm)	Observations
	%	min	Pa	g/hr	g/cm²/h	mm/h	mm	
0.000	49	240	0.9 ± 0.1	0.0	0.000	0.00	1.6	Slight particle erosion, presence of roots revealed
0.010	49	120	2.9 ± 0.2†	0.0	0.000	0.00	1.9	Nearing critical shear stress: Blocks that were already lose are lifted off by the flow
0.019	49	120	4.2 ± 0.3†	6.5	0.019	0.11	2.0	Reached critical shear stress: blocks (>2mm) are eroding
0.027	49	120	5.4 ± 0.3†	6.2	0.018	0.10	2.3	Similar patterns of mass erosion
0.036	49	146	5.9 ± 0.5†	3.9	0.011	0.07	3.2	Similar patterns of mass erosion
0.046	49	130	7.4 ± 0.8†	9.3	0.027	0.15	3.6	Similar patterns of mass erosion
0.053	49	120	7.4 ± 0.7†	10.0	0.029	0.17	3.5	Similar patterns of mass erosion
0.067	49	120	9.0 ± 1.1†	11.7	0.033	0.19	3.6	Similar patterns of mass erosion

Table 9-4. Erosion rate at applied shear stress during second erosion test of the sample in the square mould taken at the Rivière de la Tortue tributary; the tests were done a second time to verify the results

Slope	Moisture content m	Duration	Shear stress τ	Erosion rate			dz (initial: 3.2mm)	Observations
	%	min	Pa	g/hr	g/cm²/h	mm/h	mm	
0.000	47	119	0.9 ± 0.2†	0	0.000	0.00		No visible erosion

0.010	47	122	2.8 ± 0.6	0	0.000	0.00	3.0	Nearing critical stress: Large blocks (>6mm) eroded in the first hour, but only block (<2mm) in the next two hours
0.019	47	137	4.4 ± 0.5	2.5	0.007	0.04	3.2	Reached critical shear stress: blocks (>2mm) are eroding

Table 9-5. Erosion rate at applied shear stress during erosion test of the sample taken with the Sherbrooke sampler at the Rivière de la Tortue tributary

Slope	Moisture content m	Duration	Shear stress τ	Erosion rate			dz (initial: 2.2mm)	Observations
	%	min	Pa	g/hr	g/cm^2/h	mm/h	mm	
0.000	47	100	0.9 ± 0.3	0.0	0.000	0.00	3.0	No visible erosion
0.010	47	110	2.6 ± 0.5	2.0	0.024	0.14	2.9	Reached critical shear stress: cracks forming across surface and blocks (>2mm) are eroding
0.019	47	97	4.3 ± 0.5	6.8	0.083	0.48	3.5	Similar patterns of mass erosion
0.027	47	120	4.6 ± 0.5	15.1	0.185	1.07	4.8	Similar patterns of mass erosion

Table 9-6. Erosion rate at applied shear stress during erosion test of the sample in the square mould after 48hr of air-drying; taken at the Rivière de la Tortue tributary

Slope	Moisture content m	Duration	Shear stress τ	Erosion rate			dz (initial: 3.6mm)	Observations
	%	min	Pa	g/hr	g/cm^2/h	mm/h	mm	
0.000	44	35	0.8 ± 0.1	--	--	--		No visible erosion or changes
0.010		30	2.5 ± 0.3	--	--	--	2.9	No visible erosion or changes
0.019		30	4.2 ± 0.6	--	--	--	3.1	Critical shear stress reached

9.3 Site 2 – Castor River tributary

Table 9-7. Erosion rate at applied shear stress during erosion test of sample #1 taken at the Castor River tributary

Slope	Moisture content m	Duration	Shear stress τ	Erosion rate			dz (initial: 2.6mm)	Observations
	%	min	Pa	g/hr	g/cm²/h	mm/h	mm	
0.000	24	120	0.3 ± 0.1	0.0	0.000	0.00		Erosion of the surface (peeling-like erosion)
0.000		110	0.7 ± 0.2	4.1	0.051	0.25		Particle erosion occurring
0.000		127	0.9 ± 0.2	2.3	0.028	0.14	3.7	Particle erosion occurring
0.010		127	2.5 ± 0.5	22.5	0.275	1.36	4.7	Reached critical shear stress : block erosion occurring close to the edge of the mould
0.019		119	4.2 ± 0.7	7.5	0.091	0.45	5.9	Similar patterns of mass erosion
0.027		122	5.2 ± 0.8	99.5	1.218	6.01	5.2	Large block (100.0g) at the center eroded

Table 9-8. Erosion rate at applied shear stress during erosion test of the geotechnical sample taken at the Castor River tributary

Slope	Moisture content m	Duration	Shear stress τ	Erosion rate			dz (initial: 1.9mm)	Observations
	%	min	Pa	g/hr	g/cm²/h	mm/h	mm	
0.000	27	115	0.8 ± 0.3	4.6	0.056	0.28	1.8	Particle erosion
0.010		125	3.0 ± 0.6	23.7	0.290	1.47	3.0	Critical shear stress reached

Table 9-9. Erosion rate at applied shear stress during erosion test of sample #3 taken at the Castor River tributary

Slope	Moisture content m	Duration	Shear stress τ	Erosion rate			dz (initial: 5.4mm)	Observations
	%	min	Pa	g/hr	g/cm²/h	mm/h	mm	
0.000	25	105	0.8 ± 0.2	0	0	0.00	5.4	Particle erosion
0.010		55	2.7 ± 0.6	117.6	1.439	7.16	6.0	Critical shear stress reached

Table 9-10. Erosion rate at applied shear stress during erosion test of the geotechnical sample taken at the Castor River tributary after being air dried for 48 hours

Slope	Moisture content m	Duration	Shear stress τ	Erosion rate			dz (initial: 2.5mm)	Observations
	%	min	Pa	g/hr	$g/cm^2/h$	mm/h	mm	
0.000	27	85	0.9 ± 0.2	0	0	0.00	2.9	Particle erosion
0.010		60	1.9 ± 0.5	9.6	0.118	0.59	2.9	Critical shear stress reached

9.4 Site 3 – Rivière du Nord tributary

Table 9-11. Erosion rate at applied shear stress during erosion test of sample #1 taken at the Rivière du Nord tributary

Slope	Moisture content m	Duration	Shear stress τ	Erosion rate			dz (initial: 4.3mm)	Observations
	%	min	Pa	g/hr	$g/cm^2/h$	mm/h	mm	
0.000	42	125	0.3 ± 0.1	0.3	0.004	0.02	3.2	Particle erosion occurring
0.000		125	0.7 ± 0.2	7.0	0.086	0.48	3.1	Nearing critical stress: Block erosion starting to occur, larger blocks (>2mm) are visible but staying in place
0.000		123	0.8 ± 0.4	13.7	0.167	0.94	2.8	Critical shear stress reached

Table 9-12. Erosion rate at applied shear stress during erosion test of the top half of the geotechnical sample taken at the Rivière du Nord tributary

Slope	Moisture content m	Duration	Shear stress τ	Erosion rate			dz (initial: 4.3mm)	Observations
	%	min	Pa	g/hr	$g/cm^2/h$	mm/h	mm	
0.000	42	62	0.3 ± <0.1	0	0	0.00	3.7	Nearing critical stress: Block erosion starting to occur, larger blocks (>2mm) are visible but staying in place
0.000		61	0.9 ± 0.3	9.6	0.118	0.66	3.5	Critical shear stress reached

Table 9-13. Erosion rate at applied shear stress during erosion test of the bottom half of the geotechnical sample taken at the Rivière du Nord tributary

Slope	Moisture content m	Duration	Shear stress τ	Erosion rate			dz (initial: 3.5mm)	Observations
	%	min	Pa	g/hr	g/cm²/h	mm/h	mm	
0.000	41	127	0.3 ± 0.1	2.7	0.034	0.19		Nearing critical stress: Block erosion starting to occur, larger blocks (>2mm) are visible but staying in place
0.000		116	0.7 ± 0.3	3.1	0.038	0.21	3.8	Nearing critical stress: Block erosion starting to occur, larger blocks (>2mm) are visible but staying in place
0.000		130	0.8 ± 0.4	4.7	0.058	0.32	4.9	Critical shear stress reached

Table 9-14. Erosion rate at applied shear stress during erosion test of bottom half of the geotechnical sample taken at the Rivière du Nord tributary after being air dried for 48 hours

Slope	Moisture content m	Duration	Shear stress τ	Erosion rate			dz (initial: 5.7mm)	Observations
	%	min	Pa	g/hr	g/cm²/h	mm/h	mm	
0.000	43	30	0.3 ± <0.1	0	0	0.00	5.8	Nearing critical stress: Block erosion starting to occur, larger blocks (>2mm) are visible but staying in place
0.000		90	0.8 ± 0.3	4.9	0.060	0.34	3.9	Critical shear stress reached

9.5 Site 4 – A lower tributary of Chelsea Creek

Table 9-15. Erosion rate at applied shear stress during erosion test of sample #6 taken at the lower tributary of Chelsea Creek

Slope	Moisture content m	Duration	Shear stress τ	Erosion rate			dz (initial: 4.0mm)	Observations
	%	min	Pa	g/hr	g/cm²/h	mm/h	mm	
0.000	27	119	0.9 ± 0.2	0.0	0	0		No visible erosion

0.010		133	2.6 ± 0.4	0.0	0	0.00		No visible erosion
0.019		118	4.4 ± 0.7	2.4	0.007	0.03	5.5	Nearing critical shear stress: Blocks (<2mm) eroded
0.027		119	5.8 ± 0.9	3.0	0.009	0.04	5.9	Critical shear stress reached: Blocks (>2mm) eroded
0.036		115	7.1 ± 1.1	6.4	0.018	0.09	5.8	Similar patterns of mass erosion
0.046		125	8.6 ± 1.1	4.5	0.013	0.06	5.8	Similar patterns of mass erosion
0.053		116	7.8 ± 1.1	6.1	0.017	0.09	6.0	Similar patterns of mass erosion
0.067		122	10.1 ± 1.0	3.3	0.010	0.05	5.2	Similar patterns of mass erosion

Table 9-16. Erosion rate at applied shear stress during erosion test of sample #7 taken at the lower tributary of Chelsea Creek

Slope	Moisture content m	Duration	Shear stress τ	Erosion rate			dz (initial: 4.7mm)	Observations
	%	min	Pa	g/hr	g/cm²/h	mm/h	mm	
0.036	30	111	6.6 ± 0.9	0	0	0	4.9	No visible erosion
0.046		126	8.0 ± 1.3	5.4	0.016	0.08	4.7	Critical shear stress reached: Blocks (>2mm) eroded

Table 9-17. Erosion rate at applied shear stress during erosion test of sample #9 taken at the lower tributary of Chelsea Creek

Slope	Moisture content m	Duration	Shear stress τ	Erosion rate			dz (initial: 6.8mm)	Observations
	%	min	Pa	g/hr	g/cm²/h	mm/h	mm	
0.000	32	123	0.4 ± 0.2	24.0	0.069	0.36	7.4	Critical shear stress reached: Blocks (>2mm) eroded

Table 9-18. Erosion rate at applied shear stress during erosion test of sample #6 taken at the lower tributary of Chelsea Creek after being air dried for 48 hours

Slope	Moisture content m	Duration	Shear stress τ	Erosion rate	dz (initial: 5.1mm)	Observations

	%	min	Pa	g/hr	g/cm^2/h	mm/h	mm	
0.000	30	30	0.9 ± 0.2	0	0	0		No visible erosion
0.010		30	2.9 ± 0.7	0	0	0		Small blocks that were already detached (<2mm) eroded
0.027		30	5.4 ± 0.6	5.2	0.015	0.08	6.0	No visible erosion
0.036		60	7.8 ± 1.5	28.0	0.080	0.41	6.6	Critical shear stress reached: Blocks (>2mm) eroded

Table 9-19. Erosion rate at applied shear stress during erosion test of sample #9 taken at the lower tributary of Chelsea Creek after being air dried for 48 hours

Slope	Moisture content m	Duration	Shear stress τ	Erosion rate			dz (initial: 7.2mm)	Observations
	%	min	Pa	g/hr	g/cm^2/h	mm/h	mm	
0.000	29	34	0.2 ± <0.1	1.1	0.003	0.02		Small plates eroded
0.000		55	0.9 ± 0.2	9.2	0.026	0.13	6.4	Only thinner layers (<2mm) eroded
0.010		40	2.9 ± 0.4	117.0	0.334	1.70	6.9	Critical shear stress reached: Blocks (>2mm) eroded

9.6 Site 5 – An upper tributary of Chelsea Creek

Table 9-20. Erosion rate at applied shear stress during erosion test of sample #2 of an upper tributary of Chelsea Creek

Slope	Moisture content m	Duration	Shear stress τ	Erosion rate			dz (initial: 2.8mm)	Observations
	%	min	Pa	g/hr	g/cm^2/h	mm/h	mm	
0.000	68	106	0.8 ± 0.3	--	--	--		No visible erosion
0.010		104	2.8 ± 0.4	--	--	--		No visible erosion
0.019		116	4.3 ± 0.6	--	--	--		No visible erosion
0.027		112	3.8 ± 1.0	--	--	--		No visible erosion
0.036		125	6.0 ± 0.8	--	--	--		No visible erosion
0.046		115	7.5 ± 1.0	--	--	--		No visible erosion
0.053		118	4.3 ± 2.1	--	--	--		No visible erosion
0.067		130	10.4 ± 1.3	--	--	--	2.1	No visible erosion

Table 9-21. Erosion rate at applied shear stress during erosion test of sample #7 of an upper tributary of Chelsea Creek

Slope	Moisture content m	Duration	Shear stress τ	Erosion rate			dz (initial: 3.3mm)	Observations
	%	min	Pa	g/hr	$g/cm^2/h$	mm/h	mm	
0.000	80	119	0.2 ± <0.1	16.3	0.200	1.3	3.3	Critical shear stress reached

Table 9-22. Erosion rate at applied shear stress during erosion test of sample #4 after 24h of air-drying of an upper tributary of Chelsea Creek

Slope	Moisture content m	Duration	Shear stress τ	Erosion rate			dz (initial: 4.4mm)	Observations
	%	min	Pa	g/hr	$g/cm^2/h$	mm/h	mm	
0.000	72	46	0.2 ± <0.1	4.2	0.051	0.3	6.7	Critical shear stress reached

Table 9-23. Erosion rate at applied shear stress during erosion test of sample #7 after 48h of air-drying of an upper tributary of Chelsea Creek

Slope	Moisture content m	Duration	Shear stress τ	Erosion rate			dz (initial: 2.5mm)	Observations
	%	min	Pa	g/hr	$g/cm^2/h$	mm/h	mm	
0.000	70	30	0.2 ± <0.1	--	--	--		No visible erosion
0.000		30	0.8 ± 0.3	--	--	--		No visible erosion
0.019		30	4.5 ± 0.6	--	--	--		No visible erosion
0.036		30	6.4 ± 0.7	--	--	--		No visible erosion
0.053		30	7.6 ± 1.3	--	--	--		No visible erosion
0.067		110	10.9 ± 1.4	--	--	--	4.8	No visible erosion

9.7 Site 6 – Rivière St-Charles tributary

Table 9-24. Erosion rate at applied shear stress during erosion test of one sample of a tributary of Rivière St-Charles

Slope	Moisture content m	Duration	Shear stress τ	Erosion rate			dz (initial: 3.4mm)	Observations
	%	min	Pa	g/hr	g/cm^2/h	mm/h	mm	
0.000	17	119	0.8 ± 0.3	--	--	--		No visible erosion
0.010		114	2.9 ± 0.5	--	--	--		No visible erosion
0.019		112	4.7 ± 0.6	--	--	--		No visible erosion
0.027		107	5.5 ± 0.7	--	--	--		No visible erosion
0.036		113	6.5 ± 0.8	--	--	--		No visible erosion
0.046		115	7.8 ± 1.0	--	--	--		No visible erosion
0.053		115	7.6 ± 1.5	--	--	--		No visible erosion
0.067		120	11.5 ± 1.8	--	--	--	3.4	No visible erosion

Table 9-25. Erosion rate at applied shear stress during erosion test of one sample of a tributary of Rivière St-Charles after being air dried for 48 hours

Slope	Moisture content m	Duration	Shear stress τ	Erosion rate			dz (initial: 3.1mm)	Observations
	%	min	Pa	g/hr	g/cm^2/h	mm/h	mm	
0.000	11	30	0.2 ± <0.1	--	--	--	3.6	Particle erosion
0.000		85	0.9 ± 0.3	--	--	--	4.9	Critical shear reached: Particle erosion and block erosion

10 Appendix C – Erosion vs soil properties

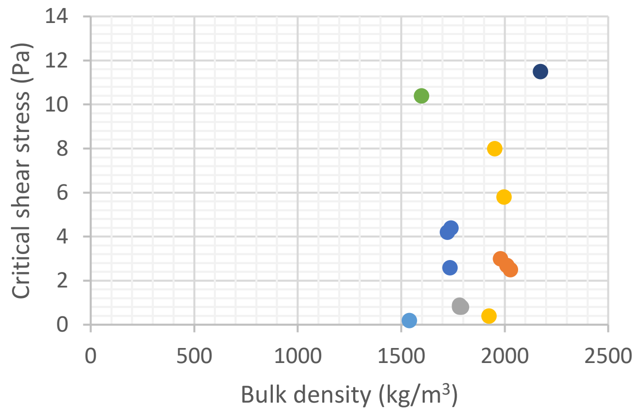

Figure 10-1. Critical shear stress and bulk density

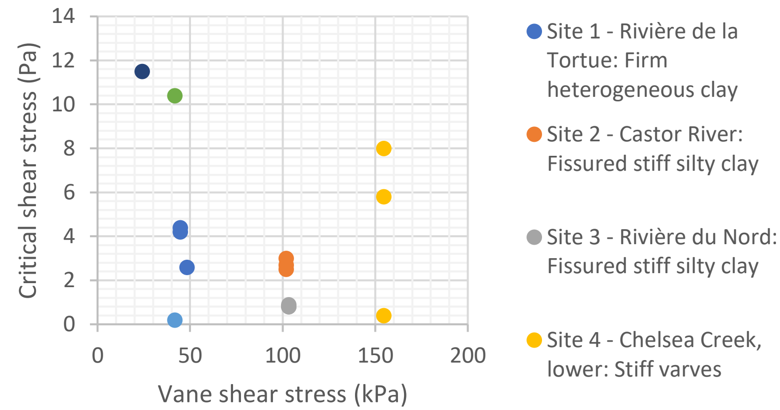

Figure 10-2. Critical shear stress and vane shear stress

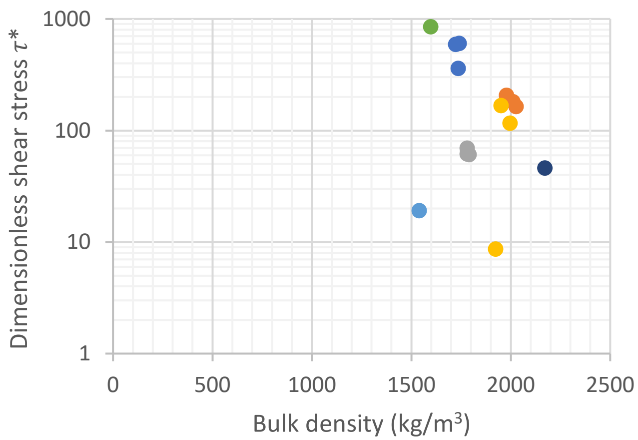

Figure 10-3. Dimensionless shear stress and bulk density

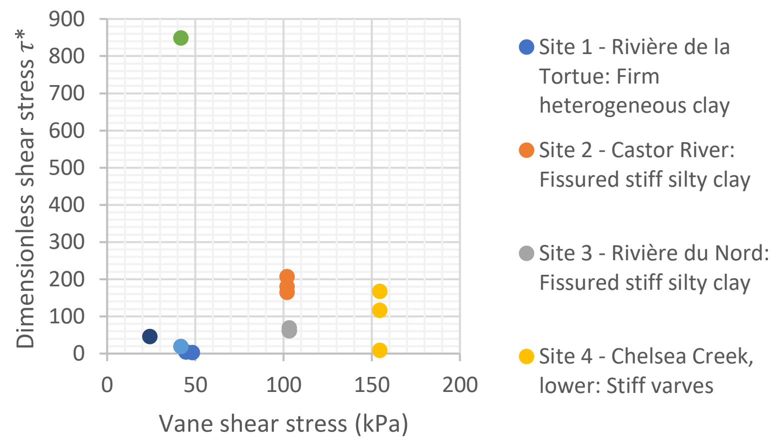

Figure 10-4. Dimensionless shear stress and vane shear stress

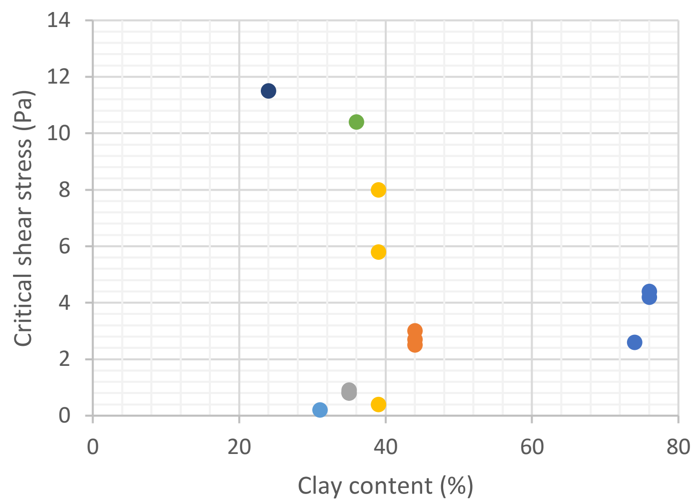

Figure 10-5. Critical shear stress and clay content

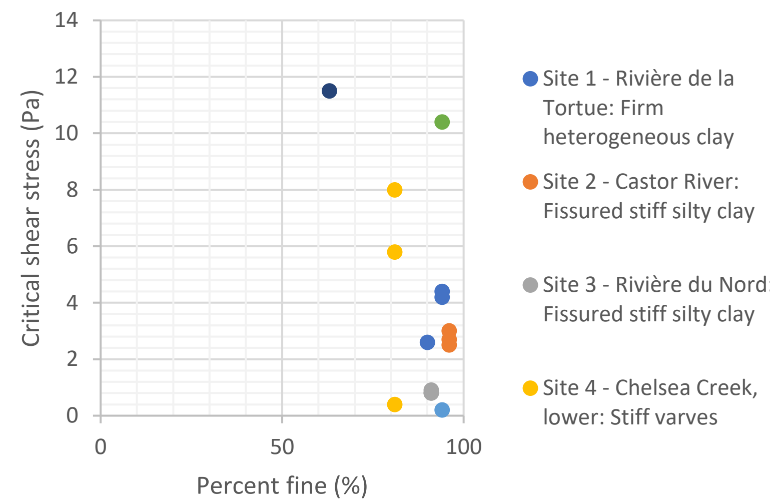

Figure 10-6. Critical shear stress and percent fine

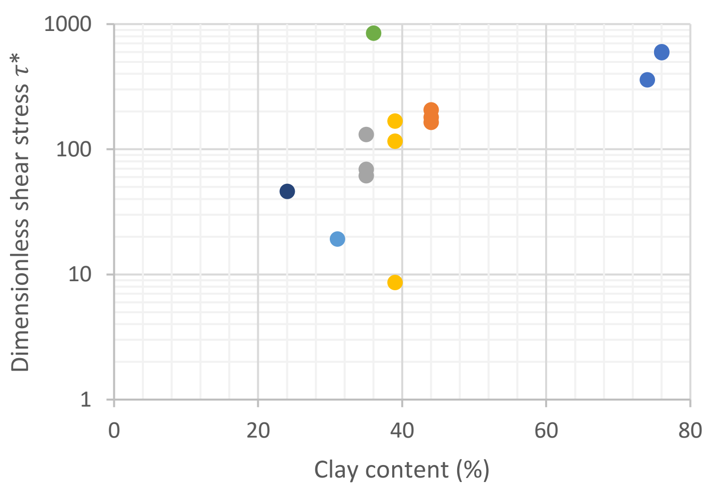

Figure 10-7. Dimensionless shear stress and clay content

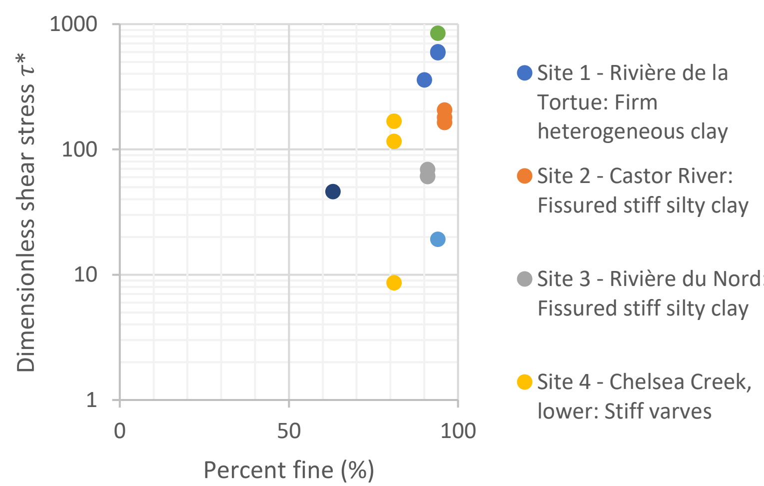

Figure 10-8. Dimensionless shear stress and percent fine

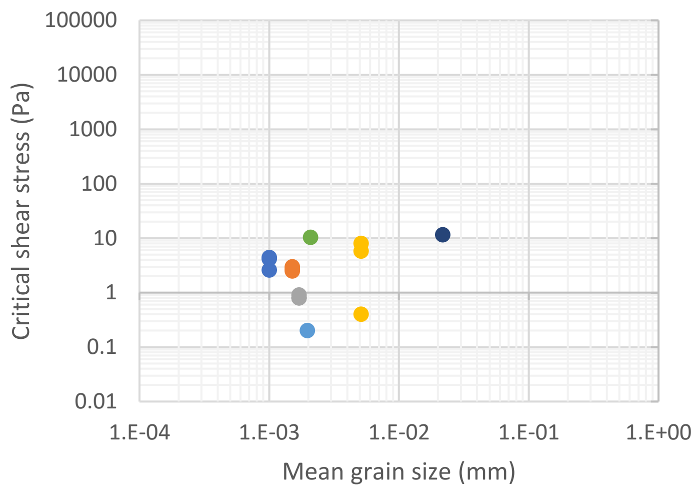

Figure 10-9. Critical shear stress and mean grain size

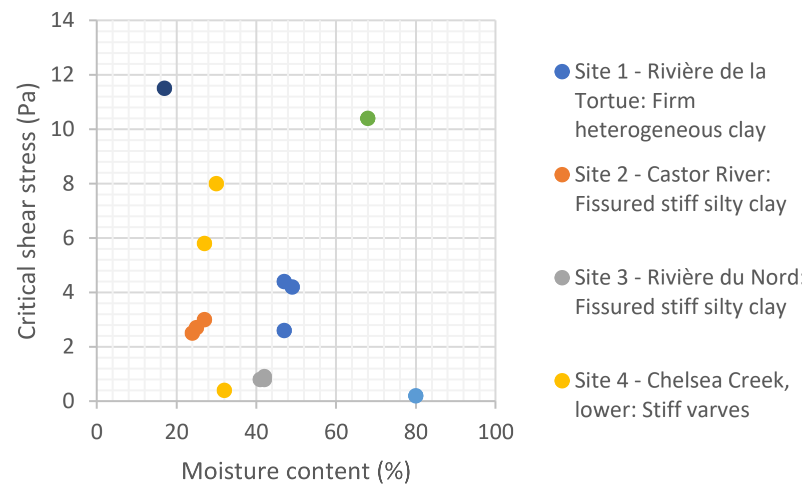

Figure 10-10. Critical shear stress and moisture content

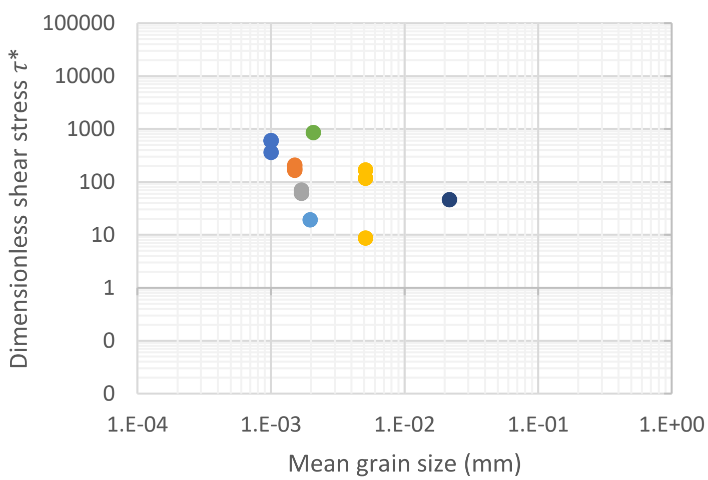

Figure 10-11. Dimensionless shear stress and mean grain size

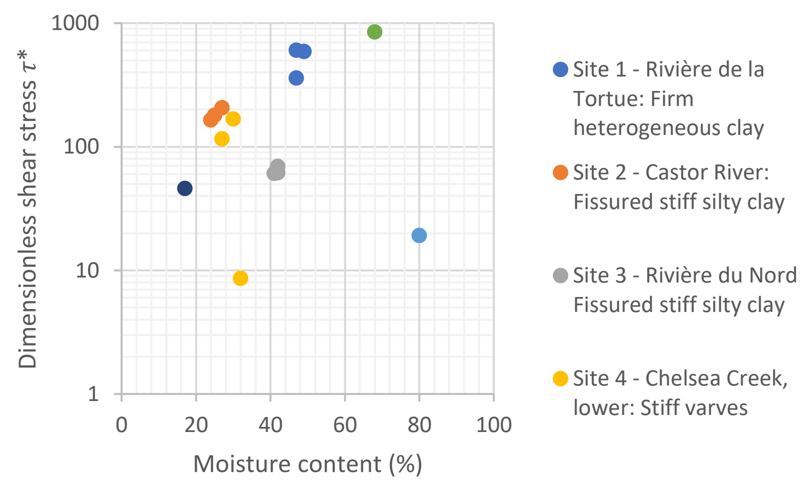

Figure 10-12. Dimensionless shear stress and moisture content

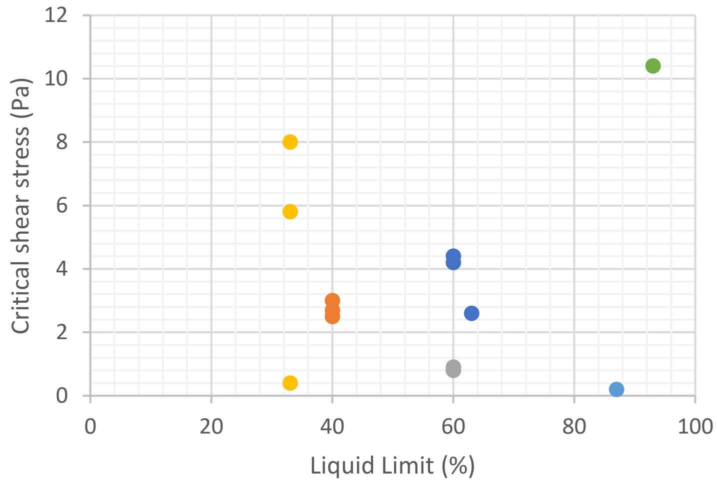

Figure 10-13. Critical shear stress and liquid limit

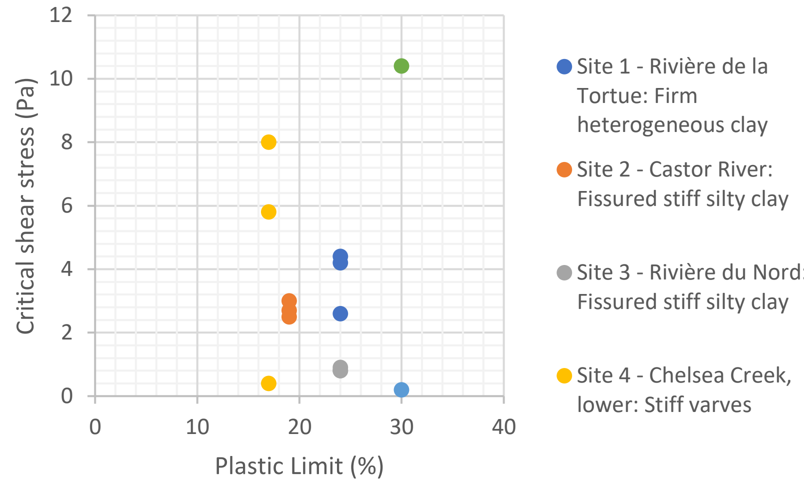

Figure 10-14. Critical shear stress and plastic limit

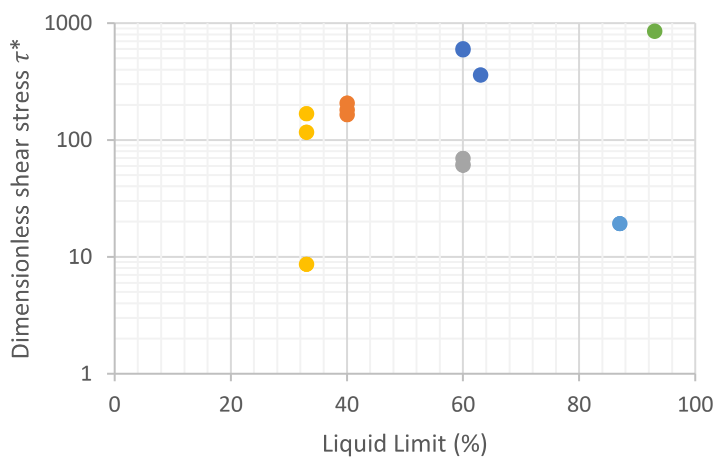

Figure 10-15. Dimensionless shear stress and liquid limit

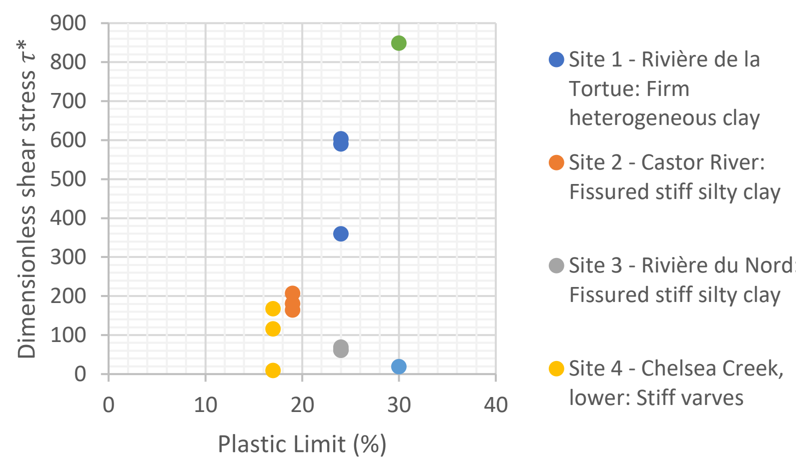

Figure 10-16. Dimensionless shear stress and plastic limit

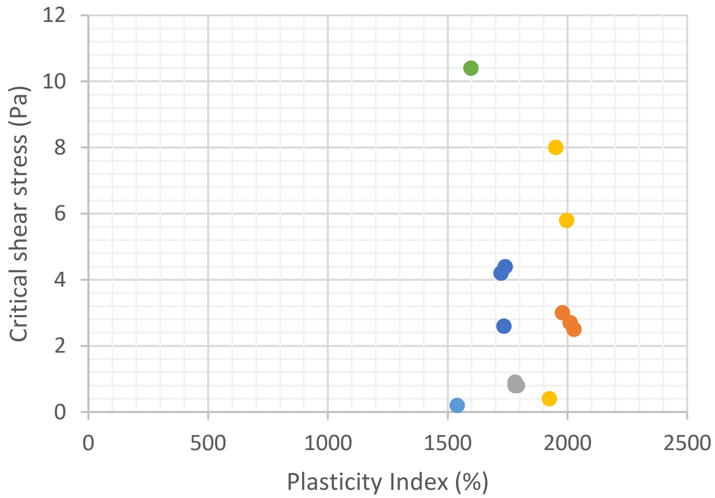

Figure 10-17. Critical shear stress and plasticity index

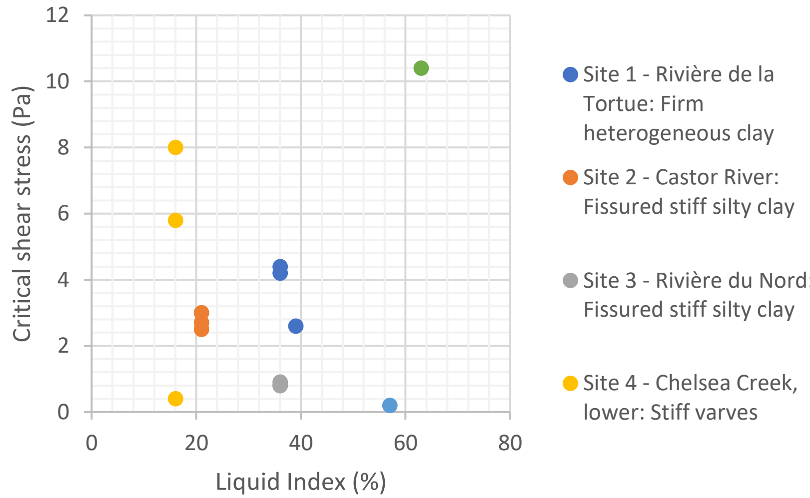

Figure 10-18. Critical shear stress and liquid index

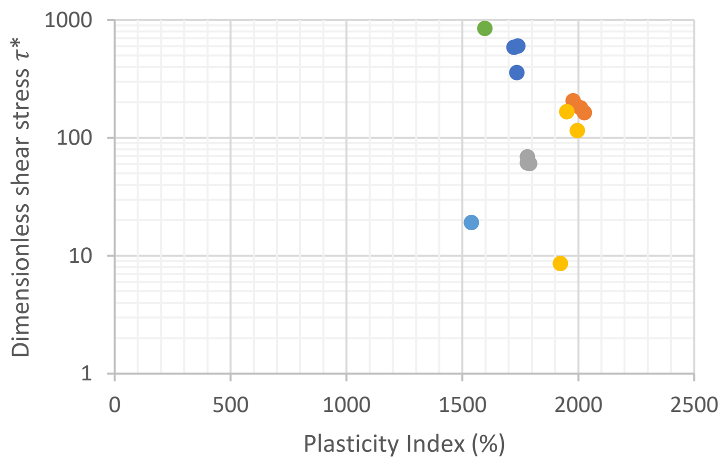

Figure 10-19. Dimensionless shear stress and plasticity index

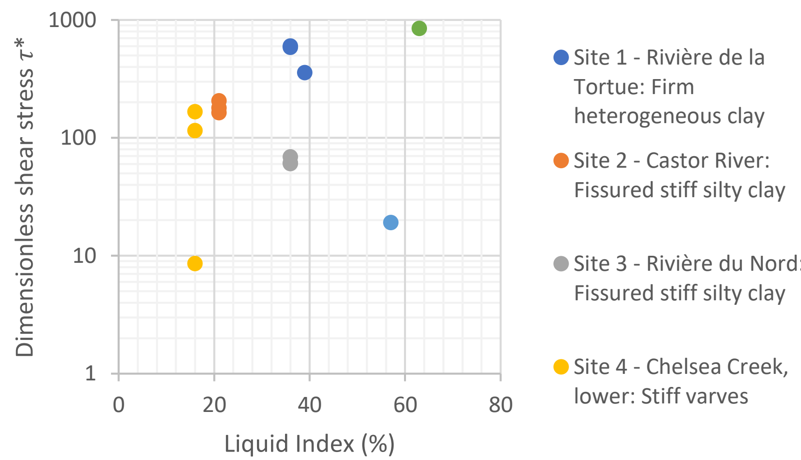

Figure 10-20. Dimensionless shear stress and liquid index